PhD Thesis

IFISC

Nonlinear Dynamics and Regime Shifts in Ecosystems

Flora Souza Bacelar

Supervisor: Emilio Hernández-García

Nonlinear Dynamics and Regime Shifts in Ecosystems *Flora S. Bacelar*

The cover background is a composition of the picture found in the back of Marine Ecology Part page and the following picture:

Photo: Cedar Creek Ecosystem Science Reserve

UNIVERSITAT DE LES ILLES BALEARS
DEPARTAMENT DE FISICA

PhD Thesis

Nonlinear Dynamics and Regime Shifts in Ecosystems

Author:
Flora Souza Bacelar

Supervisor:
Emilio
Hernández-García

Instituto de Física Interdisciplinar y Sistemas Complejos

October 7, 2010

Nonlinear Dynamics and Regime Shifts in Ecosystems

by

Flora Souza Bacelar

B.S.(Universidade Federal da Bahia) 2001
M.S. (Universidade Federal da Bahia) 2005
M.S. (Universitat de les Illes Balears) 2008

THESIS

Presented to the Physics Department of

Universitat de les Illes Balears

in Partial Fulfillment

of the Requirements

for the Degree of

DOCTOR

in

PHYSICS

October 2010

Nonlinear Dynamics and Regime Shifts in Ecosystems

Flora Souza Bacelar
Instituto de Fisica Interdisciplinar y Sistemas Complejos
IFISC (UIB-CSIC)

PhD Thesis

Supervisor: Prof. Emilio Hernández-García

This document was typeset with LaTeX

Prof. Emilio Hernandez-Garcia, as the thesis advisor, and Prof. Claudio Rubén Mirasso Santos, acting as Presenter from the UIB Physics Department, certify that this thesis has been carried out by Ms. Flora Souza Bacelar, in order to obtain the degree of Doctor in Physics. Because of that they sign the present document.

Emilio Hernández-García

Claudio Rubén Mirasso Santos

Flora Souza Bacelar

Palma de Mallorca, 7 of October of 2010.

Resum

L'objectiu fonamental de la física estadística és descriure les propietats emergents de sistemes compostos de moltes parts que interaccionen. Més en general, la denominada "ciència dels sistemes complexos" busca regularitats que permetin entendre el comportament de sistemes compostos per un gran nombre d'agents. En aquest context, els sistemes biològics han estat sempre al focus d'atenció de la física dels sistemes complexos, i l'estructura i dinàmica d'ecosistemes ha estat un dels temes rellevants. En aquesta tesi s'ha estudiat l'organització i evolució d'ecosistemes, des del punt de vista de l'estudi de sistemes complexos, emprant les eines de la dinàmica no lineal i la física estadística. Com a tema central, s'ha estudiat la fenomenología dels "canvis de règim": Tot ecosistema està exposat a canvis graduals de clima, càrrega de nutrients o fragmentació de l'hàbitat. La naturalesa en general respon a aquests canvis graduals d'una manera suau. Tanmateix estudis en ecosistemes dispars com els de llacs, oceans, o terres àrides han mostrat que respostes suaus poden ser interrompudes per canvis bruscos a estats molt diferents. En aquesta tesi s'han formulat i analitzat diversos models que permeten interpretar aquestes observacions en el marc dels conceptes de bifurcació, transicions de fase i dinàmica adaptativa. En particular s'han estudiat models de cadenes tròfiques pelàgiques, de competició d'espècies en ecosistemes litorals, de vegetació en sabanes, i d'efectes evolucionaris i ecològics en les característiques del parasitisme.

“pa toos”

Acknowledgements

First of all I would like to thank my guardian angel and the friendly spirits beside me for give me strength and energy to keep going in this hard and at the same time pleasant journey.

During my stay in Mallorca I always have support from my “big family”! Not only, my blood family but all my friends! So, there is no word to express my feelings towards all these people! But even so I will try it! It’s hard to me to say thanks to all of you using only English language, I am sorry switching languages throughout the acknowledgements, but I wanted all understand my gratitude...

Muchos cariños a todos mis “compis” que entre peleas y achuchones me han ayudado a convertirme en una persona mejor. Lo unico que puedo hacer es recordar a todos sus nombres, ya que en tan pocas lineas sería imposible relatar las experiencias compartidas con cada uno de ellos! Muchas Gracias Iacyel, Marzena, Yanne, Mirian, Mona, Jackeline, Dana, Alfredo, Marcos, Judit, Raluca, Patri, Celia, Antonio, Eva, Inês, Gerardo y Matias. Extiendo mis cariños a los vecinos ya que el piso es doble y tenemos dos plantas! hehehe Uep! Joana, Johnna, Leo y “fofinha”!! Algunas manzanas más, grandes amigos Charles e Isis.

Y la lista cresce, pues todos se conocen unos más, otros menos, pero bueno, aqui solo cuento el apoyo y cariño hacia mi, aunque lo más bonito

fue ver la familia extendiendose a grandes amistades dentro y fuera del trabajo! Molts Grácies a tots, Alejandro Herrada, Juan Carlos, Juanito, Xavi Castelló, Maria, Ismael, Claudio Tessone, Federico Vazquez, Raul Vicente, Francesco Visconti, Pau Amengual, Lluis Fita, Dani Martínez, Sigrid Jorgensen, Jade Martínez, Toni Peréz Serrano, Toni Pérez, Adrián Jacobo, Romain Modeste, Luis Lafuerza, Guadalupe, Przemek Grabowicz, Pedro Sánchez, Murat Tugrul, Jose María Aparicio (Pepe) y Teresa Martins.

Moltes gràcies a Isabel Pujol, Javier, Xisca, Francesc i Sofia per proporcionar-me bons moments i presentar-me a aquesta bonica Illa.

Muchas Gracias a mis profesoras de costura (Eva) y patchwork (Anna) en Mallorca y a la dulce Michelle! Siempre me lo paso genial con vosotras!

À minha família brasileira só louvores!!! Gente igual a vocês está por nascer! Minhas saudosas vovós, Maria Ducarmo e Moçazinha, meus saudosos vovô Homero e padrinho Jorge, Meu tio Antônio, Minha tia e madrinha Dina, meus primos Pedro e Mariana, Meu tio Edson e Rosa Maria, Minha tia Sonja, meu irmãozinho pequeno (rsrrss), minha querida sogra Estelita, vovó Luzia, Sandro e Gisele, minha irmã Dali, minhas madrinhas Lulu e Regina, minhas comadres Liu e Renata, minha princesa Ananda, Renatinho, Fêzinha, Bazinha... Infelizmente devo parar por aqui, pois não sobrará páginas para minha tese... rsrsrsr Mas saiban que nestes três pontos estão todos os que me deram carinho e apoio! Êta familia grande! Curvo-me diante de todos vocês, o apoio recebido constantemente resulta em muito mais que esta tese, mas em uma pessoa feliz por ter todos vocês ao meu lado amando-me, cuidando-me e apoiando-me. Muito obrigada!!

Não poderia deixar de destacar as pessoas mais especiais da minha vida! Meu paizinho e Minha mamãe! Vir a esse mundo de pessoas tão maravilhosas já é motivo para nascer agradecendo! Se essa tese eu dedico a todos é por vocês, pessoas que me deram amor e me ensinaram a amar, transformando minha familia não somente em um núcleo mas em o que

eu chamo da grande familia Crística. Amén.

E “meu anjo”? Você é o meu s☼lzinho! Companheiro para todos e em todos os momentos, dedico-te um agradecimento especial, pois eu sei que muitos sacrifícios foram feitos da sua parte para me acompanhar nesse meu sonho! Já passamos por muitas situações difíceis e também por muitas maravilhosas! Sou muito grata por te ter ao meu lado e poder aprender com seu exemplo diário como é ser uma pessoa boa! Por isso você é meu anjo, mas também é meu principe, mais ainda... Meu am♡r.

I would like give a special thank to my “super” supervisor Emílio Hernández-García. I admire you for the great person and great scientist you are! Thank you for give me the opportunity to complete my superior studies in Spain and your excellent guidance, respecting my thoughts and supporting my choices with a respectable way to express your opinion when punctuating my mistakes. Penso que mai no sabràs el com et sóc agraïda.

Thanks to all IFISC staff who proportioned good conferences, seminars, classes and science environment. A special thanks to Maxi San Miguel, Pere Colet, Damià Gomila, Victor M. Eguiluz, Cristóbal Lopez, Manuel Matias, Tomás Sintes, Roberta Zambrini, Alessandro Scirè , who I could learn with and receive support when I needed and specially thanks to Claudio Mirasso for accept to be the representative Professor of this thesis. Thanks to Jose Luis Lisani for giving me help in Matlab scripts. And undoubtedly thanks the wonderful people of technical and administrative support at IFISC, there is no way things work without these people! It was a great pleasure to meet the sweet Rubén Tolosa, thanks and sorry about my inconvenient computer problems(hehehe), the friendly Alex (Alexandra Casanovas) who helped me a lot when I just arrived in Mallorca and to all lovely people, Suzana Sanches, Marta Ozonas, Rosa María Rodríguez, Edu Herráiz, María Antònia Tugores Pons and Neus Verdera you are the best!

Gràcies Francesc Bonet Domenech (Xisco), Rafael Pizà Rosselló, Melcior Rotger Bauzà, Fernando de Angulo Dols, Antònia Tous Sabater,

Carme Casares Serra, Rosario (Xaro), Catalina (Cati), Tonita, Marga Prohens, Marga Moranta, al personal del Tomeu, en especial Lianka, Nuria i Cati, meus mediques Margalida Sastre i Margalida Terrasa, els de la biblioteca del mateu orfila i als meus gerents del banc Santander de la UIB, José Manuel Pellicer Martín i Toni Vidal Ferrer i als delegat de la mateixa agència Manuel Aguilera Fites i José Darder Puigserver per fer que les coses funcionin, pel vostre somriure, per facilitar un ambient agradable i acollidor a la UIB. Un especial agraïment a Gaspar Pizà Rosselló per tot el que m'ha ajudat amb la paperassa!

Obrigada Roberto, Suani, García e meu amigo Saulinho por sempre estarem presentes durante essa trajetória ajudando-me, e torcendo por mim!

Un especial Olé a todos flamencos de España y afueras. Muchos Cariños a mis amigos de la escuela flamenca La Carmeta con quienes pude compartir lindos momentos de puro arte y aprender el verdadero espirito flamenco! Un especial agradecimiento a mi maestra Carmeta y Diego Amaya, mis colegas Trini, Ica, Toni, Carmen y todos de la escuela! Muchas Gracias a José Luis Ponces, Concha, Henrique y Pilar, mis primeros maestros en la Isla del Centro de Danza Jose Luis Ponce donde he aprendido mucho y pude conocer a mis queridos amigos Dani "chichoman", la multiple Mar Forteza y Bea Vianden. A mi maestro de flamenco contemporáneo Felipe Clívio, gracias, eres un gran artista. Gracias a Alberto, Saray, Mari Paz, Miguel, Benjamin Habichuela por darme la oportunidad de bailar en los tablados de mallorca. I can't forget all those I could share flamenco experiences during my stays in Edinburgh, Edmonton and Leipzig, thanks to Jane Ogilvie, Kyla Sentes, Toshi Hayashi, Karrie Darichuk, Kin Macedo, Silvia Soto, Esperanza Santander, Marni Benavides, Susan MacGregor my flamenco friends in Edmonton, thanks to Saliha Haouachi, Bregje De Kok, Julie Ricci, Špela Ivekovič, Yashodha Govindar and Daniel Clark in Alba flamenca in Edinburgh and thanks to Irene Alvarez and to all friends in the Arrebato flamenco school in Leipzig.

And of course thanks to all people that contributed for my lovely

stays in Sant Etienne de Tinne, Leipzig, Edinburgh and Edmonton providing me a pleasant science environment, lunch times and many other things that I could learn and share with you. Regards to Andrei Akhmetzhanov, Sebastian Reyes, Jorge Mejias, Jorge Carballido, Marcelo Weber, Martjin Van Den Broek, Philip Altrock, Sten Rüdiger, Jean Luc, Mara Baudena, Katalin Kovacs, Bart Cleuren, Christian Wolff, John Robison, Bruno Escribano, Pan Li, Sabino Metta, Ignacio Peixoto, Raul Macias who I could share good experiences in south of France. A lots of kisses and hugs to my friends Isabel Martinez, Francisca Ana Soares dos Santos and Patricia Roser who I met in Leipzig. Haya! Antoine Tambue, Matthew England, Fei (Billy) Yu, Nneoma Ogbonna, Jennifer Reynolds, Yumn Suhaylah, Erengul Ozkok and Sule Sahin muy friends in Edinburgh. And in Canada, thanks Mark Lewis, Adriana Dawes, Gerda de Vries (who put me up in your beautiful house and mainly to be so nice and teaching me the art of patchwork) and Cecilia Hutchinson (a sweet and strong woman that I admire, thanks for the good moments we share together at the university, in Edmonton market and in your house). I miss you all.

I would like to record in closing my gratitude to those who have contributed directly to the realization of this work. A special thanks to my collaborators Josema Zaldivar, Sybille Dueri, Justin Calabrese, Volker Grimm, Andy White, Mike Boots and Herb Freedman for helping me in the text and giving me insightful suggestions. Thanks Abel Augusto Conceiçaão for supporting me in the fire and savanna knowledge, and thanks to all scientists that kindly gave me permission to use your beautiful pictures in this book, namely, Joel S. Levine, Claudius van de Vijver, Dan Bahauddin, Frank van Langevelde, Alain Ménesguen, Jean Yves Piriou, Alan McCormack, Alfonso Corzo and Marta Estrada.

I acknowledge support from the European Commission through the integrated project THRESHOLDS (contract 003933) and from MEC (Spain) and FEDER, through project FISICOS (FIS2007-60327) and from *Govern de les Illes Balears*.

And finally thank you for opening my PhD thesis I hope it can be useful for those are interested in Biological Physics, studies in dynamical

systems and ecological themes.

Preface

... what is needed is an altogether new instrument; one that shall envisage the units of a biological population as the established statistical mechanics envisage molecules, atoms and electrons; that shall deal with such average effects as population density, population pressure... These, in broad outline, are some of the principal land-marks in the territory ultimately to be covered by Physical Biology,

Elements of Physical Biology. Alfred J. Lotka

Last century saw an increasing application of the mathematical methodologies developed in the context of the Physical sciences (differential equation modeling, stability and control concepts, stochastic processes, etc.) to the understanding of biological processes. An early synthesis was provided by the book "Elements of Physical Bilology" authored by Alfred J. Lotka, in particular with results for population dynamics and energetics. The subject grew to a mature stage (see for example the textbook written by Murray, "Mathematical Biology") and the recent explosive increase in the availability of precise data from living systems has stressed again the need for quantitative approaches to the modeling of cells, organisms and ecosystems.

This work started in the scope of the"Thresholds of Environmental Sustainability" project (*http://www.thresholds-eu.org*) that was an integrated project in which the study of ecological discontinuities and thresholds effects as the consequence of human perturbations on ecological systems were the main related aspects. There I had the opportunity to work with two different streams, *Stream 2: Thresholds and points of no-return: thresholds definition, theory and identification* and *Stream 4: Thresholds and drivers of contaminants*.

Researchers in the Stream 4 developed several kinds of experiments and collected data from them. Specifically they performed a mesocosm experiment which had the main purpose to study effects of pyrene as a contaminant on a pelagic system including three trophic levels (algae, bacteria, zooplankton), under two nutrient conditions. Such a experiment was used to investigate direct and indirect effects of the contaminant on the studied species. Firstly my collaborators and I tried to propose models that could validate these experimental data, however our studies drove into a different path with a more general point of view, others in the group kept working in the original direction. Hence I could contribute with two different works studying regime shifts of marine ecosystems, not just considering the pyrenne case. One related to marine trophic chains affected by contaminants, changing differently the mortalities in each trophic level. And another work related to effects of eutrophication process in shallow marine ecosystems and competition between floating and submerged algae.

Then at the same perspective of the Threshold project and global change studies I drove my attention deeper inside to ecosystems that present complex behavior, discontinuities and non-linearities, i.e., systems that act through a number of motors, including climate change, desertification, land erosion, water shortage, eutrophication, pollution, biodiversity loss, succession, adaptation, natural disturbances, etc. Then I could develop different ecological models and show the versatility of a new kind of professional might be to carry out interdisciplinary projects. A professional who not only might dominate mathematical tools and bio-

logical knowledge but might have the insight to solve, interpret and make prediction to problems in nature. These are the qualities required in a professional that work in joint programs of different areas of knowledge and could be the major challenge scientists shall face in the 21st Century.

This thesis is divided in two parts. The first part is related to mathematical tools and modeling ideas used throughout the second part where the original contributions are presented. The main purpose of the first part is to introduce mathematical concepts with some illustrative examples and give the reader as many references as possible. This is maybe useful in order to help further students in preliminary studies and guide them in searching articles and books driving them deeper in the cited topics.

First Part

In the first chapter the concepts of dynamical systems are introduced and represented mathematically using differential equations language. Then, studies of fixed points and analysis of stability. Finally, in a non-rigorous way, bifurcation theory is introduced with some examples of codimension-one and codimension-two bifurcations. In the second chapter some classical and established models of biological growth and interactions of populations are depicted. Completing the tools required in the studies of Chapters 5 and 6.

Following the same logic, in the third chapter topics in discrete dynamical systems are shown. Starting with a historical perspective and the definition of cellular automata and followed by few concepts of percolation and critical phenomena theory used in Chapter 7.

And finally, closing the first part, the fourth chapter pursuits the main concepts and tools of adaptive dynamics. The definition of fitness, trade-off functions and techniques for the analysis of evolution through pairwise invadability plots (PIPs), i.e., theory used in Chapter 8 are introduced.

Second Part

The second part is divided in three chapters; one related with marine ecology, other related with tree patterns and fire in savannas and the last one is

about sex-dependent parasitism. Basically this constitutes the core of this thesis, where ecological models can be found what help the understanding of actual problems raised from interactions of natural instabilities and transformations of those ecosystems and human interventions.

Marine Ecology

Marine ecology is the study of marine organisms and their relationship with other organisms and with the surrounding environment, such as non-living, abiotic factors and living, biotic ones. Water, light, temperature, salinity, tides, currents, etc are some of the abiotic factors or physical, chemical and geological elements related to marine areas. The biotic factors comprises the interactions among living organisms. One aspect of such interactions can be described through food chains, food networks or trophic networks that describe the feeding interactions among species within an ecosystem. Food webs evolve complex networks of interactions in contrast with the simple linear pathway of the food chains. Biologists often model food web relationships in terms of the flow of solar energy, captured in photosynthesis by the phytoplankton (primary producers) and passed from organism to organism by means of feeding transfers.

Unfortunately the growing exploitation of bio-marine resources and the growing input of nutrients and contaminants due agricultural and industrial activities unbalance the correct functioning and equilibrium of such ecosystems and affects the economy of many coastal areas involving aquaculture, fishing and/or tourism. Because of this and many other reasons, interest and research activity in marine ecology are intensifying which leads to the increasing understanding of the complex interactions evolved in the marine ecosystems.

In the first work, presented in Chapter 5, we analyze the joint effect of contaminants and nutrient loading on population dynamics of marine food chains by means of bifurcation analysis. Contaminant toxicity is assumed to alter mortality of some species with a sigmoidal dose response relationship. A generic effect of pollutants is to delay transitions to complex dynamical states towards higher nutrient load values, but more counterintuitive consequences arising from indirect effects are described. In

particular, the top predator seems to be the species more affected by pollutants, even when contaminant is toxic only to lower trophic levels. This work lead to the publication Bacelar et al. (2009).

Pristine coastal shallow systems are usually dominated by extensive meadows of seagrass species, which are assumed to take advantage of nutrient supply from sediment. An increasing nutrient input is thought to favor phytoplankton, epiphytic microalgae, as well as opportunistic ephemeral macroalgae that coexist with seagrasses. The primary cause of shifts and succession in the macrophyte community is the increase of nutrient load to water; however, temperature plays also an important role. A competition model between rooted seagrass (Zostera marina), macroalgae (Ulva sp.), and phytoplankton has been developed in Chapter 6 to analyze the succession of primary producer communities in these systems. Successions of dominance states, with different resilience characteristics, are found when modifying the input of nutrients and the seasonal temperature and light intensity forcing. This chapter is related to the publication Zaldívar et al. (2009).

Patterns in Savannas

The term savanna describes ecosystems characterized by the coexistence between tree and grasses. The proportions of tree and grass can vary greatly. On the basis of general arguments(e.g. the competitive exclusion principle, see Hardin (1960)) pointing to the dominance of the fittest among competing species, one can ask about which mecanism allows this co-dominance of tree and grasses? Sarmiento (1984) formulated this argument as the ”savanna question”: *What is special about the savanna environment that allows trees and grasses to coexist, as opposed to the general pattern in other areas of the world where either one or the other functional type is dominant?* . Climate, fire, hydrology, herbivory, as well as soil nutrients, texture and depth are all important in determining the location of savanna. However recent studies have highlighted the importance of fire and tree competition for water, nutrients and light on savannas. In Chapter 7 we focused on a spatially explicit lattice model of savanna tree and grass population dynamics including these two factors.

This chapter is related to results in Bacelar et al. (2010)

Male Biased Parasitism

Males are often the “sicker” sex with male biased parasitism found in a taxonomically diverse range of species. There is considerable interest in the processes that could underlie the evolution of sex-biased parasitism. Mating system differences along with differences in lifespan may play a key role. We examine in Chapter 8 whether these factors are likely to lead to male-biased parasitism through natural selection taking into account the critical role that ecological feedbacks play in the evolution of defence. We use a host-parasite model with two-sexes and the techniques of adaptive dynamics to investigate how mating system and sexual differences in competitive ability and longevity can select for a bias in the rates of parasitism. Male-biased parasitism is selected for when males have a shorter average lifespan or when males are subject to greater competition for resources. Male-biased parasitism evolves as a consequence of sexual differences in life history that produce a greater proportion of susceptible females than males and therefore reduce the cost of avoiding parasitism in males. Different mating systems such as monogamy, polygyny or polyandry did not produce a bias in parasitism through these ecological feedbacks but may accentuate an existing bias. This chapter is related to results in Bacelar et al. (2011).

Bibliography

Bacelar, F. S., Calabrese, J. M., Hernández-García, E., 2010. Savanna-fire model: Combined effects of tree-tree establishment competition and spatially explicit fire on the spatial pattern of trees in savannas. Preprint submitted to Journal of Theoretical Biology.

Bacelar, F. S., Dueri, S., Hernández-García, E., Zaldívar, J.-M., 2009. Joint effects of nutrients and contaminants on the dynamics of a food chain in marine ecosystems. Mathematical Biosciences 218 (1), 24 – 32.

Bacelar, F. S., White, A., Boots, M., 2011. Life history and mating systems select for male biased parasitism mediated through natural selection and ecological feedbacks. Journal of Theoretical Biology 269 (1), 131 – 137.

Hardin, G., 1960. The Competitive Exclusion Principle. Science 131 (3409), 1292–1297.

Sarmiento, G., 1984. The ecology of Neotropical savannas. Harvard University Press, Cambridge.

Zaldívar, J., Bacelar, F., Dueri, S., Marinov, D., Viaroli, P., Hernández-García, E., 2009. Modeling approach to regime shifts of primary production in shallow coastal ecosystems. Ecological Modelling 220 (21), 3100 – 3110.

Part I

Introduction: General theory and Tools

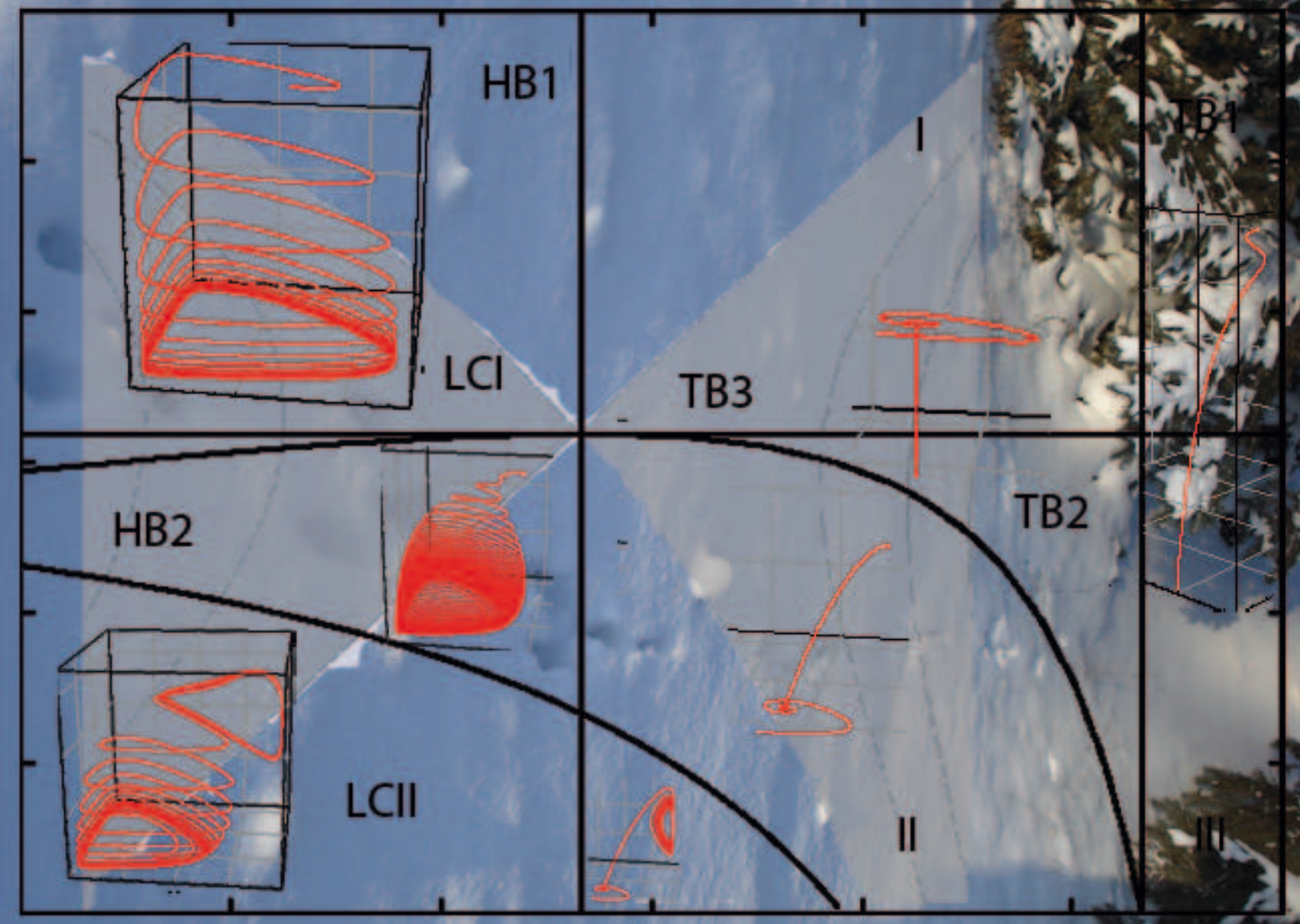
HB1
LCI
I
TB3
TB1
HB2
LCII
TB2
II
III

1

Biological Models

Things should be made as simple as possible, but not anymore simpler.
A. Einstein

In this chapter some examples of the simplest biological models will be briefly presented. They still are used to model dynamics of diverse phenomena, such as the various manifestations of populations, social and economic systems and biological organisms. And some of them are used in the chapters 5, 6 and 8 of second part of this thesis.

1.1 Models of growth

Growth is a fundamental property of biological systems, occurring at the level of populations, individual animals and plants, as well as within organisms. Even in technology, growth curves are used to forecast technological performance fitting a set of data and extrapolating the growth curve beyond the range of the data. Much research has been devoted to modeling growth processes, and there are many ways of doing this, including: mechanistic models, time series, stochastic differential equations, etc.

1.1.1 Exponential growth: Malthus Model

The Malthusian growth model, sometimes called the **exponential law of population growth**, (Malthus, 1798), describes "*if a population will grow*

(or decline) exponentially as long as the environment experienced by all individuals in the population remains constant", (Turchin, 2001). The derivation of a exponential law could be given considering all individuals in the population absolutely identical (in particular, there is no age, sex, size, or genetic structure) and they reproduce continuously. In this way the number of individuals can only change as a result of birth, death, emigration, and immigration. Malthus considered a closed population, without immigration nor emigration, in this approach, the population growth equation can be written as following:

$$\frac{dN}{dt} = (b-d)N \quad \Rightarrow \quad N(t) = N_0 e^{(b-d)t} \tag{1.1}$$

where b and d are the birth and death positive rates. If $b > d$ the population grows exponentially, if $b < d$ the population becomes extinct. Exponential growth is only realistic as long as there appears to be no limits to growth. Many systems appear to grow in this fashion for the initial periods until some capacity constraint begins to take place.

1.1.2 Gompertz curve

A model that takes into account capacity constraints is Gompertz's law. In 1825 Gompertz published "On the Nature of the Function Expressive of the Law of Human Mortality", in which he showed that "*if the average exhaustions of a man's power to avoid death were such that at the end of equal infinitely small intervals of time, he lost equal portions of his remaining power to oppose destruction*", (Winsor, 1932), then the number of survivors at any age t would be given by the equation:

$$N(t) = ke^{-be^{-ct}} \tag{1.2}$$

where k is the upper asymptote, i.e, the number of individuals in equilibrium, c is the intrinsic growth rate and b, c are positive numbers. Differentiating and taking the logarithm of the **Gompertz equation** (1.2) results

the following equations:

$$\begin{aligned} \frac{dN}{dt} &= kcbe^{-ct}e^{-be^{-ct}} = kcN(t)be^{-ct} \\ ln(N) &= ln(k)+ln(e^{-be^{-ct}}) = ln(k)-be^{-ct} \Rightarrow be^{-ct} = ln(k)-ln(N) \end{aligned}$$

combining these two results the Gompertz differential equation becomes:

$$\frac{dN}{dt} = kcN\left(ln(k)-ln(N)\right) \tag{1.3}$$

In other words this model states that, under a given number of individuals, the rate of population increase is positively proportional to the natural logarithm of the number of individuals in equilibrium divided by the given number of individuals. This model was initially used only by actuaries, but recently it has been used as a growth curve in biological and economic phenomena, mobile phone uptake and Internet, (Chow, 1967), population in a confined space and modeling of growth of tumors, (Durbin et al., 1967).

1.1.3 The Pearl-Verhulst logistic equation

Taking the Malthus model and adding a function that describes the concentration of nutrients, C, to limit the production of organisms into the dynamic equations, the following system results:

$$\frac{dN}{dt} = bCN \tag{1.4}$$

$$\frac{dC}{dt} = -\alpha bCN \tag{1.5}$$

Performing $\alpha\frac{dN}{dt}+\frac{dC}{dt}$ it is obtained: $\frac{d}{dt}(C-\alpha N)=0$, thus $(C+\alpha N)(t) = constant = C_0$. In this way $C = C_0-\alpha N$, substituting this expression in (1.4) and performing some algebraic calculation it results into a single equation called the **logistic equation**:

$$\frac{dN}{dt} = r\left(1-\frac{N}{K}\right)N \tag{1.6}$$

where the expression $r(1-\frac{N}{K})$ is called an intrinsic growth-speed and K is the carrying capacity, the maximum number of individuals that the environment can support. The logistic equation can be integrated exactly, hence the development of a population, which at initial time $t=0$ has the size N_0, is:

$$N(t) = \frac{K}{1+\frac{K-N_0}{N_0}e^{-rt}} \tag{1.7}$$

This equation initially developed for studies of demography by Verhuslt (1838), was rediscovered by Pearl and Reed (1920) , who promoted its wide and indiscriminate use.

1.1.4 The chemostat equation

The chemostat is an apparatus in which the growth of microorganisms can be controlled. Basically the system is formed by a nutrient reservoir and a growth chamber, in which the microorganisms reproduce. The name chemostat stands for **chem**ical environment is **stat**ic what means that "*the purpose of the chemostat is to have a quasi-constat microorganism concentration, N, and nutrient concentration, C, allowing a constant rate of harvest*", (Stranndberg, 2003).

Adjusting the equations (1.4) and (1.5), substituting bC in Eq. (1.4) for $K(C) = K_{max}\frac{C}{K_n+C}$, a Holling type II (see section 1.2.2), and introducing the inflow and outflow of nutrients from the reservoir and outflow of harvested microorganisms the following system is obtained:

$$\frac{dN}{dt} = K(C)N - \frac{F}{V}N \tag{1.8}$$

$$\frac{dC}{dt} = -\alpha K(C)N - \frac{F}{V}C + \frac{F}{V}C_0 \tag{1.9}$$

Where $\frac{F}{V}N$ represents flow of the harvested microorganisms, $-\frac{F}{V}C$ corresponds to the outflow and $\frac{F}{V}C$ to the inflow of nutrition. The microorganisms can not reproduce indefinitely because they are not in a chamber

of infinite concentration, the function $K(C)$ is the reproduction-rate with upper limit K_{max} and K_n is the concentration at which $K = \frac{1}{2}K_{max}$.

There are still more growth equations discussed in the literature, for instance, by Savageau (1980) , and in the articles therein. Each data described by growth equations requires different processes to be considered, in this way many specialized growth equations can be proposed in order to describe different aspects on the dynamics related to the growth. However there are enormous number of examples that are described by these basic growth equations mentioned before and some of these will be used in later chapters of this thesis.

1.2 Interacting populations models

1.2.1 Lotka-volterra model

In 1925 Alfred Lotka explained deeply the purpose of the new area called **physical biology**, which consists on the application of physical principles in the study of life-bearing systems as a whole in contrast with **biophysics** that treats the physics of individual life processes. Among some examples employed in this area he proposed a model to describe chemical reactions in which the concentrations oscillates, (Lotka, 1920). Some years hence, using the same equations, different studies were carried out by Volterra (1926). The main purpose of his work was to describe the observed variations in some species of fish in the Upper Adriatic sea. The system of equations proposed by Lotka and Volterra describes the change of prey or host density with time, and

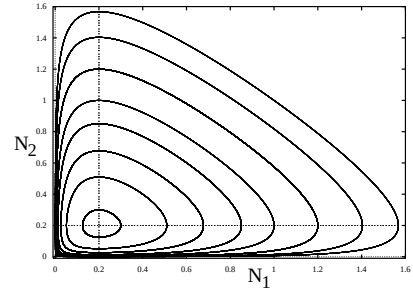

FIGURE 1.1. LOTKA-VOLTERRA PREDATOR−PREY: THE PURELY PERIODIC SOLUTIONS.

assumed, for this purpose, that the number attacked per predator was directly proportional to prey density. This model became known as **Lotka-volterra predator-prey equations**:

$$\frac{dN_1}{dt} = r_1 N_1 - \alpha N_1 N_2 \tag{1.10}$$

$$\frac{dN_2}{dt} = \delta\alpha N_1 N_2 - d_2 N_2 \tag{1.11}$$

Where N_1 is the density of prey, N_2 is the density of predator, r_1 is growth rate of prey, d_2 is the mortality rate of predator, α is the predation rate coefficient and δ is the reproduction rate of predators per 1 prey eaten (predation efficiency). This model generates **neutral stability**, see Figure 1.2.1 , but the "*assumptions are very unrealistic since very few components are included, there are no explicit lags or spatial elements, and thresholds, limits, and nonlinearity are missing*", (Holling, 1973).

The rate at which prey are taken by predators is known as the **functional response**, depending on the behavior of both the predator and the prey. A remarkable variety of functions has been proposed to characterize the functional response. In the classical Lotka-Volterra model this rate is the product αN_1 in Eq. (1.10), other functional responses are going to be shown in the next subsection. **Numerical response** is defined in different ways, however, the numerical response is usually modeled as a simple multiple of the functional response, so the numerical response assumes the same shape as the functional response like $\delta\alpha N_1$ in Eq. (1.11).

competition

Competition among two species means that the increase in one of the populations decreases the net growth rate of the second one, and vice versa. This happens when they feed on the same resources, or if they produce substances (toxins) that are toxic for the other species. A classical competition model was also introduced in Volterra (1926), and considered in a more general parameter range by Lotka (1932). It is known as the

competitive Lotka-Volterra system:

$$\begin{aligned} \frac{dN_1}{dt} &= N_1(r_1 - a_{11}N_1 - a_{12}N_2) \\ \frac{dN_2}{dt} &= N_2(r_2 - a_{21}N_1 - a_{22}N_2) \end{aligned} \tag{1.12}$$

where N_1 and N_2 are the densities of the two competing organisms. Taking $r_1, r_2 > 0$, so that each species reaches a non-vanishing stable equilibrium (at r_1/a_{11} and at r_2/a_{22}) in the absence of the other. a_{11} and a_{22} are the coefficients of intraspecific competition. The presence of one species decreases the growth of the other if $a_{12} > 0$ and $a_{21} > 0$. Symbiosis and mutualism can also be represented by taking negative interspecific competition coefficients.

1.2.2 Holling types of predation

One improvement of the predator-prey Lotka-Volterra model is to add the logistic growth of prey and besides change the type of predation, functional response, into a more realistic form. Holling in his article "The functional Response of Predators to Prey Density and its Role in Mimicry and Population Regulation", (Holling, 1965), reviewed previous papers, (Holling, 1959a,b), and analyzed a series of data of invertebrates and vertebrates species. Basically he presented three different types of predation functional responses, P, Holling types:

- Type I: Linear, the number of prey consumed per predator is assumed to be directly proportional to prey density until a saturation value after which it remains constant, so initially the fuctional response is the same used in the Lotka-Volterra model until saturation. This functional response is found in passive predators like spiders.

$$\begin{aligned} P &= \alpha N_1 N_2, \quad if\ N_1 < N_T \\ P &= \alpha N_T N_2, \quad if\ N_1 > N_T \end{aligned} \tag{1.13}$$

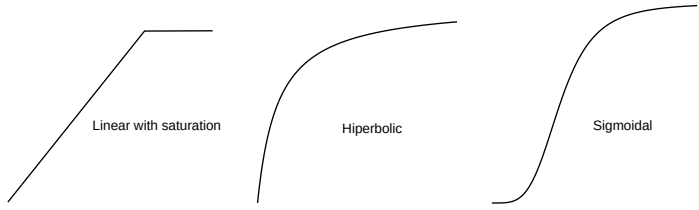

Figure 1.2: Holling Types. (a) Type I, (b) Type II, (c) Type III.

- Type II: hyperbolic functional response in which the attack rate increases at a decreasing rate with prey density until it becomes constant at satiation. This response is typical of predators that specialize on one or a few prey.

$$P = \alpha \frac{N_1}{h + N_1} N_2 \tag{1.14}$$

- Type III: S-Shape or Sigmoidal, this functional response occurs in predators which increase their search activity with increasing prey density showing a initial S-shaped rise up to a constant maximum consumption.

$$P = \alpha \frac{N_1^2}{h^2 + N_1^2} N_2 \tag{1.15}$$

α represents the rate of successful search (predation rate coefficient) and h is the half saturation of the function, see Figure 1.2. Basically in these three types only two variables affecting predation were considered, prey and predator density. They were considered by Holling in his article of 1959 to be the only essential ones, against other characteristics that were considered not to be essential, such as characteristics of the prey (e.g., reactions to predators, stimulus detected by predator, etc), density and quality of alternate foods available for the predator and characteristics of the predator (e.g., food preferences, efficiency of attack, etc). When such complex interactions are present, it is difficult to understand clearly the

principles involved in predation. In this instance a simplified situation was taken into account where some of the variables are constant or not operating.

Without more explanations it is worth citing other sort of predations functional responses in the literature:

- Gause (1934) in his book " The struggle for existence" , proposed a model that explained the behavior of predator-prey system embodied by Didiniurn-Paramecium. For large density of predator, N_2, its mortality is negligible for positive values of prey density, $N_1 > 0$. In addition, the increase of predator only slightly depends on N_1. To reduce the dependence upon N_1 the term N_1, used in the Lotka-volterra model, was substituted by $\sqrt{N_1}$ in the predation functional response.

$$P = \alpha N_1^{\frac{1}{2}} N_2 \tag{1.16}$$

- Rosenzweig generalized the expression proposed by Gause taking N_1 to the gth power $0 < g \leqslant 1$, (Rosenzweig, 1971).

$$P = \alpha N_1^g N_2, \quad 0 < g \leqslant 1 \tag{1.17}$$

- Watt proposed another non-linear connection between the relative increase of the predator and the number of prey, (Watt, 1959).

$$P = \alpha(1 - e^{-aN_1})N_2 \tag{1.18}$$

1.2.3 Rosenzweig: Paradox of Enrichment

"*Instability should often be the result of nutritional enrichment in two-species interactions*", (Rosenzweig, 1971). Rosenzweig showed for six different predator-prey models that increasing the food supply in the system can lead to destruction of the food species that are wanted in greater abundance. The enrichment was taken increasing the prey carrying capacity and he showed that for a threshold value the steady state is destroyed

while a limit cycle rises. This process was called the **paradox of enrichment**.

1.2.4 Kolmogorov general model

Kolmogorov in 1936 studied predator-prey models of the general form:

$$\begin{aligned} \frac{dN_1}{dt} &= N_1 \quad g(N_1, N_2) \\ \frac{dN_2}{dt} &= N_2 \quad h(N_1, N_2) \end{aligned} \tag{1.19}$$

where g en h are continuous functions of N_1 and N_2, with continuous first derivatives. This model was reviewed by May (1972) , who proved that limit cycle behavior is implicit in essentially all conventional predator-prey models. This model requires density dependence or resource-limitation effects at least for the prey population in contrast with the original Lotka-Volterra model which invokes exponential population growth. These sort of nonlinear two-dimensional equations possess either a stable equilibrium point or a stable limit cycle, a fact that can be guaranteed by the **Poincaré-Bendixson theorem**, (May, 1972). In three and higher dimensional systems, (Monteiro, 2006), there are two more possible attractors such as tori , (Nishiuchi et al., 2006) and strange attractors.

For more detailed information in ecological models see the books Gurney and Nisbet (1998), Murray (2002, 2003) and Neufeld and Hernández-García (2009).

Bibliography

Chow, G. C., 1967. Technological change and the demand for computers. The American Economic Review 57 (5), 1117–1130.

Durbin, P. W., Jeung, N., Williams, M. H., Arnold, J. S., 1967. Construction of a growth curve for mammary tumors of the rat. Cancer Research 27, 1341–1347.

Gause, G. F., 1934. The Struggle for Existence. Williams and Wilkins, Baltimore.

Gompertz, B., 1825. On the nature of the function expressive of the law of human mortality, and on a new mode of determining the value of life contingencies. Philosophical Transactions of the Royal Society of London 115, 513–585.

Gurney, W. S. C., Nisbet, R. M., 1998. Ecological Dynamics. Oxford University Press, New York, Oxford.

Holling, C. S., 1959a. The components of predation as revealed by a study of small-mammal predation of the european pine sawfly. The Canadian Entomologist 91 (7), 293–320.

Holling, C. S., 1959b. Some characteristics of simple types of predation and parasitism. The Canadian Entomologist 91 (7), 385–398.

Holling, C. S., 1965. The functional response of predators to prey density and its role in mimicry and population regulation. Memoir of the Entomological Society of Canada 45, 1–60.

Holling, C. S., 1973. Resilience and stability of ecological systems. Annual Re-

view of Ecologly and Systematics 4, 1–23.

Lotka, A., 1932. The growth of mixed populations: two species competing for a common food supply. J. Wash. Acad. Sci. 22, 461–469.

Lotka, A. J., 1920. Undamped oscillations derived from the law of mass action. Journal of the American Chemical Society 42 (8), 1595–1599.

Lotka, A. J., 1925. Elements of physical biology. Williams and Wilkins, Baltimore.

Malthus, T. R., 1798. An Essay On The Principle Of Population as it Affects The Future Improvement of Society. J. Johnson, London.

May, R. M., 1972. Limit cycles in predator-prey communities. Science 177, 900–902.

Monteiro, L. H. A., 2006. Systemas Dinâmicos. Editora Livraria da Física, São Paulo.

Murray, J. D., 2002. Mathematical Biology. I. An introduction, 3rd Edition. Vol. 17 of Interdisciplinary Applied Mathematics. Springer-Verlag, New York, Berlin, Heidelberg.

Murray, J. D., 2003. Mathematical Biology. II: Spatial Models and Biomedical Applications, 3rd Edition. Vol. 18 of Interdisciplinary Applied Mathematics. Springer-Verlag, US.

Neufeld, Z., Hernández-García, E., 2009. Chemical and Biological Processes in Fluid Flows: A Dynamical Systems Approach. Imperial College press.

Nishiuchi, Y., Ueta, T., Kawakami, H., 2006. Stable torus and its bifurcation phenomena in a simple three-dimensional autonomous circuit. Chaos, Solitons and Fractals 27, 941 – 951.

Pearl, R., Reed, L. J., 1920. On the rate of growth of the population of the united states since 1790 and its mathematical representation. Proceedings of the National Academy of Sciences 6 (6), 275 – 288.

Rosenzweig, M. L., 1971. Paradox of enrichment: destabilization of exploitation ecosystems in ecological time. Science 171, 385–387.

Savageau, M. A., 1980. Growth equations: A general equation and a survey of special cases. Math. Biosci. 48, 267–278.

Stranndberg, P. E., 2003. The chemostat. Tech. rep., Univeristy of Linköping, Sweden.

Turchin, P., 2001. Does population ecology have general laws? Oikos 94, 17–26.

Verhuslt, P. F., 1838. Notice sur la loi que la population suit dans son accroissement. Correpondance mathematique et Physique 10, 112–121.

Volterra, V., 1926. Fluctuations in the abundance of a species considered mathematically. Nature 118, 558–60.

Watt, K. E. F., 1959. A mathematical model for the effect of densities of attacked and attacking species on the number attacked. Canadian Entomologist 91, 129–144.

Winsor, C. P., 1932. The Gompertz curve as a growth curve. Proceedings of the national academy of sciences 18 (1), 1–8.

2

Dynamical systems: Stability and Bifurcation analysis

Science is built up with facts, as a house is with stones. But a collection of facts is no more a science than a heap of stones is a house.

La Science et l'hypothèse. Poincaré

The previous chapter presented some examples of biological models. In this chapter will be presented characteristics and some mathematical analysis of dynamical systems, tool required in chapters 5, 6 and 8 of second part of this thesis. Some explanations of continuation programs used to solve numerically some results shown in chapter 5 are in appendix A.

A system can be defined by a set of interacting elements, in such way there are cause and effect relations in the phenomena that occur to the elements of this set. In a dynamical system some characteristics of the interacting elements change over time. From the Calculus invented by Newton and independently reinvented by Leibniz it is known that the variation of an object (characteristic) $x(t)$ in a continuous time is measured by the derivative $\frac{dx(t)}{dt}$. In this sense the system evolution in time can be described mathematically by [1]:

$$\dot{\vec{x}} = \vec{f}(\vec{x}, \beta) \tag{2.1}$$

[1] $\dot{\vec{x}} = \frac{d\vec{x}(t)}{dt}$

Where $\vec{f}$ is the variation rate of the **state variables**, $\vec{x}$, and β is a parameter of the system. When $\vec{f}$ does not depend on time explicitly the system is called **autonomous**. Certain values, $\lim_{t\to\infty}\vec{x}(t) = \vec{x}^*$ with $\vec{f}(\vec{x}^*) = 0$, do not change over time, depicting a **stationary solution** of Eq. (2.1), in other words they correspond stagnation (fixed) points of the flow. These **equilibrium** points or fixed points of a system can be classified according with their stability and the topology of their **phase portrait**[2]

2.1 Stability of fixed points

According to Lyapunov, stability is a property of system behavior in neighborhoods of equilibria. When the initial conditions, $\vec{x}(0)$, fit in with a equilibrium point the system remains indefinitely in this point. However, when the initial conditions are inside a sphere of radius δ whose center is a specific equilibrium, $\vec{x}^*$, it can be defined as **asymptotically stable** when all the trajectories, $\vec{x(t)}$, converge to $\vec{x}^*$. If this sphere has a finite radius this point is **locally sable**, otherwise when $\delta \to \infty$ the point is **globally stable**. In both cases the equilibrium point is classified as a **stationary attractor** and all the set of initial conditions that converge to this point form the **basin of attraction** of this attractor.

An equilibrium point is **neutrally stable** when for a sphere of radius δ centered in such point there is another sphere with radius ε also centered in $\vec{x}^*$, with $\delta < \varepsilon$, such that every trajectory with initial condition inside the sphere of radius δ remains in the second sphere of radius ε for al $t \geq 0$. Hence $\vec{x}(t)$ does not tend to $\vec{x}^*$ when $t \to \infty$. When there is at least one trajectory with initial condition belonged to a sphere of radius δ that leaves the sphere of radius ε in a finite time the equilibrium is called **unstable**.

[2]Phase portrait, phase space or phase diagram: a plot of the system's trajectories in the state space in which the axes are the state variables. In mechanical systems the phase space usually consists of all possible values of position and momentum(or speed) variables.

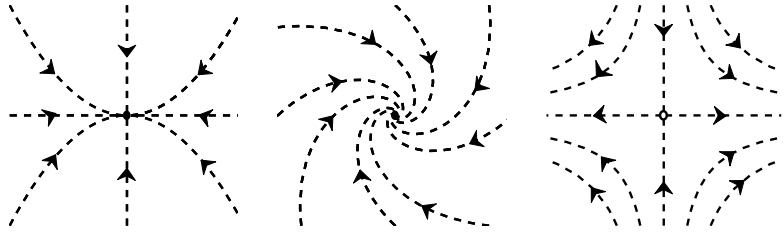

(a) **(b)** **(c)**

Figure 2.1. Fixed points in two dimensions. (a) Stable Node, (b) Stable Spiral, (c) Saddle Point. The equations that have been used are: (a) $\dot{x} = -0.5x$, $\dot{y} = -y$, (b) $\dot{x} = -x+y, \dot{y} = -x-y$, (c) $\dot{x} = x, \dot{y} = -y$.

All this classification is based on the temporal evolution of the distance between a trajectory $\vec{x}(t)$ and $\vec{x}^*$, for the complicated systems modeled by Eq. (2.1) that scientists study, explicit solutions for $\vec{x}(t)$ are rarely available. In consequence of this difficulty Lyapunov (1892), developed a method for assessing the conditions of stability indirectly. This method involves linearizing $\vec{f}$ at $\vec{x}^*$, let **J** be the jacobian matrix of $\vec{f}$ evaluated at $\vec{x}^*$.

$$\mathbf{J} = \frac{\partial \vec{f}(\vec{x}, \beta)}{\partial \vec{x}}\Big|_{\vec{x}=\vec{x}^*} \tag{2.2}$$

The **eigenvalues** of **J** determine whether $\vec{x}^*$ is stable. These are scalar values λ_i such that [3] $det(\mathbf{J} - \lambda_i \mathbf{I}) = 0$, i.e. the roots of the characteristic polynomial of **J**. In this way, if the eigenvalues are all distinct, it is possible to write a exponential combination as the for general solution of the linearized system,

$$\dot{\vec{x}} = \mathbf{J}\,\vec{x} \tag{2.3}$$

by

$$\vec{x}(t) = k_1 \vec{v}_{01} e^{\lambda_1 t} + k_2 \vec{v}_{02} e^{\lambda_2 t} + \ldots + k_n \vec{v}_{0n} e^{\lambda_n t} \tag{2.4}$$

where n is the dimension of the system, k_i are the arbitrary constants that are given by the initial conditions and the vectors $\vec{v}_{0j}$ are the

[3] **I** is the identity Matrix.

eigenvectors associated with each eigenvalue and are determined by:

$$\mathbf{J}\vec{v_{0i}} = \lambda_i \vec{v_{0i}}, \qquad (i = 1, 2, ..., n) \tag{2.5}$$

Sometimes the Jacobian matrix presents equal real eigenvalues, in this case **multiplicity**[4] of the eigenvalues has to be taken into account in order to generate linearly independent solutions. For example if a two-dimensional system has two equal eigenvalues ($\lambda_1 = \lambda_2 = \lambda$) a general solution for this **degenerate case** is:

$$\vec{x}(t) = k_1 \vec{v}_{01} e^{\lambda t} + k_2 \vec{v}_{02} t e^{\lambda t} \tag{2.6}$$

In a n-dimensional case for eigenvalues with multiplicity m the associated functions are $e^{\lambda_i t}$, $te^{\lambda_i t}$, $t^2 e^{\lambda_i t}$, ..., $t^{m-1} e^{\lambda_i t}$, thus, in the same way as for distinct eigenvalues, the general solution is the linear combination of these functions and the arbitrary constants are determined by the initial conditions.

In two dimensions, according to Poincaré, the fixed points can be classified from the trace $\mathbf{T}$ and the determinant $\mathbf{\Delta}$ of the $\mathbf{J}$ matrix:

- if $\mathbf{\Delta} < 0$, $\lambda_{1,2}$ are real and of opposite signs. The fixed point is called **saddle point** which is unstable in the sense of Lyapunov;
- if $\mathbf{\Delta} > 0$ and $\mathbf{T}^2 - 4\mathbf{\Delta} > 0$, $\lambda_{1,2}$ are real and with the same sign. If $\mathbf{T} > 0$ the point is called a **unstable node**, if $\mathbf{T} < 0$ it will be a **stable node**.
- if $\mathbf{\Delta} > 0$ and $\mathbf{T}^2 - 4\mathbf{\Delta} < 0$, $\lambda_{1,2}$ are complex conjugated. If $\mathbf{T} > 0$ the fixed point is an **unstable spiral**, if $\mathbf{T} < 0$ it is an asymptotic **stable spiral** and if $\mathbf{T} = 0$ the point is a neutrally stable **center**, where the eigenvalues are purely imaginary.

[4] The number of equal eigenvalues. If the multiplicity of an eigenvalue is 2, there are two eigenvalues of this same value. If is 3 there are three eigenvalues with this same value and so on.

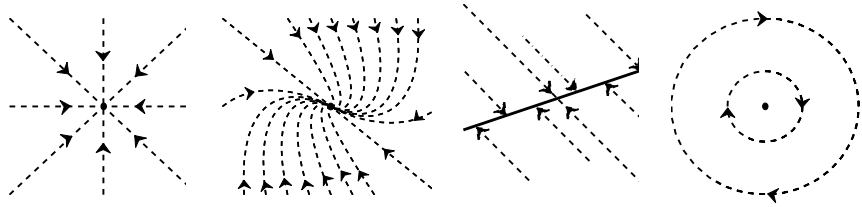

(a) **(b)** **(c)** **(d)**

Figure 2.2. Two dimensional degenerate cases of fixed points . (a) Star Node, (b) Degenerate Node, (c) Line of fixed points, (d) Center. The equations that have been used are: (a) $\dot{x} = -x, \dot{y} = -y$, (b) $\dot{x} = -x + y, \dot{y} = -x - 3y$, (c) $\dot{x} = -x + 3y$, $\dot{y} = x - 3y$, (d) $\dot{x} = y, \dot{y} = -x$.

On the line $\mathbf{T}^2 - 4\mathbf{\Delta} = 0$ are lying the **star points** and **degenerate nodes** which are cases where the system presents two equal eigenvalues. In the case of star points, only the main diagonal of **J** is different of zero with equal elements, hence the solutions are straight lines passing through x^* in the phase space. If the elements of the diagonal are positive the star is unstable, if the elements of the diagonal are negative the star is asymptotically stable. When $\mathbf{T}^2 = 4\mathbf{\Delta}$ there is a degenerate node that is stable when $\mathbf{T} < 0$ and unstable when $\mathbf{T} > 0$. If $\mathbf{\Delta} = 0$, at least one of the eigenvalues is zero and in this case there is a whole **line** or a **plane of fixed points**. Figure 2.1 shows some of the different mentioned types of fixed points and Figure 2.2 depicts the degenerate cases . Hirsch and Smale (1974, Chapter 9), give a detailed discussion of stability of fixed points as well as Strogatz (2000, Chapter 5).

Observing the form of the solution (2.4) it can be seen that it converges to stable solution when $Re\lambda_i < 0$ and diverges when at least one eigenvalue λ_i is positive. All the above refers to the phase portrait of the linearized system (2.3). But in the degenerate cases such as center, star, degenerate node and non-isolated fixed points, the linear system does not guaranty a correct picture of the phase portrait near the fixed point, degenerate points can be altered by small nonlinear terms. In such cases stability must be determined considering non-linear terms of the Taylor

series of $\vec{f}(\vec{x},\beta)$, (Andronov et al., 1973, Strogatz, 2000).

As mentioned before the stability of a equilibrium point is established by the sign of the real part of its eigenvalues. Therefore to determine the stability of this solution, taking into account that a fixed point is stable when $Re(\lambda_i) < 0$ for all i, is only necessary to know if the signs of the real parts of λ_i are negative or not. Edward John Routh and Adolf Hurwitz found independently the solution to find out whether all the roots of a polynomial have a negative real part. This criterion of stability known as **Routh-Hurwitz theorem** is very helpful specially when the characteristic polynomial for the eigenvalues of the Jacobian **J** is of order higher than five and it is in general impossible to calculate analytically its roots. The theorem says that the real part of all roots of the polynomial:

$$\lambda^n + a_1\lambda^{n-1} + a_2\lambda^{n-2} + ... + a_{n-1}\lambda + a_n = 0 \tag{2.7}$$

are negative if all the coefficients a_i are positive and if all upper-left determinants $\Delta_i(i = 1,...,n)$ of the Hurwitz matrix **H** are positive. If the jacobian matrix **J** is $n \times n$ so is **H**. The **H** matrix is made in the following way:

- The coefficients a_i with odd indices and increasing j are written in the first line . In the second line are written the coefficients with even indices and increasing j. Notice that the coefficient of λ^n, a_0, is 1. the other positions are filled up with zeros.

- The two following lines are obtained moving the first two lines one column to the right, filling-in the empty positions with zeros.

- The other lines are built repeating the procedure above until a_n occupies the lower right edge of the matrix.

In this way, for example, for $n = 6$ the Hurwitz matrix is:

$$\mathbf{H} = \begin{pmatrix} a_1 & a_3 & a_5 & 0 & 0 & 0 \\ 1 & a_2 & a_4 & a_6 & 0 & 0 \\ 0 & a_1 & a_3 & a_5 & 0 & 0 \\ 0 & 1 & a_2 & a_4 & a_6 & 0 \\ 0 & 0 & a_1 & a_3 & a_5 & 0 \\ 0 & 0 & 1 & a_2 & a_4 & a_6 \end{pmatrix}$$

and the upper-left determinants $\Delta_i (i = 1, ..., n)$ are:

$$\Delta_1 = |a_1| \, , \Delta_2 = \begin{vmatrix} a_1 & a_3 \\ 1 & a_2 \end{vmatrix} , \Delta_3 = \begin{vmatrix} a_1 & a_3 & a_5 \\ 1 & a_2 & a_4 \\ 0 & a_1 & a_3 \end{vmatrix} , \ldots , \Delta_6 = |\mathbf{H}|$$

In this section it was shown how different sorts of fixed points and their stability characterize the topology of the phase space, see Figures 2.1 and 2.2. When the phase portrait of a dynamical system changes qualitatively its topology as parameters pass through critical values the system suffers a bifurcation that will be explained in the next section.

2.2 Bifurcation analysis

The term bifurcation was introduced by Poincaré (1885) and it is strongly linked to the concept of **structural stability**. In a bifurcation fixed points can be created or destroyed, or their stability can change when varying parameters. When the dynamical system does not change quality of the flow in the phase space under small perturbations of the **control parameter** the system is structurally stable. In two-dimensional systems there is a theorem that states the necessary conditions for which the system is structurally stable, it is the known **Peixoto's theorem**, see (Peixoto, 1962).

In this section the four **local bifurcations** that occur in continuous dynamical systems will be presented: saddle-node bifurcation, transcritical bifurcation, pitchfork bifurcation and Hopf bifurcation. Then the

global bifurcations homoclinic and heteroclinic will be presented. Local bifurcations are those which can be previewed studying the vectorial field in the neighborhood of a fixed point or a closed trajectory. Normally this study is made by through the eigenvalues. Global bifurcations are those which can not be established by a local analysis.

First the **normal forms**[5] of the simplest equilibria bifurcations of codimension one will be depicted. An example of a codimension-two bifurcation will be presented in the ending of this chapter and although this work is not focused on chaos behavior, there are some regions in the bifurcation diagram of the studied system that present chaotic behavior and because of this a period doubling cascade routing to chaos will be briefly explained.

2.2.1 Codimension-one local bifurcations

Codimension counts the number of control parameters for which fine tuning is necessary to get such a bifurcation, i.e. the smallest dimension of a parameter space which contains the bifurcation in a persistent way. Four local bifurcations can occur varying the values of a unique parameter. The normal form of saddle-node, transcritical and pitchfork bifurcations are given in one-dimensional systems whereas a two-dimensional system is needed for a Hopf bifurcation.

Definition 2.2.1. A dynamical system (2.1) is said to undergo a bifurcation at parameter value $\beta = \beta_0$ if in any (small) neighborhood of $\beta_0 \in \mathbb{R}^m$ there is a β value containing dynamics that are not topologically equivalent to those at β_0.

[5] A normal form of a mathematical object is a simplified form of the object obtained by applying a transformation (often a change of coordinates) that is considered to preserve the essential features of the object.

Saddle-node bifurcation

A saddle-node bifurcation is a local bifurcation in which two fixed points coalesce into a single point that represents a bifurcation point and then this point disappears. The normal form of this bifurcation can be represented in a one-dimensional equation:

$$\dot{x} = \beta - x^2 \tag{2.8}$$

This equation[6] presents two equilibria, for $\dot{x} = 0$, $x^* = \pm\sqrt{\beta}$. When

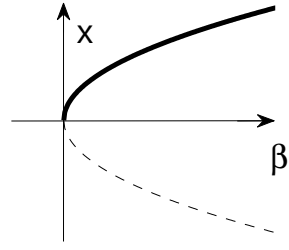

Figure 2.3. Bifurcation diagram: Saddle-node Bifurcation. The thick line is the stable solution and the dashed line is the unstable one.

$\beta < 0$ there is no equilibria, when $\beta > 0$ there are two equilibria. Then $\beta = 0$ depicts the transition in the change of flow topology in the phase space, $\beta = 0$ is the bifurcation point, β_0. A way to analyze graphically bifurcations is through the bifurcation diagram, see Figure 2.3. But in order to visualize better this bifurcation a two-dimensional equation was also plotted, see Figure2.4. In this case it expresses the collision of a stable equilibrium (node) with a unstable one (saddle).

Transcritical bifurcation

In the transcritical bifurcation, fixed points are not destroyed nor created, but for a critical value of the parameter they switch stability. The normal

[6] $\dot{x} = \beta + x^2$ is also possible as a normal form of a saddle-node bifurcation.

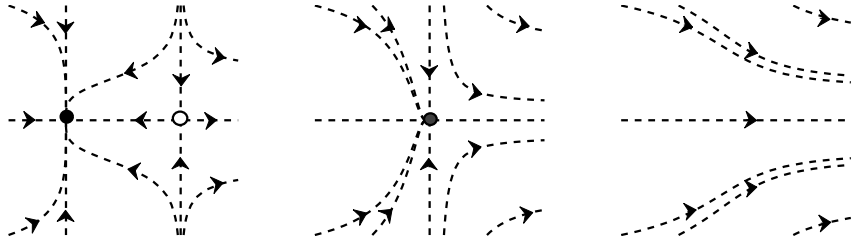

(a) **(b)** **(c)**

Figure 2.4. Phase space in two dimensions showing a saddle-node bifurcation. (a) $\beta < 0$, (b) $\beta = 0$, (c) $\beta > 0$. The equation that has been used is: (a) $\dot{x} = \beta + x^2$, $\dot{y} = -y$.

form of this bifurcation can be:

$$\dot{x} = \beta x - x^2 \tag{2.9}$$

Observe that this equation[7] presents two equilibria, $x^* = 0$ and $x^* = \beta$ and

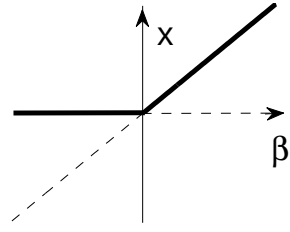

Figure 2.5: Bifurcation diagram: Transcritical Bifurcation

the eigenvalue is given by $\lambda = \beta - 2x^*$. Therefore the fixed point $x^* = 0$ has the eigenvalue $\lambda = \beta$ and the fixed point $x^* = \beta$ has the eigenvalue $\lambda = -\beta$ hence in the bifurcation point $\beta_0 = 0$ these point change stability, see Figure 2.5.

[7] $\dot{x} = \beta x + x^2$ is also possible as a normal form of a Trancritical bifurcation.

Pitchfork bifurcation

A pitchfork bifurcation occurs generically in systems with inversion or reflection symmetry. That is, an equation of motion that remains unchanged if one changes the sign of all phase space variables (or at least for one). This bifurcation has two types: supercritical or subcritical. The normal form of the supercritical pitchfork bifurcation is:

$$\dot{x} = \beta x - x^3 \tag{2.10}$$

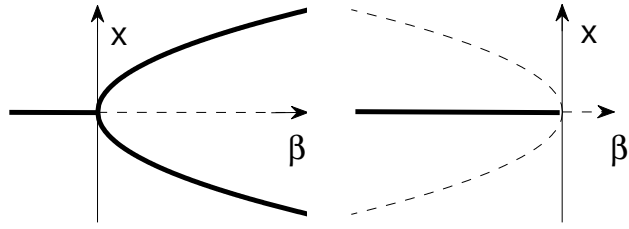

(a) **(b)**

Figure 2.6. Bifurcation diagram: Pitchfork bifurcation . (a) Supercritical, (b) Subcritical.

When $\beta < 0$ there is a stable equilibrium $x^* = 0$ at point $\beta = 0$ this point changes stability and two other equilibria $x^* = \pm\sqrt{\beta}$ appear with the same stability, in this case both are stable. And the normal form for the subcritical case is:

$$\dot{x} = \beta x + x^3 \tag{2.11}$$

In this case, for $\beta < 0$ the equilibrium at $x^* = 0$ is stable, and there are two unstable equilibria at $x^* = \pm\sqrt{-\beta}$. For $\beta > 0$ the equilibrium at $x^* = 0$ is unstable.

Hopf bifurcation

In 1942, E. F. F. Hopf established the conditions in which such bifurcation could occur in a n-dimensional system, (Hopf, 1942). This bi-

furcation was originally studied by Poincaré (1892) and studied by Andronov (1929) for two-dimensional systems. Because of this sometimes this bifurcation is called Poincaré-Andronov-Hopf bifurcation. A Hopf or Poincaré-Andronov-Hopf bifurcation is a local bifurcation in which a **limit cycle**[8] arises from an equilibrium in dynamical system, when the equilibrium changes stability via a pair of purely imaginary eigenvalues. Like in the Pitchfork bifurcation the Hopf bifurcation has two types: supercritical or subcritical. To obtain this sort of bifurcation minimally a two-dimensional system is demanded. A normal form of Hopf bifurcation could be:

$$\begin{aligned} \dot{x} &= \beta x - y + \sigma x(x^2+y^2), \\ \dot{y} &= x + \beta y + \sigma y(x^2+y^2) \end{aligned} \tag{2.12}$$

This system presents a unique fixed point, the origin ($x^* = 0$, $y^* = 0$). The eigenvalues are $\pm i + \beta$ hence the origin is asymptotically stable for $\beta < 0$ and unstable for $\beta > 0$. For $\beta = 0$ the origin changes stability, if $\sigma = -1$ a **stable limit cycle** arises in the $\beta > 0$ region and in this case the bifurcation is **supercritical**. If $\sigma = 1$ while the origin is stable for $\beta < 0$ there is a presence of a **unstable limit cycle** that collapses in the transition of stability of the origin, in this case the bifurcation is **subcritical**. All these facts can be better viewed in the polar coordinates, changing $x =$

[8] A **limit cycle** is an isolated closed trajectory that can appear in the phase portrait of nonlinear systems. An isolated trajectory means absence of other closed trajectories infinitely close. Therefore the neighboring trajectories must approach or move away from the limit cycle which is a **periodic attractor** or **repeller**. A limit cycle is asymptotically stable when the neighboring trajectories approach the limit cycle otherwise it is unstable. It is important to differentiate limit cycles from closed trajectories surrounding center points. In the last case the closed trajectories are not isolated and there could be several of them infinitely close for close initial conditions. In addition the amplitude, the period and the shape of a limit cycle are determined by the parameters of a nonlinear system while the shape, period and amplitude of closed trajectories surrounding centers depend on the initial conditions.

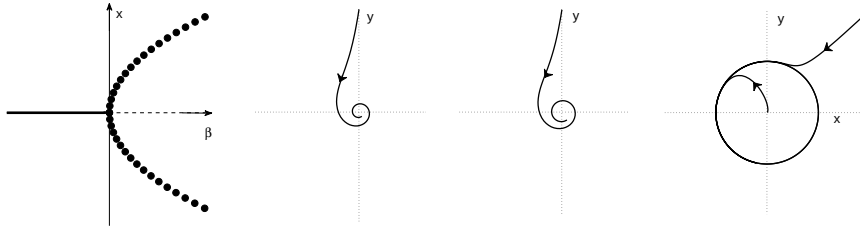

(a) **(b)** **(c)** **(d)**

Figure 2.7. Supercritical Hopf bifurcation ($\sigma = -1$). (a)Bifurcation diagram. Phase space (b) $\beta < 0$, (c) $\beta = 0$, (d) $\beta > 0$.

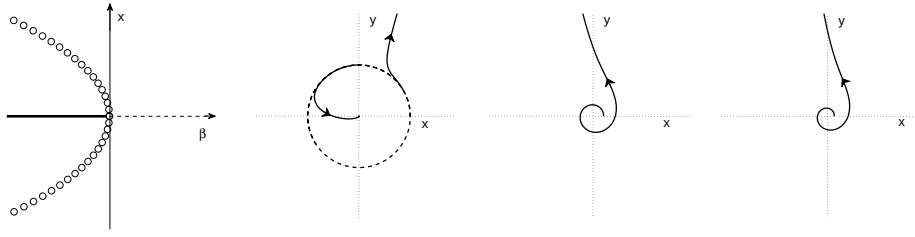

(a) **(b)** **(c)** **(d)**

Figure 2.8. Subcritical Hopf bifurcation ($\sigma = 1$). (a)Bifurcation diagram. Phase space (b) $\beta < 0$, (c) $\beta = 0$, (d) $\beta > 0$.

$r\cos\theta$ and $y = r\sin\theta$ the system becomes:

$$\begin{aligned} \dot{r} &= h(r) = \beta r + \sigma r^3, \\ \dot{\theta} &= 1 \end{aligned} \tag{2.13}$$

For $\dot{r} = 0$ there are two possibilities, the origin $r^* = 0$ and a cycle with radius $r^* = \sqrt{\frac{-\beta}{\sigma}}$, as stated before when $\sigma = -1$ the eigenvalue in polar coordinates is $\lambda = \frac{dh}{dr}\Big|_{r^*} = \beta - 3(r^*)^2$, analyzing the cycle, for $\beta > 0$, $\lambda = -2\beta$ and hence the limit cycle is stable. If $\sigma = 1$ the eigenvalue is $\lambda = \beta + 3r^2$, for $\beta < 0$, $\lambda = 4\beta$ and hence the limit cycle is unstable. See

Figures 2.7 and 2.8.

2.2.2 Codimension-one global bifurcations

Global bifurcations can not be previewed by eigenvalues of fixed points, however in 1963 V. D. Melnikov developed a method by which is possible to prove the existence of homoclinic and heteroclinic bifurcations in Hamiltonian perturbed systems, see (Melnikov, 1963). In this subsection the homoclinc and heteroclinic bifurcations will be presented briefly .

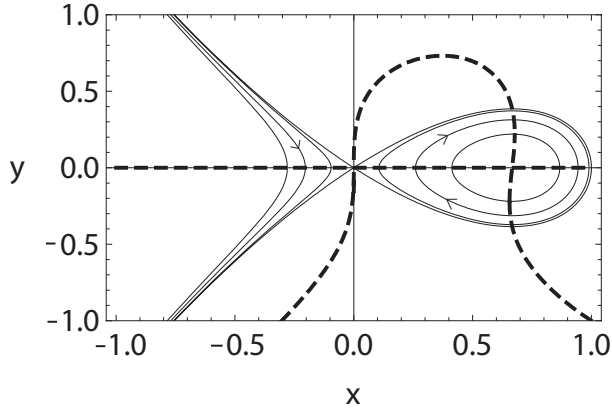

Figure 2.9. Phase space: Homoclinic bifurcation. The limit cycle get close to the saddle point (0,0) when increasing β. The dashed lines are the nullclines for $\beta = -0.1$ and the solid lines are the trajectories ($x^3 - x^2 + y^2 = \beta$) for the increasing values of β, $\beta = -0.1$, $\beta = -0.05$, $\beta = -0.01$ and finally $\beta = 0$ that represents the homoclinic orbit.

Homoclinic Bifurcation

A point is called a **homoclinic point** when it lays down in a trajectory that is, at the same time, a stable and unstable manifold of a saddle point, this trajectory is a **homoclinic orbit**[9]. A bifurcation that leads to a destruction

[9]Homoclinic trajectory or homoclinic loop

of a of a homoclinic orbit is a **homoclinic bifurcation** . As an example, the following system proposed by Hale and Koçak (1991), presents a homoclinic bifurcation:

$$\begin{aligned} \dot{x} &= 2y \\ \dot{y} &= 2x - 3x^2 - y(x^3 - x^2 + y^2 - \beta) \end{aligned} \tag{2.14}$$

This system presents two fixed points, observe the intersection of the **nullclines**[10] in Figure 2.9. The origin $(x^* = 0, y^* = 0)$ and the point $(x^* = \frac{2}{3}, y^* = 0)$ are the fixed points of this system. The origin is always a saddle point with eigenvalues $\lambda_i = \frac{1}{2}\left(\beta \pm \sqrt{\beta^2 + 16}\right)$ independently of the values of β. But the point ($\frac{2}{3}$, 0) changes stability when β varies, and its eigenvalue is $\lambda_i = \frac{1}{54}\left(27\beta + 4 \pm \sqrt{729\beta^2 + 216\beta - 11648}\right)$. Observe that at $\beta^* = -\frac{4}{27}$ the system suffers a supercritical Hopf bifurcation before which this point is a stable spiral, and than it converts into a unstable spiral. For $-\frac{4}{27} < \beta < 0$ one can see the presence of an orbitally asymptotically periodic orbit, alias limit cycle and at $\beta^* = 0$ the periodic orbit is absorbed by a homoclinic loop, i.e, a homoclinic bifurcation happens, see Figures 2.9 and 2.10, in this case for $\beta > 0$ the homoclinic orbit is destroyed.

Heteroclinic Bifurcation

When the unstable manifold of a steady point becomes the stable manifold of another steady point, thus connecting two steady points, then the system presents a heteroclinic connection, alias **heteroclinic cycle**. A **Heteroclinic bifurcation** happens when the steady points connection is broken. Observe the following system proposed by Hale and Koçak

[10] Nullclines or Zero-Growth isoclines of a two-dimensional dynamical system are the boundary between regions where $\dot{x}$ or $\dot{y}$ switch signs. In this way setting either $\dot{x} = 0$ or $\dot{y} = 0$ the nullclines of the system will be found. The intersections between x and y nullclines are the equilibrium points.

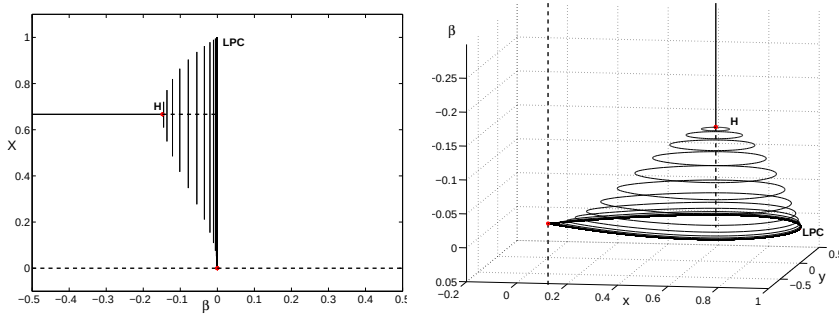

(a) **(b)**

Figure 2.10. Bifurcation diagram: Homoclinic Bifurcation . (a) 2D Bifurcation diagram, (b) 3D Bifurcation diagram. The dashed lines are unstable solutions and thick lines the stable ones.

(1991):

$$\begin{aligned} \dot{x} &= \beta + 2xy \\ \dot{y} &= 1 + x^2 - y^2 \end{aligned} \tag{2.15}$$

In Figure 2.11 depicts the phase portrait for three different values of the parameter. At $\beta = 0$ the system presents two fixed points, $(0,1)$ and $(0,-1)$, both of which are saddle points. The orbit in the y-axis between the two points has the stable manifold of $(0,1)$ and the unstable manifold of $(0,-1)$ thus the system has a heteroclinic orbit for $\beta = 0$. For $\beta \neq 0$ the saddle connection is broken hence a heteroclinic bifurcation happens.

2.2.3 Codimension-two bifurcations

As mentioned before the number of control parameters necessary to get a bifurcation determined the codimension of this bifurcation. Therefore when two control parameters are necessary to get a bifurcation, such a bifurcation is told to be codimension two. There are several sorts of codimension two bifurcations, such as Bautin, Bogdanov-Takens, Cusp, Fold-

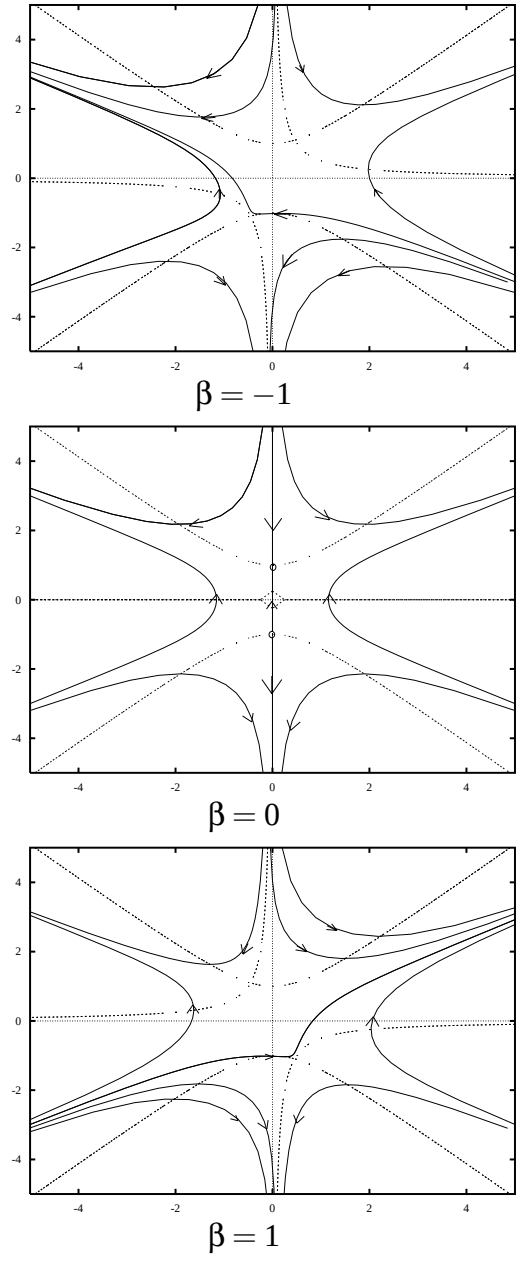

Figure 2.11. Phase space: Heteroclinic Bifurcation. Dashed lines are the nullclines and thick lines are some trajectories.

Holpf and Hopf-Hopf bifurcations. As an example observe the system that was studied by Takens (1974) and Bogdanov (1975) ,:

$$\begin{aligned} \dot{x} &= y \\ \dot{y} &= \beta_1 + \beta_2 x - x^2 + xy \end{aligned} \tag{2.16}$$

When $\beta_1 > 0$ there is no equilibrium. For $\beta_1 = 0$ and $\beta_2 = 0$ the origin is the unique equilibrium and its two eigenvalues are zero. For $\beta_1 < 0$ there are two equilibria: $(\sqrt{-\beta_1}, 0)$ and $(-\sqrt{-\beta_1}, 0)$. In this way $\beta_1 = 0$ is a saddle-node bifurcation point. The first fixed point is a saddle with eigenvalues:

$$\lambda_{1,2} = \frac{1}{2}\left(\beta_2 - \sqrt{-\beta_1} \pm \sqrt{\beta_2^2 - 2\sqrt{-\beta_1}\beta_2 - \beta_1 + 8\sqrt{-\beta_1}}\right) \tag{2.17}$$

the second one has the eigenvalues:

$$\lambda_{1,2} = \frac{1}{2}\left(\beta_2 + \sqrt{-\beta_1} \pm \sqrt{\beta_2^2 + 2\sqrt{-\beta_1}\beta_2 - \beta_1 - 8\sqrt{-\beta_1}}\right) \tag{2.18}$$

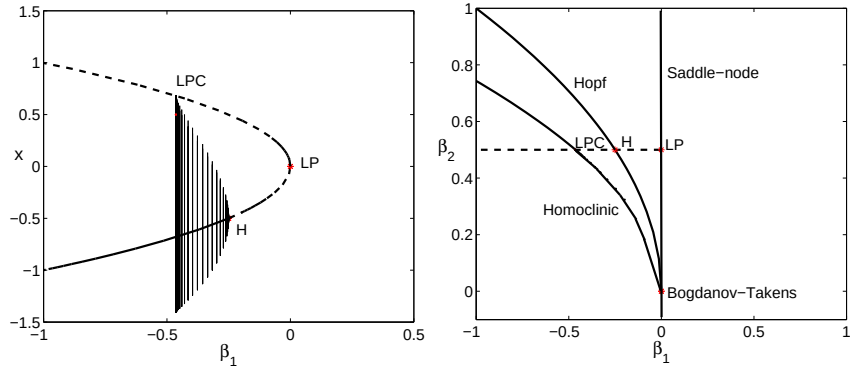

(a) **(b)**

Figure 2.12. Bogdanov-Takens Bifurcation. The first graph is the bifurcation diagram for $\beta_2 = 0.5$. The second one is the two-parameter bifurcation diagram.

For $\beta_2 < -\sqrt{-\beta_1}$ this point is asymptotically stable and unstable for $\beta_2 > -\sqrt{-\beta_1}$. And observing the eigenvalues of the second point

one can see that a subcritical Hopf bifurcation happens at $\beta_2 = -\sqrt{-\beta_1}$, the decreasing β_1 from this value a limit cycles arises. Decreasing further more the value of β_1 the cycle is destroyed into a homoclinic bifurcation when it merges with the saddle point, see Figure 2.12(a). In the two-parameter graph in Figure 2.12(b), it can be seen that a Bogdanov-Takens bifurcation happens. The origin of the parameter plane, coincides with the origin in the cartesian plane and, as mentioned before, this point has two zero eigenvalues and corresponds to the critical value of the **Bogdanov-Takens bifurcation**. Three codimension-one bifurcations occur nearby: a saddle-node bifurcation, a Poincaré-Andronov-Hopf bifurcation and a homoclinic bifurcation.

2.2.4 Period Doubling Cascade and Chaos

Differently to the previous bifurcations a **period doubling** bifurcation or **flip** bifurcation is a local bifurcation related to cycles and has no correspondence for equilibria in continuous systems. In this bifurcation a cycle loses its stability, while another cycle with twice the period of the original cycle rises. If the secondary path is stable the bifurcation is **supercritical** (subtle), conversely, when the secondary path is unstable the bifurcation is **subcritical** (catastrophic). This bifurcation requires at least a three-dimensional phase space and a supercritical period doubling cascade converges to chaotic behavior. This can be seen in the following example.

Rössler equations

Rössler proposed the following system in 1976:

$$\begin{aligned} \dot{x} &= -y - z \\ \dot{y} &= x + ay \\ \dot{z} &= b + z(x - c) \end{aligned} \tag{2.19}$$

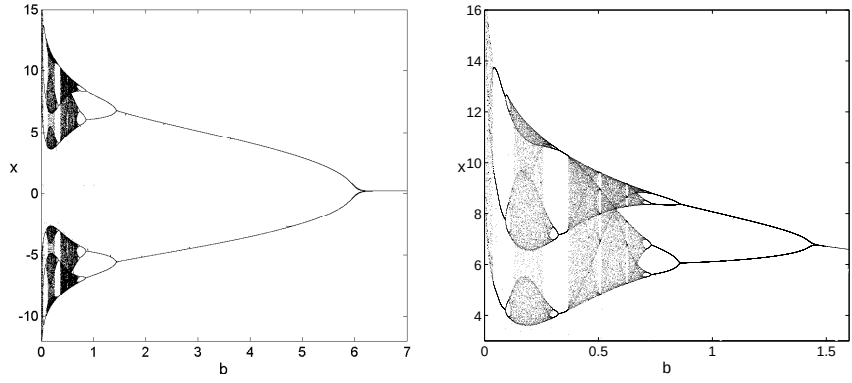

Figure 2.13. Period Doubling Cascade and Chaos for Rössler system, varying the b parameter and fixing $a = 0.2$ and $c = 5.7$. The first picture depicts the complete bifurcation diagram, where line between $b = 5.99$ and $b = 7$ is the fixed point that bifurcates in a Hopf bifurcation at b value, 5.99. The other lines represent the maximum and minimum of the cycles. The second picture shows the higher sequence of bifurcations amplified.

It is minimal for continuous chaos for at least three reasons: Its phase space has the minimal dimension three, its nonlinearity is minimal because there is a single quadratic term, and it generates a **chaotic attractor**[11] with a single lobe, in contrast to the Lorenz attractor which has two lobes, (Lorenz, 1963).

This system presents stationary, periodic and chaotic attractors depending on the value of the parameters (a, b, c). The Figure 2.13 shows the sequence of bifurcations for certain range of parameters, in the first plot a complete bifurcation scenario is plotted, observe that there is a stable fixed point that converts into unstable via a Hopf bifurcation at b value

[11] Also called Strange Attractors , (Ruelle and Takens, 1971). Actually, in many texts in the literature, the word strange is related to the geometrical structure of attractor, strange attractors are fractals and demonstrate infinite self similarity, while the word chaotic refers to the dynamics of orbits on the attractor. The attractor that will be shown here is a strange chaotic attractor, but it is important to bear in mind, although it will not be shown in this thesis, the existence of **strange nonchaotic attractors**, (Romeiras and Ott, 1987).

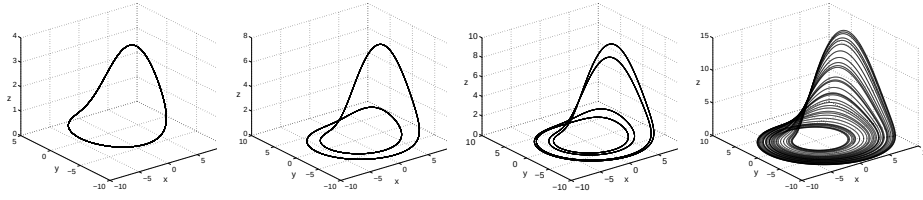

(a) **(b)** **(c)** **(d)**

Figure 2.14. Rössler Phase Space: (a) $b = 2.0$, (b) $b = 1.0$, (c) $b = 0.8$, (d) $b = 0.4$. fixed $a = 0.2$ and $c = 5.7$.

of 5.99 then the stable cycle loses stability through a period doubling bifurcation $b = 1.43$. Another period doubling happen at 0.85 and then at 0.73. Afterwards a cascade of supercritical bifurcations occurs leading to a chaotic attractor, see the last picture of Figure 2.14. More information can be also found in the book of Thompson and Stewart (2002, Chapter 12).

The theory of dynamical systems is not an innovation and excellent books have already been published in this issue, specially it's worth citing Strogatz (2000), Hale and Koçak (1991), Thompson and Stewart (2002), Gugenheimer and Holmes (1993) and Monteiro (2006, in Portuguese). The purpose of this chapter was a quick review and a summary of dynamical systems theory. The graphs were drawn using a MATLAB package for numerical bifurcation analysis of ODEs (Matcont), (Dhooge et al., 2003), XPPAUT, (Doedel et al., 1997, Ermentrout, 2002) and my own program codes, see appendix A.

Bibliography

Andronov, A. A., 1929. Les cycles limites de poincaré et la théorie des oscillations auto-entretenues, , , vol. , pp. . Comptes Rendus de l'Académie des Sciences de Paris 189, 559–561.

Andronov, A. A., Leontovich, E. A., Gordon, I. I., Maier, A. G., 1973. Qualitative Theory of Second-Order Dynamic Systems. Wiley, New York.

Bogdanov, R. I., 1975. Versal deformations of a singular point on the plane in the case of zero eigenvalues. Func. Anal. Appl. 9, 144–145.

Dhooge, A., Govaerts, W., Kuznetsov, Y., 2003. Matcont: A matlab package for numerical bifurcation analysis of odes. ACM Trans. Math. Software 29, 141 – 164.

Doedel, E., Champneys, A., Fairgrieve, T., Kuznetsov, Y., Sandstede, B., Wang, X., 1997. Auto 97: continuation and bifurcation software for ordinary differential equations. Technical report, Concordia University, Montreal, Canada.

Ermentrout, B., 2002. Simulating, Analyzing, and Animating Dynamical Systems: A Guide to Xppaut for Researchers and Students (Software, Environments, Tools). SIAM: Society for Industrial and Applied Mathematical.

Gugenheimer, J., Holmes, P., 1993. Nonlinear oscillations, dynamical systems and bifurcations of vector fields. Vol. 42. Applied mathematical sciences, Springer-Verlag, New York Inc.

Hale, J. K., Koçak, H., 1991. Dynamics and bifurcations. Springer-Verlag, New York.

Hirsch, M. W., Smale, S., 1974. Differential equations, dynamical systems, and linear algebra. Academic Press, New York.

Hopf, E. F. F., 1942. Abzweigung einer periodischen losung van einer stationaren losung eines differential- systems. Berichte der Mathematisc- Physikalischen Konoglich-Sachsischen Academie der Wissenschaften Leipzig, 94, 1–22.

Lorenz, E. N., 1963. Determinisctic nonperiodic flow. Journal of the Atmosferic Sciences 20, 130–141.

Lyapunov, A., 1892. The General Problem of the Stability of Motion. Taylor and Francis, London.

Melnikov, V., 1963. On the stability of the center for timeperiodic perturbations. Tr. Moscow Math. Soc. 12, 3–52.

Monteiro, L. H. A., 2006. Systemas Dinâmicos. Editora Livraria da Física, São Paulo.

Peixoto, M., 1962. Structural stability on two-dimensional manifolds. Topology 1, 101–120.

Poincaré, H., 1885. Sur l'équilibre d'une masse fluide animée d'un mouvement de rotation. Acta Mathematica 7, 259–380.

Poincaré, H., 1892. Les méthodes nouvelles de la mécanique céleste. Gauthier-Villars, Paris.

Romeiras, F. J., Ott, E., 1987. Strange nonchaotic attranctors of the damped pendulum with quasiperiodic forcing. Physical Review A 35 (10), 4404–4413.

Rössler, O., 1976a. An equation for continuous chaos. Physical Letters A 57, 397–398.

Ruelle, D. P., Takens, F., 1971. On the nature of turbulence. Communications of Mathematical Physics 20, 167–192.

Strogatz, S. H., 2000. Nonlinear dynamics and chaos: With applications to physics, biology, chemistry, and engineering. Perseus Books group, Cambridge, Massachusetts.

Takens, F., 1974. Singularities of vector fields. Pub. Math. IHES 43, 47–100.

Thompson, J., Stewart, H., 2002. Nonlinear Dynamics and Chaos, 2nd Edition. John Wiley and Sons, Chichester, UK.

3

Cellular Automata

The sciences do not try to explain, they hardly even try to interpret, they mainly make models. By a model is meant a mathematical construct which, with the addition of certain verbal interpretations describes observed phenomena. The justification of such a mathematical construct is solely and precisely that it is expected to work.

John von Neumann

It is known in the history of science that new areas of basic science are developed from the appearance of new technologies. For example, telescope technology was what led to modern astronomy, microscope technology led to modern biology and at the same way computer technology has led to what Wolfram called in his book the new kind of science, (Wolfram, 2002), the era of cellular automata ,which together with simulations and other individual based modeling started since then. At the beginning the standard intuition in traditional science, more focused in equation-based methods or top-down approaches, showed no interest in the agent/individual-based modeling, a bottom-up approach, thinking that the results in this kind of modeling wouldn't be interesting...

However since the release of Conways Game of Life (Gardner, 1970), cellular automata have been developed and progressively used to model a great variety of dynamical systems in different application domains such as physical and spatial sciences, biology, mathematics and computer science, image processing (Rosin, 2006, 2010) and as well as in the social sciences.

Historically CA were first defined and studied in the 1950's by John

Von Neumann and Stanislaw Ulam as ideal structures for modeling self-reproducing "machines", (Von Neumann, 1951, Von Neumann and Burks, 1966), in 1970, the mathematician Jon Conway proposed his now famous Game of Life published by Martin Gardner in the mathematical games column in Scientific American (Gardner, 1970). In 1980's systematic studies were pioneered by Wolfram in a family of one-dimensional cellular automata rules . Many interesting behaviors encountered in continuous systems are seen in such discrete dynamical systems, as seen for example in (Wolfram, 2002). In the following sections the basic theory used in the studied model in chapter 7 is presented.

3.1 Definition

Cellular automata (CA) are an idealization of physical/dynamical systems in which space and time are discrete, and physical quantities (state variables) take only a finite set of values. Basically it consists of a grid of cells/sites (lattice), where each cell's value (state) is updated in discrete time steps according to a **transition rule** (or **updating rule**). The transition rules of a CA can be deterministic or, in a more general case, probabilistic and there are several ways to implement them. These implementations are an essential part of the definition of a model, since they generally produce different transients, stationary states and averages of physical quantities. There are three basic ways of implementing the update rules which are common for practical purposes like in computer simulations. They are called parallel, sequential and random sequential update.

3.1.1 Updating rules

The **deterministic** updating rules can be seen as functions which can be linear or nonlinear whose argument is the state at time t of itself and the neighboring cells, and whose value is the next state of the considered cell at time $t+1$. In **probabilistic** or **stochastic** CA, local rules may have a

probabilistic element to them; rather than dictating the state of an updated cell (Coe et al., 2008, Domany, 1984, Grassberger et al., 1984, Lebowitz et al., 1990, Szabó and Borsos, 2002).

In the models defined in terms of **parallel updating** rules, the state of every cell in the model is updated together, before any of the new states influence other cells and it can be performed synchronously (Burstedde et al., 2001, Wang et al., 1999). Implementations of **synchronous updating** can be analyzed in two phases. The first, interaction, calculates the new state of each cell based on the neighborhood and the update rule. State values are held in a temporary store. The second phase updates state values by copying the new states to the cells.

In contrast, **asynchronous updating** does not necessarily separate these two phases: in the simplest case (fully asynchronous updating), changes in state are implemented immediately in such a way that the new state of a cell affects the calculation of states in neighboring cells. The two most common asynchronous updating implementation are the **sequential** and **random sequential** update. In the first, also known as **ordered asynchronous** updating, includes any process in which the updating of individual states follows a systematic pattern (Cornforth et al., 2005). In the second, also known as **random asynchronous** updating, at each time step, a cell is chosen at random with replacement (Braun et al., 1998, Cornforth et al., 2005).

3.1.2 Neighborhoods

The two most commonly used neighborhood types in a two dimensional square lattice are the Von Neumann and Moore neighborhood. The **Von Neumann neighborhood** consists of four adjacent cells orthogonally surrounding a central cell on a two-dimensional square lattice. They are also called by physicists as “nearest neighbors sites”. The **Moore neigh-**

borhood[1] comprises the eight cells surrounding a central cell on a two-dimensional square lattice, the four of Von Neumann's one and the four diagonal neighbors which touch at one corner only, called by physicists the "next nearest neighbors". It was the neighborhood used by John Conway's "Game of Life" (Gardner, 1970). These neighborhoods can be expanded, and the number of cells are given by $(2r+1)^2$ and $2r(r+1)+1$ respectively, where r is the range of the neighborhood ($r = 0, 1, 2, 3, \ldots$). In Figure 3.1 Von Neumann and Moore neighborhood can be seen for ranges 1 and 2.

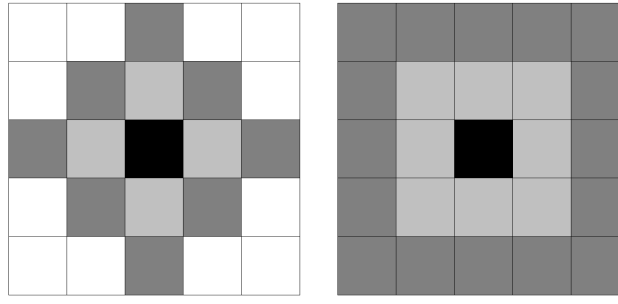

Figure 3.1. Most common square lattice neighborhoods: (a) Von Neumann and (b) Moore neighborhoods. Black represents the analyzed central cell, light gray the neighborhood in the range 1 and dark gray together with light gray represent the neighborhood in range 2.

The simplest implementation of a CA is a one-dimensional array of cells (possibly two way infinite). Many examples of one-dimensional CA can be find in the Wolfram's book "A new kind of science" (Wolfram, 2002). The most used in literature are the two-dimensional CA, normally representing a square lattice. However other sort of geometrical structures can been found in the literature such as hexagonal/honeycomb lattice (Domany, 1984) and triangular lattice (Kong and Cohen, 1991).

[1]This neighborhood takes its name from Edward Forrest Moore, the inventor of the Moore finite state machine (Moore, 1956)

In Figure 3.2 the most common neighborhood in a hexagonal lattice and triangular lattice can be seen.

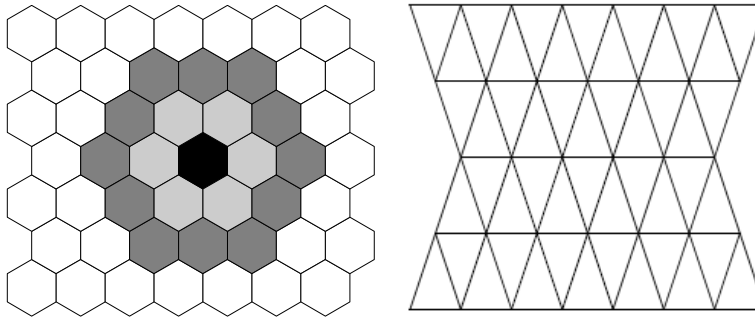

Figure 3.2: (a) Hexagonal lattice neighborhoods. (b) Scheme of a triangular lattice.

3.1.3 Dynamics and Boundary conditions

The dynamics begins with an initial condition that is known by the initial configuration of the cellular automaton and may be given or randomly generated. In the systematic studies performed by Wolfram (1984), he showed that starting from random initial conditions, order can emerge or even the system can became more and more complex and indeed sometimes the produced behavior appears completely random. The different structures (attractors) generated by cellular automata evolution were grouped in four basic behavior classes : **Class 1**: Independently of the initial state the output generated are lead to exactly the same uniform final state, analogous to **fixed point**. **Class 2**: There are many different possible final states, but all of them consist just of a certain set of simple structures that either remain the same forever or repeat every few steps, analogous to **limit cycle**. **Class 3**: A more complicated behavior is reached and seems in many aspects random, although triangles and other small-scale structures are seen always at some level (**fractals**), analogous to **Chaotic ("strange") attractors** . **Class 4**: Involves a mixture of order

and randomness: localized structures are produced and interact with each other in very complicated ways. See the snapshots of the different final configurations of each class in Figure 3.3.

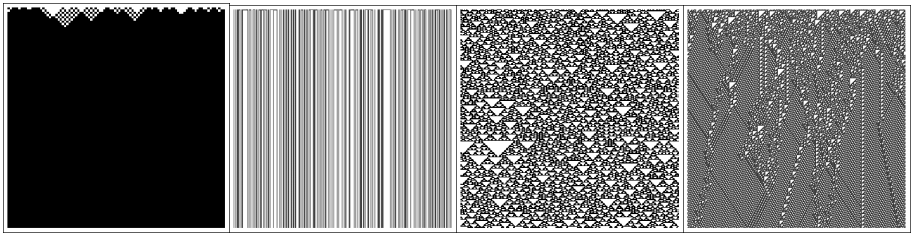

Figure 3.3. Examples of the four basic classes of behavior seen in the evolution of one-dimensional cellular automata from random initial conditions (Wolfram, 2002) and periodic boundary conditions. These figures were generated with Wolfram *Mathematica* program with the code $ArrayPlot[CellularAutomaton[rule,"Initialconditions",t]]$ for 250, 108, 126 and 110 rules respectively, representing class 1 to class 4.

In thereby a CA could consist of an infinite grid of cells, however for practical reasons and computer memory limitations, CA are often simulated on a finite grid rather than an infinite one. One issued problem is how to handle the cells on the edges. For that, many different boundary conditions arose for different problems modeled. For example **open boundary conditions** can be found for example in a vehicular traffic models (Kai Nagel and Michael Schreckenberg, 1992), pedestrian dynamics models (Burstedde et al., 2001) and others (Rajewsky and Schreckenberg, 1997). In this kind of boundary condition the elements of the model (pedestrians, cars, etc.) are introduced/eliminated through the edges. **Fixed boundary condition** is the condition where cell values on the boundary (virtual neighbors) are not allowed to change with time, in the case a null value is chosen this condition is known as **null boundary condition** (Cho, 2005, Rubio et al., 2004). In the **reflexive boundary condition** the virtual neighbors assume the same value of the present state of cells in the edges (Kobuchi and Nishio, 1973, Yacoubi and Jai, 2002). And finally the **periodic boundary condition** where the extreme cells are adjacent

(Rubio et al., 2004). In Figure 3.4 three different schematic representations of the virtual neighborhood near the boundary in a square lattice are represented, namely fixed, reflexive and periodic boundary conditions.

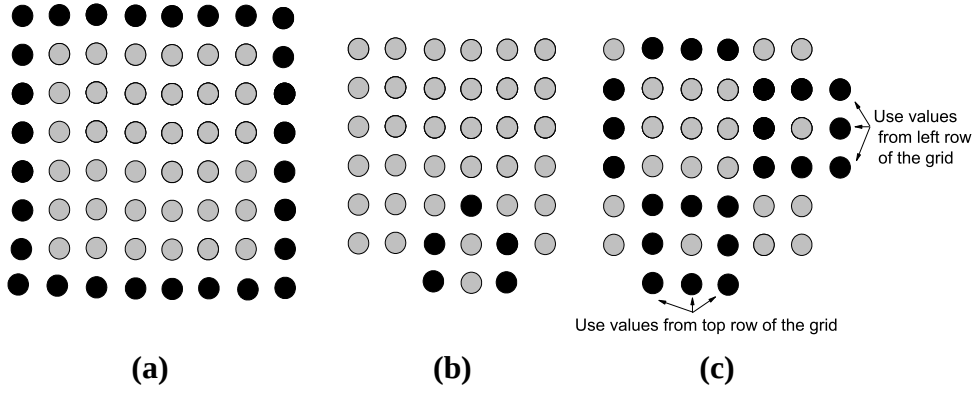

Figure 3.4. Examples of common used boundary conditions: (a) constant boundary condition, (b) reflexive boundary condition and (c) virtual Moore neighborhood in the periodic boundary condition which uses left,right rows to extend the grid horizontally and the top, bottom rows to extend the grid vertically

Some reviews of cellular automata can be found in Sarkar (2000) and Yang and Young (2005).

3.2 Percolation clusters

Percolation is a model for random connectivity, associated with systems with a critical state. In biological systems the role of the connectivity of different elements is of great importance (Green, 1993). Basically percolation deals with groups of neighboring occupied sites with the same state in the lattice and these groups are called **clusters**. Usually, in literature, Von Neumann neighborhood is the most considered neighborhood in the formation of these clusters, like in the example showed in Figure 3.5. However other kinds of neighborhood can be considered as well (see

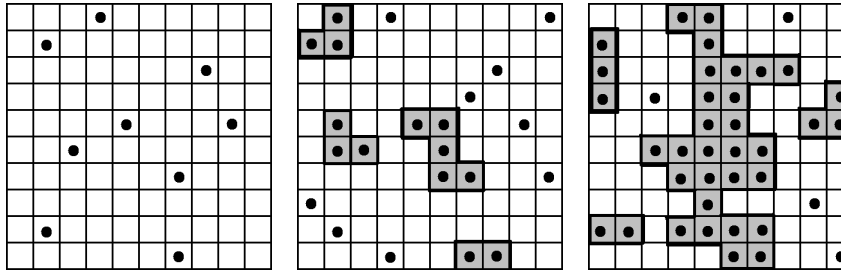

Figure 3.5. Site percolation: (a) system in which few cells at occupied state are randomly distributed throughout the lattice. (b) A system in which some cells at occupied state are randomly distributed so that some clusters may form (encircled). (c) A system in which enough cells at occupied state have been randomly added so that a probability exists of a cluster forming that spans the system (encircled).

chapter 7). Percolation is widely observed in chemical systems and historically, it was first recognized by Flory and Stockmayer as a method to describe how small, branched molecules react to form polymers, ultimately leading to an extensive network connected by chemical bonds (Flory, 1941a,b,c, Stockmayer, 1943, 1944).

The term “percolation” and the mathematical concept were introduced by Broadbent and Hammersly in the late 1950s, who studied the spreading of hypothetical fluid particles through a random medium, making the distinction between diffusion and percolation processes (Broadbent and Hammersley, 1957). Thereafter, percolation theory has been found useful to characterize many disordered systems (Andrade et al., 2000). Stauffer described the application of percolation theory to conductivity and diffusivity (Stauffer and Ahorony, 1985).

In order to understand percolation phenomena observe Figure 3.5. In Figure 3.5(a) it is possible to see how occupied cells are distributed randomly. Because of the low density of this occupied cells no physical contact is encountered. In this sense no information in the system is exchanged. If increasing the density of occupied cells in the lattice a finite probability arises for these cells to form some clusters which per-

mits some exchange of information within the clusters, but the clusters are isolated so the information exchange is confined within each cluster, see Figure 3.5(b). If enough occupied cells are randomly added to the system, some clusters may appear as a single cluster which spans the entire length or width of the system.

This spanning cluster produces a conduit through which an uninterrupted flow of information is possible across the system. This situation of uninterrupted flow is called **percolation** (Figure 3.5(c)). The minimum number of occupied cells in the system necessary to have a finite probability of percolation occurring is called the **percolation threshold** or **percolation point** (Kier et al., 1999). In this process the cells are not necessarily distributed independently (i.e. randomly) in the lattice but the cells positions may be correlated, i.e., determined by rules which depends on the cells positions in cellular automata models, like the positions of molecules in a real gas, forest fire through clusters of trees or infected people in spreading diseases.

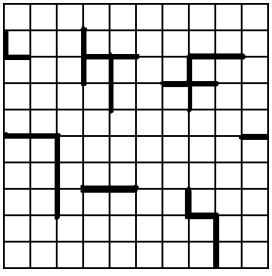

Figure 3.6: Bond Percolation

There are two types of percolation: Bond percolation and site percolation. A **bond percolation** considers the lattice edges as the relevant entities; a **site percolation** considers the lattice vertices/cells as the relevant entities. In Figure 3.5 shows an example of site percolation and Figure 3.6 an illustration of bond percolation. The transition from a non-percolating state to a percolating state is a kind of **phase transition**. The major difference between percolation and other phase transition models is the absence of a Hamiltonian. Instead, the theory is based entirely on probabilistic arguments (Essam, 1980). Good reviews in percolation theory can be found in Essam (1980), Stauffer (1979) and Fortunato (2000).

3.2.1 Cluster size distribution

Once defined the problem, it is possible to study percolation phenomena quantitatively. Since percolation is related to a random process, in repeating the procedure over and over clusters of different sizes and shapes will be encountered. Hence it is possible to study the averages of quantities related to the clusters, studying the statistics of these clusters. The **size of a cluster**, s can be defined as the number of sites (bonds) belonging to it. In percolation theory one of the statistics studies is to see how the clusters are distributed according to their size. Hence the number of clusters of size s per lattice site can be expressed as following:

$$n_s = \lim_{V \to \infty} \frac{N_V(s)}{V} \tag{3.1}$$

where V is the number of sites (volume) of a finite lattice and N_V the number of clusters of size s on that lattice which depends also on occupation probability p.

As illustrated in Figure 3.5, depending on the density of occupied cells it is possible to find some clusters, increasing the density of occupied cells when increasing the occupation probability p, the cluster sizes and the number of clusters increase until a certain critical point, p_c, where the biggest cluster spans through the lattice. Near this transition[2] , when $p = p_c$, cluster sizes become statistically correlated over large scales, and can even become scale invariant. Thus the distribution of clusters sizes obeys a power-law:

$$n_s \propto s^{-\tau} \tag{3.2}$$

Where τ is a critical exponent. This is the connection of percolation and critical phenomena, what lead in the 80's to growth of popularity of this subject among physicists.

[2]It is called by physicists as a second-order transition since it is characterized by a continuous vanishing of the order/control parameter

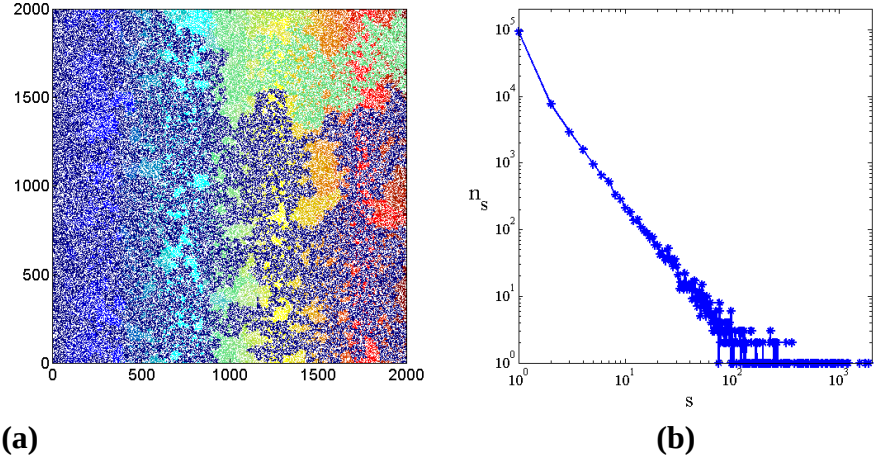

Figure 3.7. (a) Snapshot of a 2000×2000 square lattice. Sites are randomly occupied or empty (white cell)when occupation probability $p = p_c \approx 0.593$ (which is the percolation threshold on site percolation in the square lattice). Occupied sites with the same color pertain to the same cluster. (b) Log-log plot of the cluster distribution shown in (a). The slope of the straight line gives an approximated estimate of the critical exponent τ.

Bibliography

Andrade, J. S., Buldyrev, S. V., Dokholyan, N. V., Havlin, S., King, P. R., Lee, Y., Paul, G., Eugene Stanley, H., 2000. Flow between two sites on a percolation cluster. Phys. Rev. E 62 (6), 8270–8281.

Braun, O. M., Hu, B., Filippov, A., Zeltser, A., 1998. Traffic jams and hysteresis in driven one-dimensional systems. Phys. Rev. E 58 (2), 1311–1324.

Broadbent, S., Hammersley, J., 1957. Percolation processes i. crystals and mazes. Proc. Cambridge Philos. Soc. 53 (03), 629–641.

Burstedde, C., Klauck, K., Schadschneider, A., Zittartz, J., 2001. Simulation of pedestrian dynamics using a two-dimensional cellular automaton. Physica A: Statistical Mechanics and its Applications 295 (3-4), 507 – 525.

Cho, S.-J., 2005. Analysis of pseudo-noise sequences generated by null boudnary cellular automata. J. Appl. Math. & Computing 18 (1 - 2), 287 – 300.

Coe, J. B., Ahnert, S. E., Fink, T. M. A., 2008. When are cellular automata random? EPL (Europhysics Letters) 84 (5), 50005.

Cornforth, D., Green, D. G., Newth, D., 2005. Ordered asynchronous processes in multi-agent systems. Physica D: Nonlinear Phenomena 204 (1-2), 70 – 82.

Domany, E., 1984. Exact results for two- and three-dimensional Ising and Potts models. Phys. Rev. Lett. 52 (11), 871–874.

Essam, J. W., 1980. Percolation theory. Rep. Prog. Phys. 43 (7), 833.

Flory, P. J., 1941a. Molecular size distribution in three dimensional polymers. I. Gelation. J. Am. Chem. Soc. 63 (11), 3083–3090.

Flory, P. J., 1941b. Molecular size distribution in three dimensional polymers. II. trifunctional branching units. J. Am. Chem. Soc. 63 (11), 3091–3096.

Flory, P. J., 1941c. Molecular size distribution in three dimensional polymers. III. tetrafunctional branching units. J. Am. Chem. Soc. 63 (11), 3096–3090.

Fortunato, S., 2000. Percolation and deconfinement in SU(2) Gauge theory. Ph.D. thesis, Physics Faculty, University of Bielefeld.

Gardner, M., 1970. Mathematical games: The fantastic combinations of John Conway's new solitaire game 'Life'. Sci. Am. 223 (4), 120–123.

Grassberger, P., Krause, F., von der Twer, T., 1984. A new type of kinetic critical phenomenon. Journal of Physics A: Mathematical and General 17 (3), L105.

Green, D. G., 1993. Emergent behavior in biological systems. In: In: D.G. Green and T.J. Bossomaier (Editors), Complex Systems: From Biology to Computation. IOS. IOS Press, pp. 24–35.

Kai Nagel, Michael Schreckenberg, 1992. A cellular automaton model for freeway traffic. J. Phys. I France 2 (12), 2221–2229.

Kier, L. B., Cheng, C.-K., Testa, B., 1999. A cellular automata model of the percolation process. J. Chem. Inf. Comput. Sci. 39 (2), 326–332.

Kobuchi, Y., Nishio, H., 1973. Some regular state sets in the system of one-dimensional iterative automata. Information Sciences 5, 199 – 216.

Kong, X. P., Cohen, E. G. D., 1991. Diffusion and propagation in triangular lorentz lattice gas cellular automata. Journal of Statistical Physics 62, 737–757.

Lebowitz, J. L., Maes, C., Speer, E. R., 1990. Statistical mechanics of probabilistic cellular automata. Journal of Statistical Physics 59, 117–170.

Moore, E. F., 1956. Gedanken experiments on sequential machines. In: Automata Studies. Princeton U., pp. 129–153.

Rajewsky, N., Schreckenberg, M., 1997. Exact results for one-dimensional cellular automata with different types of updates. Physica A: Statistical and Theoretical Physics 245 (1-2), 139 – 144.

Rosin, P., 2006. Training cellular automata for image processing. IEEE Transactions on Image Processing 15 (7), 2076–2087.

Rosin, P. L., 2010. Image processing using 3-state cellular automata. Computer Vision and Image Understanding 114 (7), 790 – 802.

Rubio, F., Encinas, C. H., White, L. H., del Rey, S. M., Snchez, A. R., Gerardo, 2004. The use of linear hybrid cellular automata as pseudorandom bit generators in cryptography. Neural Parallel Sci. Comput. 12, 175–192.

Sarkar, P., 2000. A brief history of cellular automata. ACM Computing Surveys 32 (1), 80–107.

Stauffer, D., 1979. Scaling theory of percolation clusters. Phys. Rep. 54 (1), 1 – 74.

Stauffer, D., Ahorony, A., 1985. Introduction to Percolation Theory, revised second edition Edition. Taylor & Francis, London.

Stockmayer, W. H., 1943. Theory of molecular size distribution and gel formation in branched-chain polymers. J. Chem. Phys. 11 (2), 45–55.

Stockmayer, W. H., 1944. Theory of molecular size distribution and gel formation in branched polymers ii. general cross linking. J. Chem. Phys. 12 (4), 125–131.

Szabó, G., Borsos, I., 2002. A cellular automaton with two phase transitions. J. Phys. A 35 (13), L189.

Von Neumann, J., 1951. The general and logical theory of automata. In: Jeffress, L. A. (Ed.), Cerebral Mechanisms in Behavior - The Hixon Symposium. John Wiley & Sons, New York, pp. 1–31.

Von Neumann, J., Burks, A. W., 1966. Theory of Self-Reproducing Automata. University of Illinois Press, Champaign, IL.

Wang, B. H., Kwong, Y. R., Hui, P. M., Hu, B., 1999. Cellular automaton models of driven diffusive frenkel-kontorova-type systems. Phys. Rev. E 60 (1), 149–158.

Wolfram, S., 1984. Universality and complexity in cellular automata. Phys. D 10 (1-2), 1–35.

Wolfram, S., 2002. New Kind of Science. A. Wolfram Media, Inc.

Yacoubi, S. E., Jai, A. E., 2002. Cellular automata modelling and spreadability. Mathematical and Computer Modelling 36 (9-10), 1059 – 1074.

Yang, X.-S., Young, Y., 2005. Cellular Automata, PDEs and Pattern Formation. Handbook of Bioinspired Algorithms and Applications. Chapman & Hall/CRC Press, Ch. 18, pp. 271–282.

4

Evolutionary dynamics

It is clearly impossible to say what the "best" phenotype is unless one knows the range of possibilities. If there were no constraints on what is possible, the best phenotype would live forever, would be impregnable to predators, would lay eggs at an infinite rate, and so on. It is therefore necessary to specify the set of possible phenotypes, or in some other way describe the limits of what can evolve.

Maynard Smith

The basic principle of evolution, natural selection, was outlined by Darwin (1859) in his book On the origin of species. Darwin expressed his arguments verbally, but many attempts since then have been made to formalize the theory of evolution, such as population genetics (Roughgarden, 1979), quantitative genetics (Falconer and Mackay, 1996) and evolutionary game theory (Hofbauer and Sigmund, 1998).

John Maynard Smith introduced game theory to biology in the 1980s, including the evolutionarily stable strategy (ESS), a population-genetic counterpart to the Nash competitive equilibrium (NCE) of game theory (Nash, 1951, Roughgarden et al., 2006). An ESS is a strategy that when played by most of the population is unbeatable by any other strategy. "*A major advantage of the ESS is that it can be resolved from phenotypic considerations alone without having to account explicitly for the (often unknown) underlying genetic detail. Moreover, by circumventing the intricacies of diploid Mendelian inheritance, more complex ecological interactions and adaptations can be explored than is usually possible with a fully genetic approach. In those cases where a comparison with*

more complete approaches is possible, ESS-theory has been shown to be largely compatible with both quantitative genetics and population genetics" (Geritz et al., 1998, and references therein).

Evolutionary invasion analysis, also known as adaptive dynamics, is a mathematical theory for studying long-term phenotypical evolution and was formally developed during the 1990s. It links population dynamics to long-term evolution driven by mutation and natural selection providing methods of model formulation and analysis that relate phenomena on an evolutionary time scale to processes and structures defined in ecological and population dynamical terms. A key factor is that mutant strategies must be successful in an environment shaped by current resident strategies. Successful mutations can become established and therefore alter the environment for future mutant strategies. In this way there is a feedback between the population dynamics (the environment) and the evolutionary dynamics.

This chapter introduces the fundamental ideas behind adaptive dynamics and the methods that were used in the studies shown in chapter 8.

4.1 Adaptive dynamics

In **adaptive dynamics** the **phenotypes** are represented as a **strategy** that can vary continuously. The **resident** population can be assumed to be in a dynamical equilibrium when new **mutants** appear, and the eventual fate of such mutants can be inferred from their initial growth rate when rare in the environment consisting of the resident. Following the same notation as in Geritz et al. (1997) consider a population with a single strategy x. The growth of the population can be described by the equation:

$$\frac{d}{dt}\vec{N} = M(x, E_x) \cdot \vec{N} \tag{4.1}$$

where $\vec{N}$ is the state vector or variable of the population, $M(x, E_x)$ is the matrix that contains the demographic parameters for birth, death, migration and depends on strategy x as well as on the environment $E_x = E_x(\vec{N})$. Fixing condition of the environment the population would increase exponentially with growth rate $r(x, E_x)$, which is the real leading eigenvalue of the matrix M, i.e., the long-term exponential growth rate of the phenotype in a given environment, also called **fitness** (Metz et al., 1992).

The equilibrium of the resident population is the solution of $r(x, E_x) = 0$ and is assumed to be unique. Adaptive dynamics considers the fate of a new mutant with strategy y emerging in a population of residents with strategy x. Since the mutant population is rare it does not contribute to change the environment and so its fitness can be written as:

$$s_x(y) = r(y, E_x) \tag{4.2}$$

Analysis of the mutant fitness in the environment set by the resident, $s_x(y)$ can determine the evolutionary behavior of the system.

If $s_x(y) > 0$ the mutant can spread but it is not guaranteed to persist, since random extinction can happen due the small initial amount of mutants. But if $s_x(y) < 0$ the mutant population will die out. If $s_x(y) > 0$ and $s_y(x) < 0$, it means that the mutant can spread but the resident cannot recover when its population is rare and in this situation it is common for the mutant to replace the resident strategy (and therefore become the new resident). It is possible to assess the evolutionary behavior by re-writing the mutant fitness expression. Since mutations are small it is possible to apply a linear approximation of the mutant's fitness:

$$s_x(y) = s_x(x) + D(x)(y - x) \tag{4.3}$$

where $D(x)$ is the local fitness gradient and can be defined when mutant and resident population are equal:

$$D(x) = \frac{\partial s_x(y)}{\partial y}\Big|_{y=x} \tag{4.4}$$

since $s_x(x) = r(x, E_x) = 0$ for all x, the sign of $D(x)$ determines whether mutants can invade. Evolution progresses in the direction of the fitness

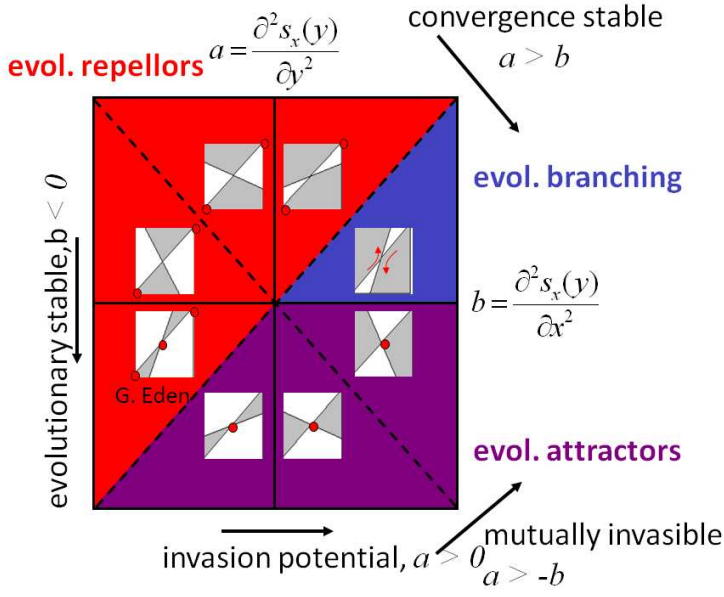

Figure 4.1. Classification of the singular strategies according to the second partial derivatives of $s_x(y)$. The small plots are the local PIPs near to the singular strategy in the center of each graph.

gradient until reaching a strategy for which the local fitness gradient is zero, called an **evolutionary singular strategy**, x^*.

4.1.1 Pairwise invasibility plots

In monomorphic populations, considered up to now, where there is only one analyzed strategy, the evolution can be analyzed graphically by means of a **pairwise invasibility plot** (PIP). And close to a singular strategy there are only eight possible generic local configurations of PIP (see Figure 4.1 and each configuration represents a different evolutionary scenario that can be determined analytically in terms of the second-order derivatives of $s_x(y)$ at singular evolutionary point ($x = y = x^*$) and interpreted in terms of four properties of singular strategy (Geritz et al., 1998, 1997):

1. $\frac{\partial s_x(y)}{\partial y^2} < 0$, means that x^* is locally ESS-stable and no nearby mutant

can invade;

2. $\frac{\partial s_x(y)}{\partial x^2} > \frac{\partial s_x(y)}{\partial y^2}$, means that x^* is convergence stable (CS), a population of nearby phenotypes can be invaded by mutants that are even closer to x^*;

3. $\frac{\partial s_x(y)}{\partial x^2} > 0$, means that the singular strategy x^* can spread in other populations when itself is initially rare;

4. $\frac{\partial s_x(y)}{\partial x^2} > -\frac{\partial s_x(y)}{\partial y^2}$, the two strategies x and y can mutually invade and hence give rise to a dimorphic population.

In practice the evolutionary behavior at the singular strategy can be determined by considering the ESS and CS properties only. If x^* is ESS and CS then it is necessarily an evolutionary attractor and will be an end point of evolution; if it is not ESS and not CS, it is an evolutionary repellor and strategies will evolve away from x^*. If x^* is ESS but not CS it is known as a Garden of Eden strategy. Here, if at x^*, no other strategies can invade but nearby strategies evolve away from the singular strategy. The phenomenon of evolutionary branching occurs when x^* is CS but not ESS. Here strategies evolve towards x^* but when close by they undergo disruptive selection and two distinct strategies co-exist either side of x^*. Branching points are at the forefront of theoretical attempts to explain speciation.

4.2 Intraspecific competition in predator-prey models

The adaptive dynamics techniques can be understood more clearly by considering a specific example. Bowers et al. (2003) considered a classical predator-prey model and examined the evolutionary behavior when the prey had an explicit or implicit carrying capacity. They argued that implicit carrying capacities, where individual properties evolve and act

on natural selection are more appropriate for evolutionary models. The model of Bowers et al. (2003) with an implicit carrying capacity is formulated as follows:

$$\begin{aligned} \frac{dN}{dt} &= N(r - hN - cP) \\ \frac{dP}{dt} &= P(-d + ceN) \end{aligned} \tag{4.5}$$

Here, N represents the density of the prey and P the density of the predator. All parameters are positive and r is the intrinsic growth rate of prey, c is the rate of predation , d is the death rate of the predator and e is the rate of conversion of predation into predator births. The parameter h represents the susceptibility to crowding for the prey (prey self-regulation) and in the absence of the predator the prey reaches a carrying capacity $N = r/h$ which depends on model parameters. Bowers et al. (2003) consider the evolution of the prey parameters r and c (all other parameters are fixed). A key property of evolutionary theory is that a benefit through changes in one life history parameter must be bought at a cost in terms of other parameters. Therefore we link the parameters r and c with a **trade-off** ($r = f(c)$) such that the benefit of an increase in host reproduction rate, r, is bought at a cost of an increase on the predation rate, c. Therefore the only evolving parameter is c (and r is linked to c through the trade-off).

The fitness, $\overline{s}$, of a mutant prey type with parameter $\overline{c}$ in a resident predator-prey environment at a stable point equilibrium where the resident prey has parameter c is as follows:

$$\overline{s} = f(\overline{c}) - hN - \overline{c}P \tag{4.6}$$

Where now N and P denote the resident equilibrium population densities and, therefore, depend only on resident parameters. A singular strategy, c^*, occurs when:

$$\frac{\partial \overline{s}}{\partial \overline{c}}\Big|_{\overline{c}=c} = 0 \qquad \Rightarrow \qquad f'(c^*) = P \tag{4.7}$$

The behavior at the singular points is determined by the ESS and CS properties which satisfy the following conditions:

$$\text{ESS: } \frac{\partial^2 \overline{s}}{\partial \overline{c}^2}\Big|_{c^*} < 0 \qquad \Rightarrow \qquad f''(c^*) < 0 \tag{4.8}$$

$$\text{CS: } \frac{\partial^2 \overline{s}}{\partial c^2}\Big|_{c^*} - \frac{\partial^2 \overline{s}}{\partial \overline{c}^2}\Big|_{c^*} > 0 \qquad \Rightarrow \qquad f''(c^*) < \frac{hd}{e(c^*)^3} \tag{4.9}$$

Therefore if $f''(c^*) < 0$ the singular strategy is ESS and CS and is therefore an evolutionary attractor. If $f''(c^*) > hd/e(c^*)^3$ then the singular strategy is neither ESS or CS and it is an evolutionary repellor. If $0 < f''(c^*) < hd/e(c^*)^3$ then the singular strategy is CS but it is not ESS which leads to evolutionary branching. This example highlights how the shape of the trade-off function (the cost structure of the trade-off) determines the evolutionary behavior.

Simulations of the adaptive dynamics process can be undertaken to verify this evolutionary behavior. In the simulations, the population dynamics were numerically solved for a fixed time (t) according to population dynamical equations (4.5) starting with a monomorphic population. Mutant strategies were generated by small deviations around the current strategies and introduced at low density. Explicitly the solved system is:

$$\begin{aligned} \frac{dN_i}{dt} &= N_i(r_i - hN_i - c_iP) \\ \frac{dP}{dt} &= P(-d + \sum c_i e N_i) \end{aligned} \tag{4.10}$$

where i represents all non-zero populations or prey, resident or mutant, and all prey have the same susceptibility to crowding, h. Then the population dynamics were solved for a further time t with strategies whose population density fell below a low threshold considered extinct and removed before considering new mutations. In this way, the parameter c

could evolve (see Bowers et al. (2003) for further details). By choosing the trade-off $r = f(c) = \alpha c^2 + 2c + \alpha + 1$ the singular strategy can become an evolutionary attractor, a repellor or a branching point by choosing different values of α, see Figure 4.2.

This example highlights how adaptive dynamics can be used to understand the evolution of phenotypes (represented by differences in the parameter c in Bowers et al. (2003)) and the importance of trade-offs in determining the evolutionary behavior. These techniques will be used to examine the evolution of male-biased parasitism in chapter 8.

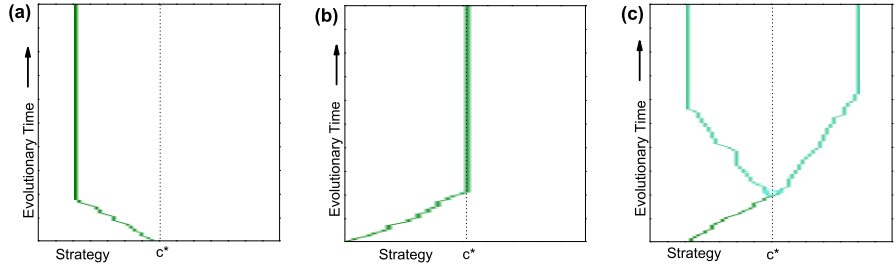

Figure 4.2. Simulations of equations (4.10), showing how strategy c evolves over time. In each panel the singular strategy, c^*, is represented by the vertical dotted line. The solid line represents the way c evolve in the adaptive dynamics simulation process, i.e., the density of prey with non-zero c_i. Parameters are $h = 1$, $d = 1$ and $e = 1$. In (a) $\alpha = -0.5$ and therefore, $\frac{\partial^2 f(c^*)}{\partial^2 \bar{c}} < 0$ and c^* is an evolutionary attractor. In (b) $\alpha = 0.8$ and $\frac{\partial^2 f(c^*)}{\partial^2 \bar{c}} > hd/e(c^*)^3$ and c^* is an evolutionary repellor. In (c) $\alpha = 0.3$ and $0 < \frac{\partial^2 f(c^*)}{\partial^2 \bar{c}} < hd/e(c^*)^3$ and c^* is an evolutionary branching point.

Bibliography

Bowers, R. G., White, A., Boots, M., Geritz, S. A. H., Kisdi, E., 2003. Evolutionary branching/speciation: contrasting results from system with explicit or emergent carrying capacities. Evolutionary Ecology Research 5, 1–9.

Darwin, C., 1859. On the Origin of Species by Means of Natural Selection, or the Preservation of Favoured Races in the Struggle for Life. John Murray, United Kingdom.

Falconer, D. S., Mackay, T. F. C., 1996. Introduction to quantitative genetics, 4th Edition. Prentice Hall, Malaysia.

Geritz, S., Kisdi, E., Meszéna, G., Metz, J., 1998. Evolutionarily singular strategies and the adaptive growth and branching of the evolutionary tree. Evol. Ecol. 12, 35–57.

Geritz, S. A. H., Metz, J. A. J., Kisdi, E., Meszéna, G., 1997. Dynamics of adaptation and evolutionary branching. Phys. Rev. Lett. 78 (10), 2024–2027.

Hofbauer, J., Sigmund, K., 1998. Evolutionary games and population dynamics. Cambridge University Press, Cambridge, UK.

Metz, J. A. J., Nisbet, R. M., Geritz, S. A. H., 1992. How should we define 'fitness' for general ecological scenarios? TREE 7 (6), 198–202.

Nash, J., 1951. Non-cooperative games. The Annals of Mathematics 54 (2), pp. 286–295.

Roughgarden, J., 1979. Theory of Population Genetics and Evolutionary Ecology: an introduction. Macmillian Publishing Co, Inc.

Roughgarden, J., Oishi, M., Akcay, E., 2006. Reproductive Social Behavior: Cooperative Games to Replace Sexual Selection. Science 311 (5763), 965–969.

Smith, J. M., 1982. Evolution and the theory of games. Cambridge Univ. Press., Cambridge.

Smith, J. M., Price, G. R., 1973. The logic of animal conflict. Nature 246, 15–18.

Part II

Original research

Marine ecology

Photo: André Luis Sousa Sena

5

Joint effects of nutrients and contaminants on the dynamics of a food chain in marine ecosystems

5.1 Introduction

Marine waters and in particular coastal waters are increasingly exposed to anthropogenic pressures represented not only by the growing input of nutrient and contaminants related to urban, agricultural and industrial activities, but also by the exploitation of coastal areas for aquaculture, fishing and tourism. Since the resources of the coastal zone are exploited by different stake holders it is essential to improve the knowledge on the ecosystem's vulnerability to stressors and protect those areas through a sensible management.

The interaction of pollutants and nutrients on aquatic ecosystems is difficult to evaluate, since many direct and indirect effects have to be considered. Contaminants can have instantaneous effects, such as massive killings after an accidental contaminant release. Other toxic effects, such as genotoxicity and reproductive failure are less evident and they act on a longer time-scale; however, they represent an important risk for the ecosystem. Furthermore, if the contaminant is lipophilic[1], bioaccumulation[2] should be considered. On the other hand, an increase of the nutrient load can have the direct effect of raising the primary production at the bottom of the food chain and consequently increase the concentration of

[1]The ability of a chemical compound to dissolve in fats, oils, lipids.

[2]An increase in the concentration of a chemical in a biological organism over time.

the organic matter in the system. But the higher concentration of organic matter can affect the bioavailability of the contaminants and therefore the fate of pollutants in the aquatic environment and their effects on the impacted ecosystem (Gunnarsson et al., 1995).

Thus, contaminants affect aquatic ecosystems through direct and indirect effects (Fleeger et al., 2003), from acute and/or chronic toxicity on sensitive species to disruption in the food web structure. Some species might be more sensitive than others to a certain chemical, but since the different populations are linked to each other by competition and predation, species which are not directly stressed may respond indirectly (Fleeger et al., 2003). Within a food web, community-level relations arise from unobservable indirect pathways. These relations may give rise to indirectly mediated relations, mutualism and competition (Fath, 2007). In some cases environmental perturbations alter substantially the dynamics or the structure of coastal ecosystems and the effect may produce the occurrence of a trophic cascade and eventually the extinction of some species (Jackson et al., 2001). A better understanding of the relative importance of top-down (e.g. overfishing) versus bottom-up (e.g. increased nutrient input causing eutrophication) controls is essential and can only be achieved through modelling (Daskalov, 2002).

Sudden regime shifts and ecosystem collapses are likely to occur in stressed ecosystems. Catastrophic regime shifts have been related to alternative stable states which can be linked to a critical threshold in such a way that a gradual increase of one driver has little influence until a certain value is reached at which a large shift occurs that is difficult to reverse (Scheffer and Carpenter, 2003, Scheffer et al., 2001). The shape of ecotoxicological[3] dose-response curves (Suter II, 1993), showing a sharp increase in the effect of toxic substances above a critical value, facilitates the occurrence of regime shifts under pollutant pressure.

This study considered the combined effects of contaminant sub-

[3] "The branch of toxicology concerned with the study of toxic effects, caused by natural or synthetic pollutants, to the constituents of ecosystems, animal (including human), vegetable and microbial, in an integral context."

stances and nutrient load in the framework of a simple tritrophic food chain model. The study was restricted to contaminants, such as s-triazines[4], which affect the mortality in particular trophic levels, but which do not bioaccumulate neither in time nor along the food chain. When studying the dynamics of simple food chain and food web models it is also important to bear in mind that the response might depend on the complexity of the represented system. Chaotic dynamics, for example, seems to be more frequent in simple ecosystem models or in models with a high number of trophic levels (Fussmann and Heber, 2002). Thus, only the first qualitative changes of behavior occurring when increasing nutrients from low values, and how this is changed by pollutants, will be focused. And not the complex sequences of chaotic states which may occur at high nutrient availability, whose details are more affected by the trophic structure of the model.

Since no microbial recycling loop was included, sediment or oxygen dynamics, or shading effects, complex eutrophication behavior typical of coastal ecosystems (Zaldívar et al., 2003), e.g. anoxic crises, alteration of nutrient cycling, macroalgal blooms, etc. will not occur in the model. The study was rather concentrated in the simplest scenarios occurring during enrichment and its modification by contaminants, discussing particularly the indirect effects which lead to counterintuitive behavior.

5.2 Model formulation

The Canale's chemostat model (CC) was considered, (Boer et al., 1998, 2001, Canale, 1970, Gwaltney and Stadtherr, 2007), which is an extension of the tri-trophic food-chain Rosenzweig-MacArthur model (RMA) that

[4]s-triazine is one of three organic chemicals, isomeric with each other, whose empirical formula is $C_3H_3N_3$. The three isomers of triazine are distinguished from each other by the positions of their nitrogen atoms, and are referred to as 1,2,3-triazine, 1,2,4-triazine, and 1,3,5-triazine or s-triazine. Among other usages triazine is used in the manufacture of resins and as the basis for various herbicides.

has been extensively studied in theoretical ecology (Abrams and Roth, 1994, DeFeo and Rinaldi, 1997, Gragnani et al., 1998, Gwaltney et al., 2004, Hastings and Powell, 1991, Klebanoff and Hastings, 1994, Kuznetsov and Rinaldi, 1996, McCann and Yodzis, 1994). This model was previously used to analyze the dynamics of a food chain consisting of bacteria living on glucose, ciliates and carnivorous ciliates (Boer et al., 1998, 2001), but can be adapted to represent an aquatic food chain with a constant nutrient input. The CC model is similar to the RMA model, but there is an additional equation representing the input of nutrient and it considers the losses due to the flushing rate:

$$\dot{N} = D(I-N) - P\frac{a_1 N}{b_1+N}, \tag{5.1}$$

$$\dot{P} = P\left[e_1\frac{a_1 N}{b_1+N} - \frac{a_2 P}{b_2+P} - d_1 - f_1 D\right], \tag{5.2}$$

$$\dot{Z} = Z\left[e_2\frac{a_2 P}{b_2+P} - \frac{a_3 F}{b_3+Z} - d_2 - f_2 D\right], \tag{5.3}$$

$$\dot{F} = F\left[e_3\frac{a_3 Z}{b_3+Z} - d_3 - f_3 D\right]. \tag{5.4}$$

In this study the variables N, P, Z, F represent the nitrogen concentration in the different compartments of the system (nutrient, phytoplankton, zooplankton and fish, which will be also denoted with the alternative names of nutrient, prey, predator, and top-predator, respectively) expressed in units of mgN/l. The default parameters, see Table 5.1, were derived from the parameters of the aquatic food chain model presented in Mosekilde (1998) and from the pelagic ecosystem model in Lima et al. (2002). I is the nutrient load or nutrient input into the system. D is a flow rate quantifying water re-

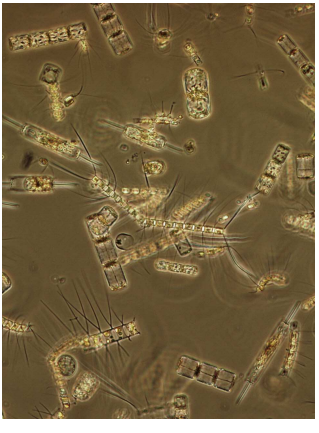

Figure 5.1. Phytoplankton of winter-spring proliferation in the Catalan-Balearic sea. Photo:Marta Estrada

newal in the system, which affects the species through the flushing rates f_i ($i = 1,2,3$). d_i are the specific mortalities, b_i half saturation constants for the Holling type-II predation functions, a_i are maximum predation rates, and e_i efficiencies. The following condition should be satisfied by the equation parameters:

$$e_i a_i > d_i + D f_i \quad (i = 1,2,3), \tag{5.5}$$

since this "avoids the case where predator and top-predator cannot survive, even when their food is infinitely abundant" (Kuznetsov et al., 2001). Contaminant toxicity is incorporated in the model by an increase in mortality.

Three different scenarios were considered in each of which the contaminant affects the mortality of only one of the compartments:

$$d_j = d_j^{(0)} + \Delta d_j \left(\frac{(C_j)^6}{(C_j)^6 + 0.5^6} \right) \tag{5.6}$$

$j = 1,2$, and 3 labels the three trophic levels: prey, predator and top-predator, C_j is the dimensionless concentration of the contaminant affecting the level j, normalized in such a way that for $C_j = 0.5$ the toxicity achieves half its maximum impact on mortality, and a sigmoidal function (Figure 5.2) has been used to model the mortality increase from a baseline value, $d_j^{(0)}$, to the maximum mortality, $d_j^{(0)} + \Delta d_j$, attained at large contaminant concentrations. This represents typically the shape of the dose-response curves found when assessing toxic effects of chemical on biological populations (Suter II,

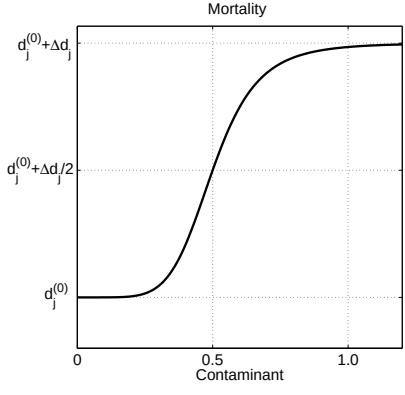

Figure 5.2. Sigmoidal response of mortality to the concentration of the toxic contaminant, according to Eq.(5.6)).

1993). Other works that have studied bifurcations due to mortality changes in the CC model (Gwaltney and Stadtherr, 2007) have normally considered a linear increase. The values of $d_j^{(0)}$ and Δd_j used are written in Table 5.2.

Table 5.1: Parameters of the CC model.

Parameters		value	Units
Nutrient input	I	0.15	mg N/l
Inflow/outflow rate	D	0.02	day^{-1}
Max predation rate	a_1	1.00	day^{-1}
	a_2	0.50	day^{-1}
	a_3	0.047	day^{-1}
Half saturation cont	b_1	0.008	mg N/l
	b_2	0.01	mg N/l
	b_3	0.015	mg N/l
Efficiency	e_1	1.00	-
	e_2	1.00	-
	e_3	1.00	-
Mortality(base values)	d_1	0.10	day^{-1}
	d_2	0.10	day^{-1}
	d_3	0.015	day^{-1}
Flushing rate	f_1	0.01	day^{-1}
	f_2	0.01	day^{-1}
	f_3	0.01	day^{-1}

Table 5.2: Contaminant parameters for the three compartments, $j = 1, 2, 3$.

j	$d_j^{(0)}$	Δd_j
1 (prey)	0.1	0.5
2 (predator)	0.1	0.3
3 (top-predator)	0.015	0.015

5.3 Steady states

This system presents the following set of fixed points: The nutrient-only state (Nu):

$$\begin{aligned} N &= I, \\ P &= 0, \\ Z &= 0, \\ F &= 0. \end{aligned} \tag{5.7}$$

The nutrient-phytoplankton state (NP):

$$\begin{aligned} N &= \frac{b_1(d_1+Df_1)}{a_1e_1-d_1-Df_1}, \\ P &= \frac{De_1\left(\frac{b_1(d_1+Df_1)}{a_1e_1-d_1-Df_1}+I\right)}{d_1+Df_1}, \\ Z &= 0, \\ F &= 0. \end{aligned} \tag{5.8}$$

There are two solutions (NPZ) characterized by the absence of the top predator:

$$\begin{aligned} N &= \frac{b_1D+a_1P-DI\pm\sqrt{4b_1D^2I+(-b_1D-a_1P+DI)^2}}{2D}, \\ P &= \frac{b_2(d_2+Df_2)}{a_2e_2-d_2-Df_2}, \\ Z &= -\frac{(b_1d_1+b_1Df_1+d_1N-a_1e_1N+Df_1N)(b_2+P)}{a_2(b_1+N)}, \\ F &= 0. \end{aligned} \tag{5.9}$$

but only the one with the positive sign of the square root is positive definite.

And finally there are three internal fixed points (NPZF), in which all species are alive. From the equation for $\dot{N}$, (5.1), an equation for P

as a function of N is obtained. Introducing it into (5.2) together with the expression for $Z = \bar{Z}$ which is obtained from (5.4), the following equation for N is obtained:

$$[A_1 N^3 + A_2 N^2 + A_3 N + A_4] = 0 \tag{5.10}$$

where

$$\begin{aligned}
A_1 &= D(a_1 e_1 - d_1 - D_0 f_1), \\
A_2 &= -a_1^2 b_2 e_1 - D(d_1 + D f_1)(2b_1 - I) + a_1(b_1 D e_1 + b_2(d_1 + D f_1) \\
&\quad + a_2 \bar{Z} - D e_1 I), \\
A_3 &= b_1(-D(d_1 + D f_1)(b_1 - 2I) + a_1(b_2(d_1 + D f_1) + a_2 \bar{Z} - D e_1 I)), \\
A_4 &= b_1^2 D(d_1 + D f_1 I).
\end{aligned} \tag{5.11}$$

The values of the remaining variables at the three internal fixed point solutions can be written in terms of $\bar{Z}$ and of the three values of $N = \bar{N}$ obtained from the cubic (5.10):

$$\begin{aligned}
N &= \bar{N}, \\
P &= D_0(I - \bar{N})\frac{b_1 + \bar{N}}{a_1 \bar{N}}, \\
Z &= \bar{Z} = \frac{b_3(d_3 + D f_3)}{a_3 e_3 - d_3 - D f_3}, \\
F &= \frac{(a_2 e_2 P - b_2 d_2 - b_2 D f_2 - d_2 P - D f_2 P)(b_3 + \bar{Z})}{a_3(b_2 + P)}.
\end{aligned} \tag{5.12}$$

It turns out that only one of the three fixed point solutions is positive for the parameter values in Table 5.1.

Mathematically there are four additional solutions but they are not feasible biologically since they lead to negative populations: the state characterized by the absence of phytoplankton ($N = I, P = 0, Z \neq 0, F \neq 0$), by the absence of nutrient and of the top-predator ($N = 0, P \neq 0, Z \neq 0, F = 0$), by the absence of the nutrient and of phytoplankton ($N = 0, P = 0, Z \neq 0, F \neq 0$), and by the absence of nutrient ($N = 0, P \neq 0, Z \neq 0, F \neq 0$).

5.4 Stability and bifurcation analysis

The dynamics of the CC food-chain models has been analyzed for several parameter values by direct numerical integration of the model equations, and by bifurcation analysis carried on with the software XPPAUT, (Doedel et al., 1997, Ermentrout, 2002). Background on the different types of bifurcations can be found in (Gugenheimer and Holmes, 1993, Strogatz, 2000). Only bifurcations of positive solutions were considered and, as stated in the introduction, the routes to chaotic behavior occurring at high nutrient loadwere not described in detail. For low and intermediate nutrient load the relevant attractors are the fixed points described above, and also two limit cycles, one involving the variables N, P and Z, lying on the $F = 0$ hyperplane, and another one in which all the species are present. These attractors are represented in Figure 5.3.

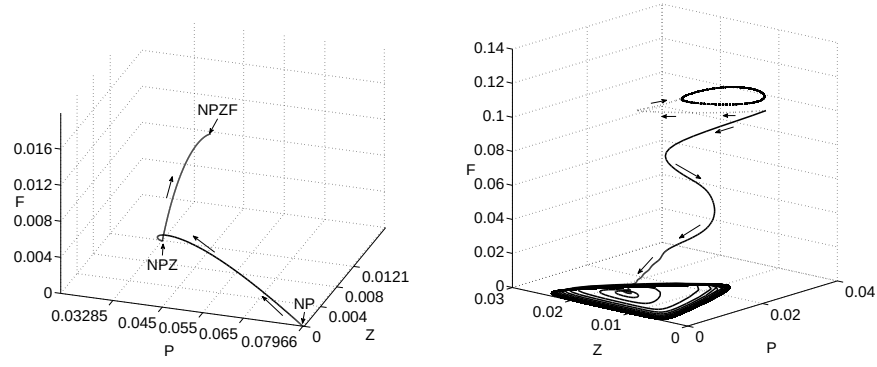

Figure 5.3. a) Projection on the PZF subspace of a trajectory which starts close to the NP fixed point, approaches the NPZ one, and finally is attracted by the NPZF fixed point. $I = 0.4\ mgN/l$, $C_1 = C_3 = 0$, and $C_2 = 0.8$. This shows the approximate location of these points and that only the NPZF one is stable for these parameter values. (b) Cyclic behavior: Thick line is a trajectory leading to an attracting limit cycle on the NPZ hyperplane for $I = 0.1\ mgN/l$, $C_1 = C_2 = 0$, and $C_3 = 0.8$; dotted line is a trajectory attracted by the limit cycle involving all the variables for $I = 0.24\ mgN/l$, $C_1 = C_2 = 0$, and $C_3 = 0.2$.

5.4.1 The non-contaminant case

First, system behavior for the case of mortalities at their base values was considered, i.e. in the absence of contaminants. This will serve as a reference for later inclusion of contaminants. Figure5.4 shows the sequence of bifurcations when increasing the nutrient input I. For very low input, only nutrients are present in the system (solution (5.7)). When $I > I^{TB1}$, with

$$I^{TB1} = \frac{b_1(d_1 + Df_1)}{a_1e_1 - d_1 - Df_1}\ , \tag{5.13}$$

phytoplankton becomes positive in a transcritical bifurcation (which was called TB1) at which the NP state (5.8) becomes stable. Since $I^{TB1} = 0.0008909$ is very small, this bifurcation can not be clearly seen in Figure 5.4. From this value on, further enrichment leads to a linear increase of phytoplankton (5.8), until a second transcritical bifurcation, TB2, at which zooplankton becomes positive and the NPZ solution (5.9) becomes stable. It happens at

$$I^{TB2} = \frac{(d_1 + Df_1)(P^{NPZ}d_1 - P^{NPZ}a_1e_1 - b_1De_1 + P^{NPZ}Df_1)}{De_1(d_1 - a_1e_1 + Df_1)} \tag{5.14}$$

where P^{NPZ} is the expression for P in the NPZ solution, (5.9). From this point the zooplankton starts increasing (keeping phytoplankton concentration at a constant value) until a new bifurcation TB3 occurs, at which the fish concentration starts to grow from zero while zooplankton remains constant, phytoplankton increases, and nutrients decrease (this is the positive interior solution NPZF, Eq. (5.12)). The value of I^{TB3} is given implicitly by:

$$d_3^{TB3} = \frac{Z^{NPZ}a_3e_3 - Z^{NPZ}Df_3 - b_3Df_3}{Z^{NPZ} + b_3} \tag{5.15}$$

where Z^{NPZ} is the expression for Z in the NPZ solution, (5.9).

One of the first counterintuitive indirect effects present in the food-chain dynamics has been noticed here: In the NPZF solution, increase of nutrient input leads to decrease in nutrient concentration (see Figure 5.4).

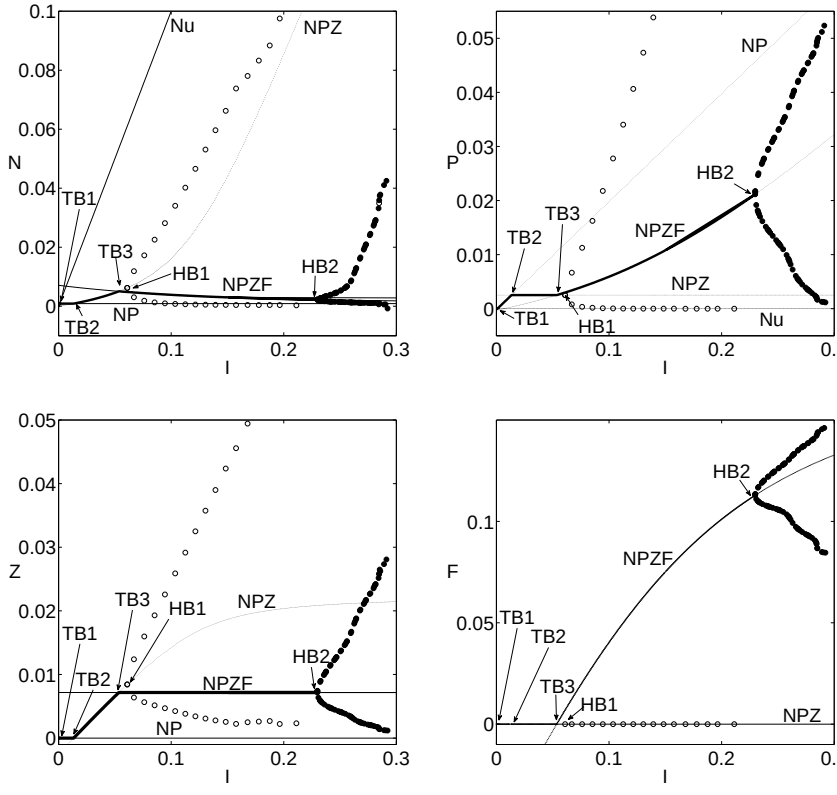

Figure 5.4. Bifurcation diagrams of the four variables as a function of nutrient input parameter I. Thick lines and full symbols denote stable fixed points and maxima and minima of stable cycles, respectively, and thin lines and open symbols, unstable ones. The name of the fixed points is indicated. The relevant bifurcations (described in the main text) occur at $I^{TB1} = 0.0008909\ mgN/l$, $I^{TB2} = 0.01345\ mgN/l$, $I^{TB3} = 0.05352\ mgN/l$, $I^{HB1} = 0.06101\ mgN/l$, and $I^{HB2} = 0.2298\ mgN/l$, locations which are indicated by arrows.

The reason is the top-down control that the higher predator begins to impose on zooplankton, leading to positive and negative regulation on the compartments situated one or two trophic levels below Z, respectively.

Shortly after becoming unstable at TB3, the fixed point NPZ experiences a Hopf bifurcation (HB1) which leads to a limit cycle on the NPZ hyperplane. Since the whole hyperplane has become unstable before this bifurcation occurs, this cycle has no direct impact on long time dynamics, although it can affect transients, and it will become relevant when adding contaminants. The steady coexistence of the three species at the NPZF fixed point remains stable until a new Hopf bifurcation HB2 occurs at which the fixed point becomes unstable and oscillations involving the three species and the nutrients (Figure 5.3) occur. The destabilization of steady coexistence by the appearance of oscillations, which could facilitate extinctions if the amplitude of oscillation is sufficiently large, is the well known "paradox of enrichment", first mathematically described by Rosenzweig (1971). A good overview of the studies connected with this issue can be found in the paper of Jensen and Ginzburg (2005). See also Bell (2002), Fussmann et al. (2000), Kirk (1998), Shertzer et al. (2002).

Gragnani et al. (1998) demonstrated that the dynamics of Canale's model for increasing nutrient supply is qualitatively similar to the one of the RMA model. After the stationary and cyclic states described above, chaotic behavior followed a different cyclic behavior with higher frequency are found. Also, the maximal average density of top-predator is attained at the edge between chaotic and high frequency cyclic behavior. We will not further describe these states but we will concentrate in the modifications arising from toxic effects of contaminants on the dynamics, for small and moderate nutrient loading.

5.4.2 Contaminant toxic to phytoplankton

Now the contaminant C_1 is introduced. It increases the mortality of phytoplankton according to expression (5.6) for $i = 1$. Expressions for the bifurcation lines TB1, TB2 and TB3 as a function of I and C_1 can be obtained simply by replacing the mortality (5.6) into the corresponding expressions (5.13), (5.14), and (5.15), respectively. The same can be done numerically for the Hopf bifurcation lines HB1 and HB2. The result is

shown in the 2-parameter bifurcation diagrams of Figure 5.5.

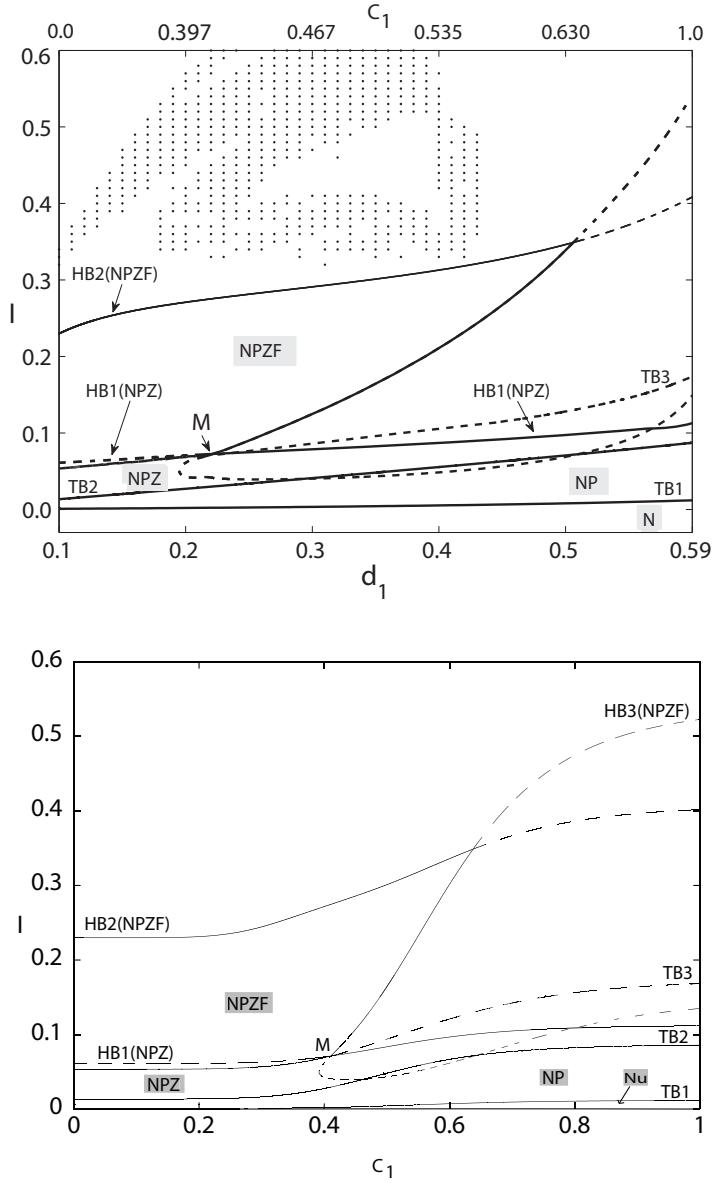

Figure 5.5

Figure 5.5. Upper graph: Some of the bifurcations occurring as a function of nutrient input I and the phytoplankton mortality d_1, in the range of values determined by the presence of contaminant C_1 affecting phytoplankton. Values of C_1 are also indicated in the upper horizontal axis. Lower graph: same plot but displayed in terms of C_1 instead of d_1. The name of the bifurcation lines is indicated (for the case of the Hopf lines HB1, HB2 and HB3, the name of the fixed point involved in the bifurcation is shown in parenthesis). Crossing the continuous lines involves a qualitative change for the state attained by the system. Inside regions surrounded by continuous lines, the name of the relevant stable fixed point is shown inside grey squares. Crossing the discontinuous bifurcation lines does not involve a change in the stable state (because, e.g., they correspond to bifurcations of already unstable states). Immediately above the HB2 line, a limit cycle involving all the species is the relevant attractor for low values of d_1 (or C_1). The limit cycle on the $F = 0$ hyperplane is the relevant attractor above the HB1 line for large d_1. Additional bifurcations (not shown) occur in other regions of the open areas above HB1 and HB2. M is a codimension-2 point described in the main text. In the upper graph the dotted region identifies areas where chaotic solutions have been found.

Because of the sigmoidal effect of the contaminant (5.6), its impact is mild for $C_1 \ll 0.5$, and it will saturate for $C_1 \gg 1$. Thus, in both limits the bifurcation lines become parallel to the horizontal axis. The interesting behavior is for intermediate values of C_1, where the bifurcation lines are displaced towards higher values of I. That is, the first effect of the contaminant is to stabilize the simplest solutions, the ones stable at lower nutrient load, delaying until higher nutrient loads the transitions to the most complex ones.

But this stabilizing effect is different for the different solutions, and the most important qualitative change occurs at point M in Figure5.5. It is a codimension-2 point at which the transcritical bifurcation TB3, involving the NPZ and the NPZF fixed points, and the Hopf bifurcation HB1 of the NPZ point, meet. A new Hopf bifurcation line of the NPZF equilibrium, HB3, emerges also from that point. The cycle created at HB3 consists in oscillations of all the four variables, similarly to the cycle created at HB2. Other characteristics of the organizing center M is that the Hopf bifurcations change subcritical to supercritical character across it, and also that a line (not shown) of saddle-node bifurcations of the cycles

created at HB1 and HB3 emerges also from M. There are a number of additional structures in parameter space emerging from double-Hopf points, and transcritical bifurcations of cycles which were not described further here.

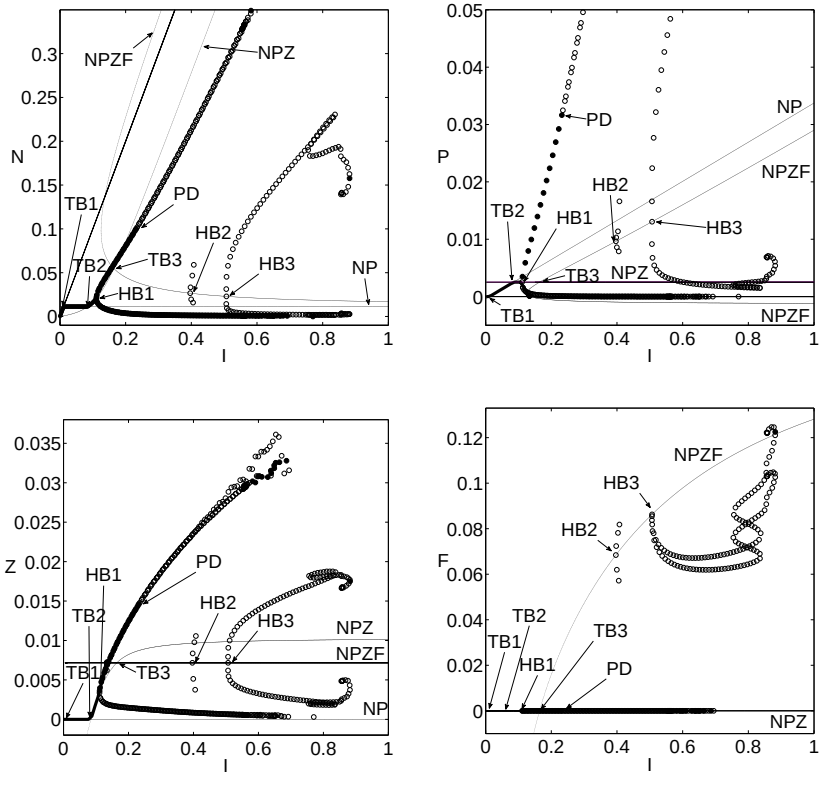

Figure 5.6. Bifurcation diagrams of the four variables as a function of nutrient input parameter I, at a constant high value of the contaminant affecting phytoplankton, $C_1 = 0.9$. Thick lines and full symbols denote stable fixed points and maxima and minima of stable cycles, respectively, and thin lines and open symbols, unstable ones. The name of the fixed points is shown. The bifurcation points are identified by arrows. PD is a period doubling bifurcation.

Despite the complexity of the above scenario, its effect on the bifur-

cation sequence when increasing nutrient level (up to moderate levels) in the presence of contaminant values beyond M is rather simple (see Figure 5.6): since the lines TB3 and HB1 have interchanged order, the Hopf bifurcation HB1 in which a stable limit cycle is created in the hyperplane $F = 0$ occurs before the appearance of a positive NPZF equilibrium. As a consequence, fish remains absent from the system even at relatively high nutrient levels. This is one of the counterintuitive outcomes of indirect effects: adding a substance which is toxic for phytoplankton makes fish to disappear, whereas the oscillating phytoplankton levels are indeed comparable with the ones at zero contaminant (see Figure 5.6). As in the absence of contaminant, period doubling and transition to chaos, which have not been analyzed in detail, occur when increasing further the value of I.

A different view of the transitions can be given by describing the bifurcations occurring by increasing the contaminant concentration at constant I. Figure 5.7 and 5.8 shows that for an intermediate value of the nutrient load, $I = 0.15\ mgN/l$. The NPZF fixed point is stable at low contaminant, but oscillations appear when crossing the HB3 lines. Very shortly after that, this limit cycle involving all species approaches the $F = 0$ hyperplane until colliding with the cycle lying on that plane, which involves only the N, P, and Z species. At this transcritical bifurcation, this limit cycle from which fish is absent becomes stable and is the observed solution for larger C_1 or d_1. As before, adding a substance which is toxic for the bottom of the trophic chain has the main effect of suppressing the top-predator.

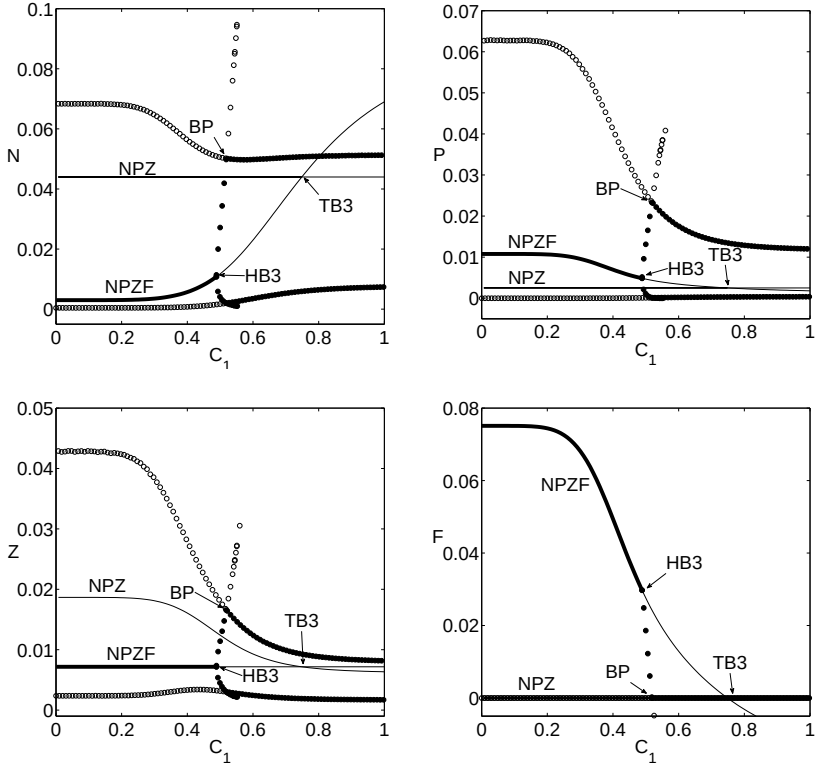

Figure 5.7. Bifurcation diagrams of the four variables as a function of C_1, at constant nutrient input $I = 0.15\ mgN/l$. Thick lines and full symbols denote stable fixed points and maxima and minima of stable cycles, respectively, and thin lines and open symbols, unstable ones. BP is a transcritical bifurcation of cycles. The name of the fixed points is shown. The bifurcation points are identified by arrows.

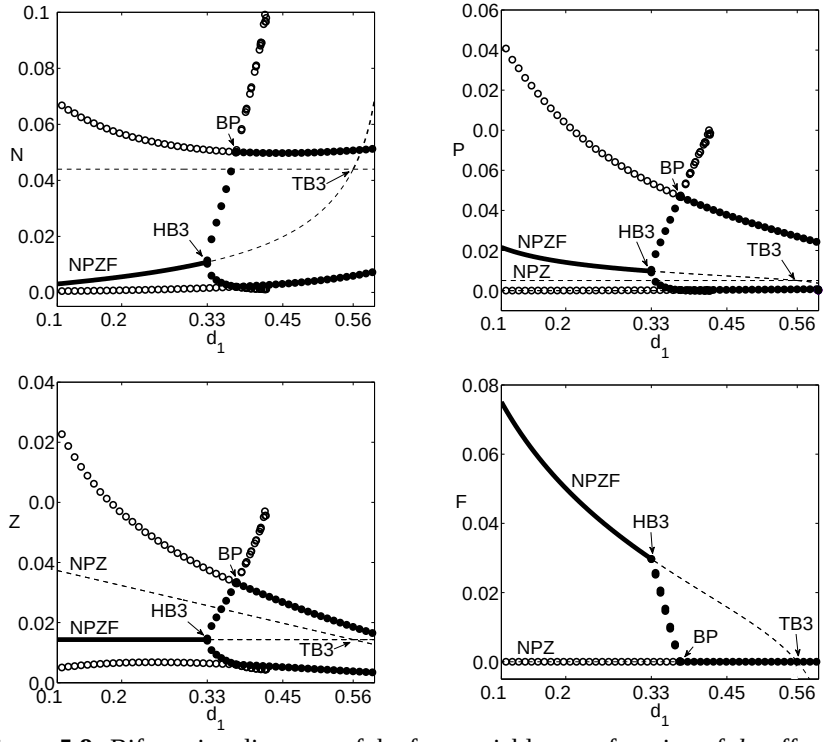

Figure 5.8. Bifurcation diagrams of the four variables as a function of d_1, affected by contaminant C_1, at constant nutrient input $I = 0.15\ mgN/l$. Thick lines and full symbols denote stable fixed points and maxima and minima of stable cycles, respectively, and thin lines and open symbols, unstable ones. BP is a transcritical bifurcation of cycles. The name of the fixed points is shown. The bifurcation points are identified by arrows.

5.4.3 Contaminant toxic to zooplankton

As before, the mortality expression (5.6) for $j = 2$ can be inserted in the expressions (analytical or numerical) for the bifurcations TB1, TB2, TB3, HB1, and HB2 to elucidate the impact of the contaminant C_2, acting on zooplankton, into the food chain dynamics. As in the C_1 case, the bifurcation lines become displaced to higher nutrient load values, so that the sequence of bifurcations of Figure 5.4 becomes delayed to higher values of I.

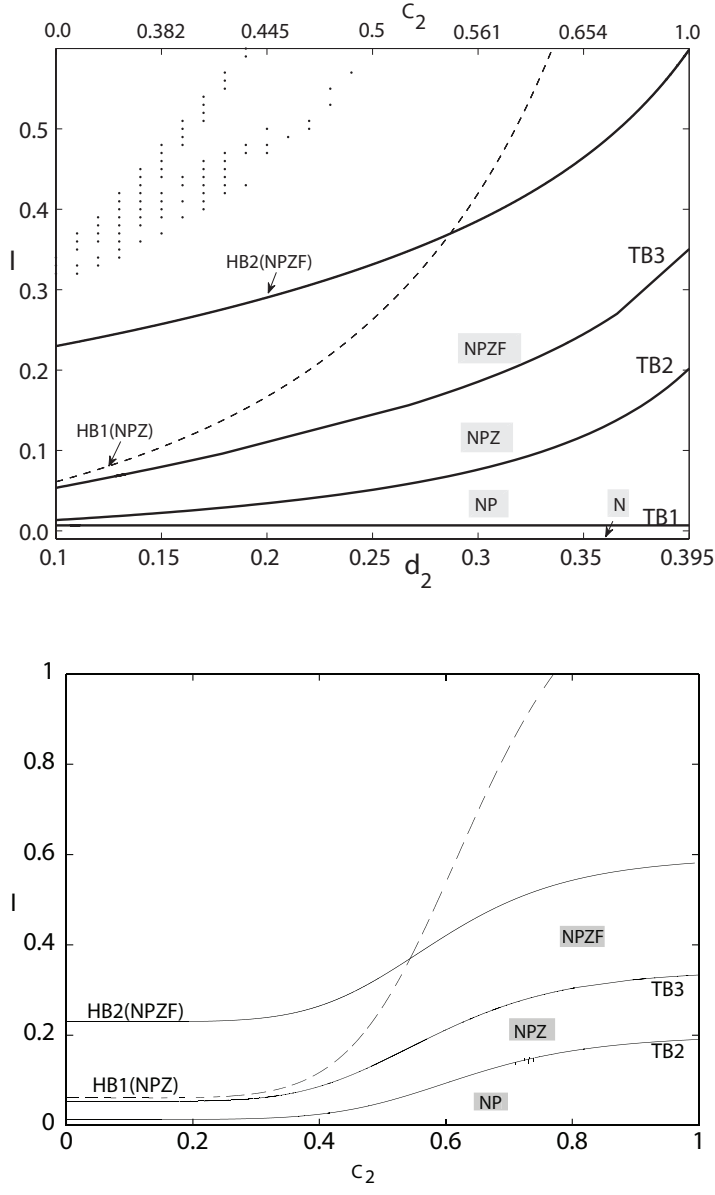
c2
0.0
0.382
0.445
0.5
0.561
0.654
1.0
I
HB2(NPZF)
TB3
NPZF
TB2
HB1(NPZ)
NPZ
NP
N
TB1
d2
0.1
0.15
0.2
0.25
0.3
0.35
0.395
I
NPZF
TB3
HB2(NPZF)
NPZ
TB2
HB1(NPZ)
NP
c2

Figure 5.9

Figure 5.9. Upper graph: some of the bifurcations occurring as a function of nutrient input I and zooplankton mortality d_2, in the range of values determined by the presence of contaminant C_2 affecting zooplankton. Values of C_2 are also indicated in the upper horizontal axis. Lower graph: same plot but displayed in terms of C_2 instead of d_2. Names of fixed points and bifurcation lines as in Figure 5.5, as well as the meaning of continuous and discontinuous lines. Immediately above the HB2 line, the relevant attractor is a limit cycle involving all the species. Additional bifurcations (not shown) occur at higher values of I. In the upper graph the dotted region identifies areas where chaotic solutions have been found

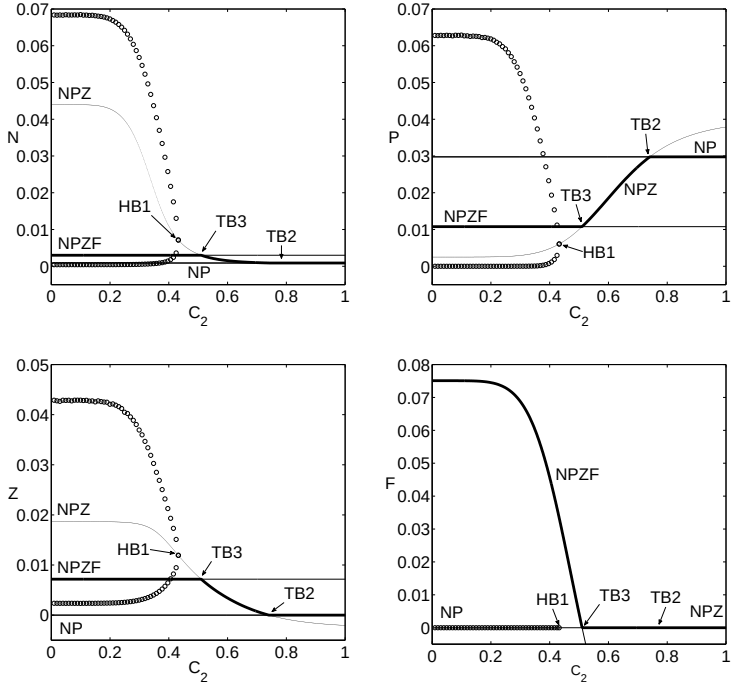

Figure 5.10. Bifurcation diagrams of the four variables as a function of C_2, for a constant nutrient load $I = 0.15\ mgN/l$. Thick lines denote stable fixed and thin lines and open symbols, unstable fixed points and maxima and minima of unstable cycles. The name of the fixed points is shown. The bifurcation points are identified by arrows.

This is seen in the 2-parameter bifurcation diagram of Figure 5.9. At difference with the C_1 case, the TB3 and HB1 lines do not cross, so that there are no further qualitative changes with respect to the case without contaminants (Figure 5.4), at least up to moderate values of I.

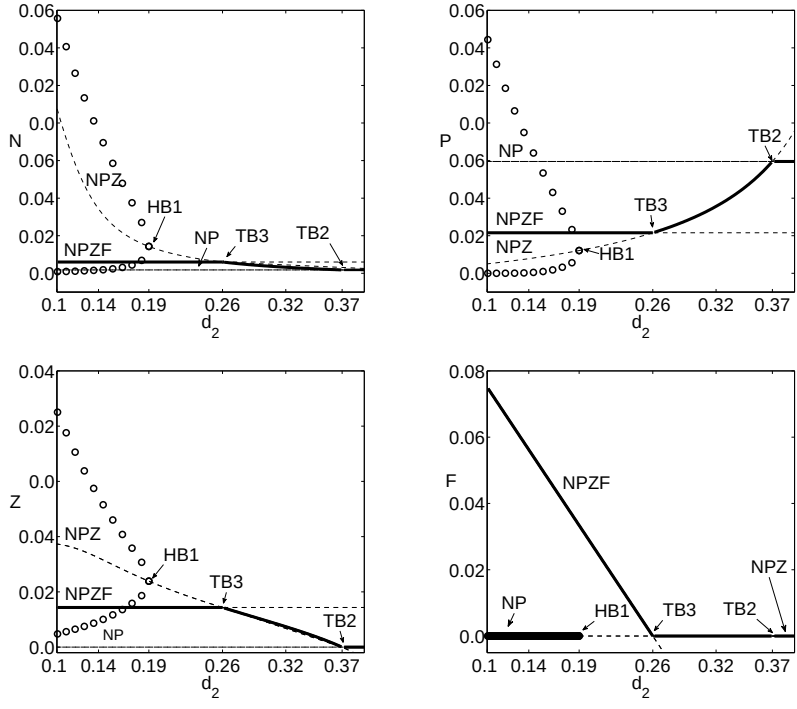

Figure 5.11. Bifurcation diagrams of the four variables as a function of d_2, affected by contaminant C_2, for a constant nutrient load $I = 0.15\ mgN/l$. Thick lines denote stable fixed and thin lines and open symbols, unstable fixed points and maxima and minima of unstable cycles. The name of the fixed points is shown. The bifurcation points are identified by arrows.

Another view of the consequences of Fig. 5.9 can be seen in Figures 5.10 and 5.11, which shows the different regimes attained at a fixed intermediate value of I ($I = 0.15\ mgN/l$) and increasing C_2 or d_2. The most remarkable indirect effect is that, for $d_2 < d_2^{TB3} = 0.2592\ day^{-1}$ ($C_2 < C_2^{TB3} = 0.5103$), zooplankton remains constant despite the increase

of C_2 which is toxic to it. The net effect of C_2 in this range is to decrease the amount of fish until extinction. Only for $C_2 > C_2^{TB3}$ contaminant kills zooplankton until extinction at $d_2 = d_2^{TB2} = 0.374\ day^{-1}$ ($C_2 = C_2^{TB2} = 0.7406$).

5.4.4 Contaminant toxic to fish

The simplest bifurcation lines are shown in Figure 5.12 as a function of I and C_3, the contaminant affecting fish mortality. As in the cases before, bifurcations are delayed to higher values of I when contaminant is present. As in the C_1 case, this delay is different for the different lines, resulting in a crossing of TB3 and HB1 in a codimension-2 point M, joining there also a new Hopf bifurcation HB3 of the NPZF fixed point and other bifurcation lines (not shown).

Additional structures emerging from other codimension-2 points, such as double-Hopf points are also presented but they were not studied in detail. The qualitative behavior when increasing I at large C_3 (Figure 5.13) is similar to the C_1 case: there is a succession of N, NP and NPZ fixed points followed by a Hopf bifurcation which leads to oscillations of the N, P and Z variables, remaining the fish absent from the system.

Only at relatively high nutrient values does the NPZF steady state become stable at the subcritical branch of the Hopf bifurcation HB3 before becoming unstable again at HB2. Two of the NPZF internal solutions (5.12) which, in contrast with the $C_3 = 0$ case, are positive here, collide at a limit point. In Figure 5.12 the line of these points as a function of the I and C_3 parameters is labelled as LP.

The two solutions exist above that line, and cease to exist below. The sequence of bifurcations encountered when increasing C_3 at constant intermediate values of I is also similar to the C_1 case of Figure 5.7 in that the NPZF stable fixed point becomes a cycle involving all the variables when HB3 is crossed, and in that this falls onto the $F = 0$ plane shortly afterwards. The details are, however, more complex because of the pres-

ence in phase space of additional unstable cycles.

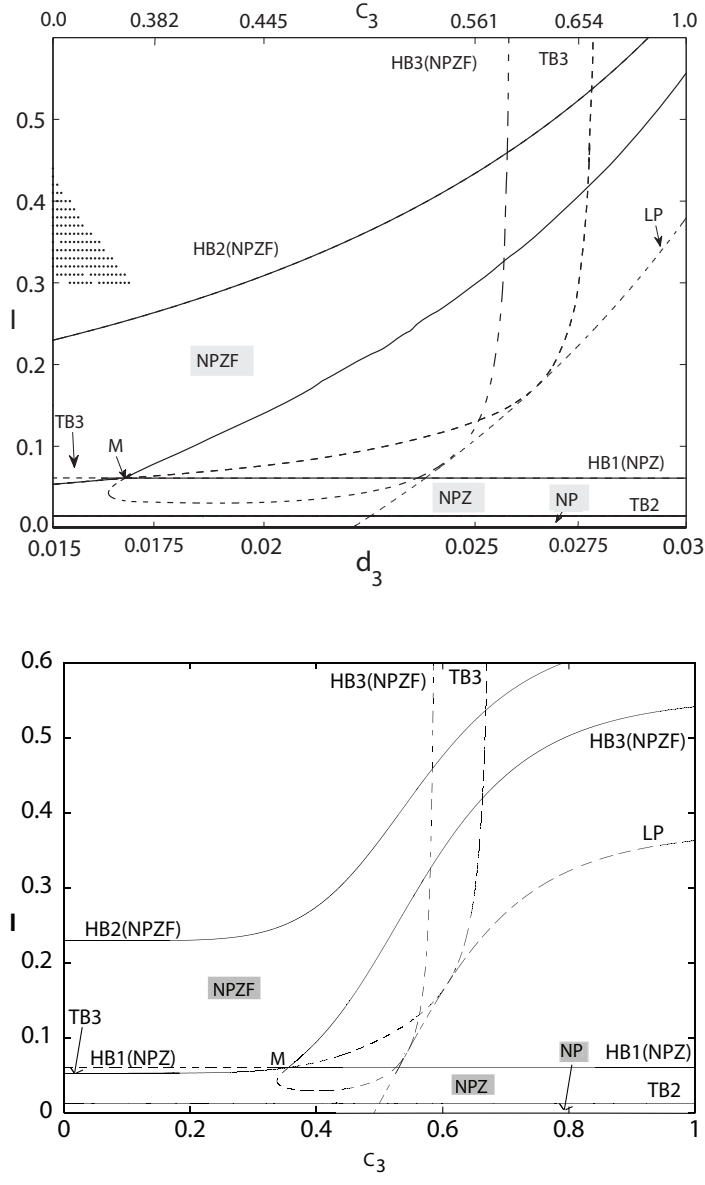

Figure 5.12

Figure 5.12. Upper graph: some of the bifurcations occurring as a function of nutrient input I and fish mortality d_3, in the range of values determined by the presence of contaminant C_3 affecting fish. Values of C_3 are also indicated in the upper horizontal axis. Lower graph: same plot but displayed in terms of C_3 instead of d_3. Names of fixed points and bifurcation lines as in Figure 5.5, as well as the meaning of continuous and discontinuous lines. Immediately above the HB2 line, the relevant attractor is a limit cycle involving all the species. Additional bifurcations (not shown) occur at higher values of I. There is a region of the area labelled as NPZF in which this stable fixed point coexists with a stable limit cycle on the $F = 0$ hyperplane.

5.5 Discussion and conclusion

We have seen that, because of the assumed sigmoidal influence of contaminant on mortality, toxic effects on our food chain model have a distinct effect at low and at large concentrations, with rather fast transition behavior in between.

At small and moderate contaminant concentrations the main effect is a displacement of the different bifurcations towards higher nutrient load values, so that transitions to states containing less active compartments, and states without oscillations, become relatively stabilized. Contaminants increase the stability of the food chain with respect to oscillations caused by increased nutrient input. A similar outcome has been observed in Upadhayay and Chattopadhayay (2005) for a food-chain model composed of a toxin producing phytoplankton, zooplankton and fish population. In that study chaotic dynamics can be stabilized by increasing the strength of toxic substance in the system.

For higher contaminant values, in most of the cases there is a reordering of the different transitions, giving rise to the appearance of new bifurcations which change qualitatively the sequence of states encountered by increasing nutrient input. The main effect, even in the cases in

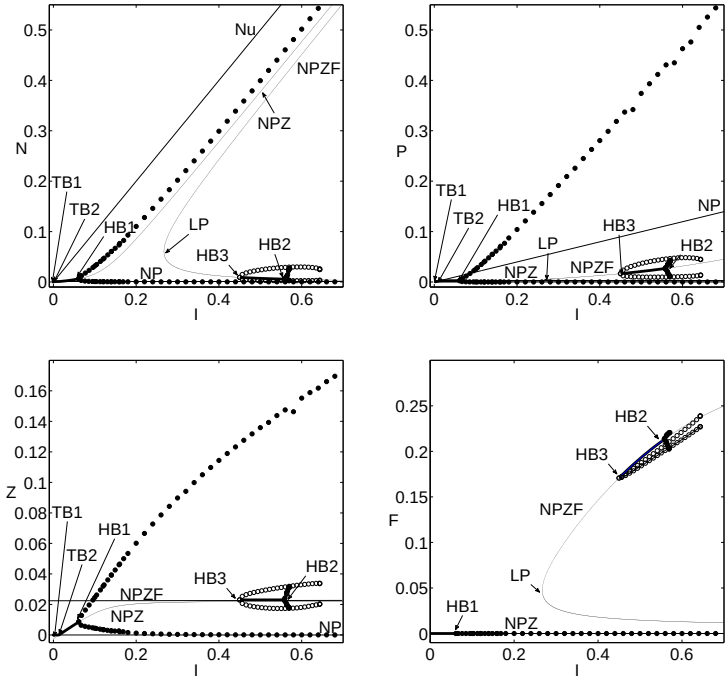

Figure 5.13. Bifurcation diagrams of the four variables as a function of nutrient input rate parameter I for a high value of the contaminant affecting fish, $C_3 = 0.7$. Thick lines and full symbols denote stable fixed points and maxima and minima of stable cycles, respectively, and thin lines and open symbols, unstable ones. The name of the fixed points is shown. The bifurcation points are identified by arrows. There is a small region of coexistence (between HB3 and HB2) of the stable NPZF fixed point and a stable limit cycle on the $F = 0$ hyperplane, which leads later to coexistence of two limit cycles.

which such reordering does not occur (the case of C_2 contaminant), is that the top predator becomes the most depleted, being even brought to extinction. This strong impact of the contaminant on the higher predator occurs even in the cases in which the direct toxic effect is on lower trophic levels. It seems that the increased mortality at lower trophic levels becomes nearly compensated by a debilitation of top-down control exerted by higher predators. Obviously, the top predator can not benefit from this mechanism, thus becoming the most affected.

Extrapolation of the above findings for real ecosystems may be problematic, because of the much higher food web complexity found in nature. We believe however that the counterintuitive indirect effects described above should be kept in mind when analyzing the complex responses that ecosystems display to changes in external drivers such as nutrient load and pollutants, and that the detailed identification of them performed here can help to interpret some aspects of the behavior of real ecosystems.

Bibliography

Abrams, P. A., Roth, J. D., 1994. The effects of enrichment of three-species food chains with non-linear functional responses. Ecology 75, 1118–1130.

Bell, T., 2002. The ecological consequences of unpalatable prey: phytoplankton response to nutrient and predator additions. Oikos 99, 59–68.

Boer, M. P., Kooi, B. W., Kooijman, S. A. L. M., 1998. Food chain dynamics in the chemostat. Math. Biosci. 150, 43–62.

Boer, M. P., Kooi, B. W., Kooijman, S. A. L. M., 2001. Multiple attractor and boundary crises in a tri-trophic food chain. Math. Biosci. 169, 109–128.

Canale, R. P., 1970. An analysis of models describing predator-prey interaction. Biotechnology and Bioengineering 12, 353–358.

Daskalov, G. M., 2002. Overfishing drives a trophic cascade in the Black sea. Mar. Ecol. Prog. Ser. 225, 53–63.

DeFeo, O., Rinaldi, S., 1997. Yield and dynamics of tritrophic food chains. The American Naturalist 150 (3), 328–345.

Doedel, E., Champneys, A., Fairgrieve, T., Kuznetsov, Y., Sandstede, B., Wang, X., 1997. Auto 97: continuation and bifurcation software for ordinary differential equations. Technical report, Concordia University, Montreal, Canada.

Ermentrout, B., 2002. Simulating, Analyzing, and Animating Dynamical Systems: A Guide to Xppaut for Researchers and Students (Software, Environments, Tools). SIAM: Society for Industrial and Applied Mathematical.

Fath, B. D., 2007. Network mutualism: Positive community-level relations in

ecosystems. Ecol. Model. 208, 56–67.

Fleeger, J. W., Carman, K., R.M.Nisbet, 2003. Indirect effects of contaminants in aquatic ecosystems. Sci. Total Environ. 317, 207–233.

Fussmann, G. F., Ellner, S. P., Sherzer, K. W., Jr, N. G. H., 2000. Crossing the Hopf bifurcation in a live predator-prey system. Science 290, 1358–1360.

Fussmann, G. F., Heber, G., 2002. Food web complexity and chaotic population dynamics. Ecol. Lett. 5, 394–401.

Gragnani, A., Feo, O. D., Rinaldi, S., 1998. Food chain dynamics in the chemostat: Relationships between mean yield and complex dynamics. Bull. Math. Biol. 60, 703–719.

Gugenheimer, J., Holmes, P., 1993. Nonlinear oscillations, dynamical systems and bifurcations of vector fields. Vol. 42. Applied mathematical sciences, Springer-Verlag, New York Inc.

Gunnarsson, J. S., D.Broman, Jonsson, P., Olsson, M., Rosenberg, R., 1995. Interactions between eutrophication and contaminants: towards a new research concept for the european aquatic environment. AMBIO 24, 383–385.

Gwaltney, C. R., Stadtherr, M. A., 2007. Reliable computation of equilibrium states and bifurcations in ecological systems analysis. Computers and Chemical Engineering 31 (8), 993 – 1005.

Gwaltney, C. R., Styczynski, M. P., Stadtherr, M. A., 2004. Reliable computation of equilibrium states and bifurcations in food chain models. Comput. Chem. Eng. 28, 1981–1996.

Hastings, A., Powell, T., 1991. Chaos in a three-species food chain. Ecology 72(3), 896–903.

Jackson, J. B. C., Kirby, M. X., Berger, W., Bjorndal, K., Botsford, L. W., Bourque, B. J., Bradbury, R. H., Cooke, R., Erlandson, J., Estes, J. A., Hughes, T. P., Kidwell, S., Lange, C. B., Lenihan, H. S., Pandolfi, J. M., Peterson, C. H., Steneck, R. S., Tegner, M. J., Warner, R. R., 2001. Historical overfishing and the recent collapse of coastal ecosystems. Science 293, 629–638.

Jensen, C. X. J., Ginzburg, L. R., 2005. Paradoxes or theoretical failure? the jury is still out. Ecol. Model. 188, 3–14.

Kirk, K. L., 1998. Enrichment can stabilize population dynamics: autotoxins and density dependence. Ecology 79 (7), 2456–2462.

Klebanoff, A., Hastings, A., 1994. Chaos in three-species food chains. J. Math. Biol. 32 (5), 427–451.

Kuznetsov, Y. A., Feo, O. D., Rinaldi, S., 2001. Belyakov homoclinic bifurcations in a tritrophic food chain model. SIAM J. Appl. Math. 62, 462–487.

Kuznetsov, Y. A., Rinaldi, S., 1996. Remarks on food chain dynamics. Math. Biosci. 134, 1–33.

Lima, I. D., Olson, D. B., Doney, S. C., 2002. Intrinsic dynamics and stability properties of size-structured pelagic ecosystem models. J. Plankton Res. 24 (6), 533–556.

McCann, K., Yodzis, P., 1994. Biological conditions for chaos in a three-species food chain. Ecology 75 (2), 561–564.

Mosekilde, E., 1998. Topics in Nonlinear Dynamics. Application to Physics, Biology and Economic Systems. World Scientific publishing, Singapore.

Rosenzweig, M. L., 1971. Paradox of enrichment: destabilization of exploitation ecosystems in ecological time. Science 171, 385–387.

Scheffer, M., Carpenter, S. R., 2003. Catastrophic regime shifts in ecosystems: linking theory to observation. Trends Ecol. Evol. 18, 648–656.

Scheffer, M., Carpenter, S. R., Foley, J. A., Folke, C., Walker, B., 2001. Catastrophic shifts in ecosystems. Nature 413, 591–596.

Shertzer, K. W., Ellner, S. P., Fussmann, G. F., Jr, N. G. H., 2002. Predator-prey cycles in an aquatic microcosm: testing hypotheses of mechanism. J. Anim. Ecol. 71, 802–815.

Strogatz, S. H., 2000. Nonlinear dynamics and chaos: With applications to physics, biology, chemistry, and engineering. Perseus Books group, Cambridge, Massachusetts.

Suter II, G. W., 1993. Ecological Risk Assessment. Lewis Publishers,Boca Raton, Florida.

Upadhayay, R. K., Chattopadhayay, J., 2005. Chaos to order: role of toxin producing phytoplankton in aquatic systems. Nonlinear analysis: modeling and control 10 (4), 383–396.

Zaldívar, J. M., Cattaneo, E., Plus, M., Murray, C. N., Giordani, G., Viaroli, P., 2003. Long-term simulation of main biogeochemical events in a coastal lagoon: Sacca di Goro (Northern Adriatic coast, Italy). Cont. Shelf Res. 23,

1847–1876.

6

Modeling approach to regime shifts of primary production in shallow coastal ecosystems

6.1 Introduction

Shallow transitional water systems (McLusky and Elliott, 2007) are intrinsically unstable and highly variable over wide temporal and spatial scales (Kjerfve, 1994, Zaldívar et al., 2008). These ecosystems, being interfaces between terrestrial and aquatic ecosystems, provide essential ecological functions influencing the transport of nutrients, material and energy from land to sea (Wall et al., 2001). Biodiversity can attain low values, but its functional significance remains high (Sacchi, 1995). Therefore, shifts in diversity are likely to have important and profound consequences for ecosystem structure and functioning (Levin et al., 2001). Invasions, competitive advantages, and non-linear feedback interactions may lead to alternating states and regime shifts (Scheffer et al., 2001), which, once occurred, may pose limits for remediation strategies since it may be difficult, if not impossible, returning to the original state (Webster and Harris, 2004).

Contrary to open seas, where primary production is dominated by phytoplankton, in transitional waters a considerable portion of primary production is performed by angiosperms, epiphytic algae[1], macroalgae and epibenthic microalgae. In addition, shallow aquatic ecosystems do

[1] Attached algae on natural substrates.

not show the typical correlation between nutrient inputs and chlorophyll-a in water (Nixon et al., 2001), as already demonstrated for deeper coastal waters and lakes (Vollenweider, 1976).

Regime shift phenomena occurring in shallow coastal areas (Flindt et al., 1999, Nienhuis, 1992, Sand-Jensen and Borum, 1991, Schramm, 1999, Viaroli et al., 1996) have been already documented as the result of the competition between free floating plants and submerged phanerogams.

Several authors have proposed a conceptual scheme that considers nutrient inputs as the main driver in the succession from benthic[2] vegetation to phytoplankton or floating seaweeds in shallow transitional waters (Borum, 1996, Hemminga, 1998, Nienhuis, 1992, Nixon et al., 2001, Valiela et al., 1997). This conceptual scheme is based on the evolution of benthic communities through several phases as the level of nutrients increases. In the pristine stage, the community is dominated by phanerogams species from a relatively small number of genera, i.e. Zostera, Thalassia, Halodule, Cymodocea, and Ruppia. Nutrient enrichment leads to an increase in epiphytic microalgae, followed by the increase in floating ephemeral macroalgae as Ulva and Gracilaria which compete for light and nutrients thus producing the disappearance of perennial seagrass species. Finally, at high levels of nutrient input, phytoplankton growth increases water turbidity enough to depress macroalgal growth thus leading to a dominance of phytoplankton species.

Even though the decline of seagrasses due to anthropogenic eutrophication is a world wide phenomenon (Orth et al., 2006, Short et al., 2006), there is no direct causality evidence from field data (Ralph et al., 2006). In addition, it is not evident from experimental studies where the limit lies for the dominance shift between these two competing type of organisms are (Hauxwell, 2004, Schramm, 1999). Field studies demonstrate that the decrease of seagrass meadows is directly related to nitrogen loadings (Hauxwell, 2004, Nelson, 2003) and the dominance of macroalgae, especially Ulvaes, becomes apparent in eutrophic environ-

[2]The benthic zone is the ecological region at the lowest level of a body of water such as an ocean or a lake, including the sediment surface and some sub-surface layers.

ments (Borum, 1996). An overview of seagrass responses to nutrient enrichment and/or eutrophication events is presented in Burkholder et al. (2007), whereas the evolution of several Mediterranean coastal lagoons from pristine conditions to the present situation is summarized in Viaroli et al. (2008).

Although nutrient loading is one of the main drivers of regime shifts in transitional waters, light and temperature have been also recognized as key abiotic factors controlling algal growth (Schramm, 1999). Furthermore, in transitional water ecosystems hydrological and hydrodynamic conditions affect community persistence (Dahlgreen and Kautsky, 2004, Marinov et al., 2007).

Regime shifts occurring in shallow aquatic ecosystems were analyzed by Scheffer and Carpenter (2003), who developed a minimum model with two ordinary differential equations, one considering floating plants and the other for submerged aquatic vegetation (SAV). Competition between floating vegetation and SAV was found to cause alternate attractors, since floating plants out compete SAV when light is the only limiting factor, whereas SAV species dominate at low nutrient concentrations since they are able to uptake nutrients from the sediments. The model, although not fully validated with experimental data, was the first to provide a comprehensive explanation of several observed phenomena.

In this work, we have studied the regime shifts from SAV to floating macroalgae in shallow brackish ecosystems. We have developed a basic model that accounts for the competition between Zostera marina and Ulva sp. using existing models by Bocci et al. (1997), Coffaro and Bocci (1997) and Solidoro et al. (1997a,b). To deal with the ability of seagrass to survive at low nutrient conditions, we have also included the dynamics of inorganic nitrogen (nitrates and ammonium) in the water column and in the sediments (Chapelle, 1995). A simple phytoplankton model (Plus et al., 2003) has been also incorporated in the main model.

The integrated model is able to simulate successions of dominance states, with different resilience characteristics according with the concep-

tual scheme. Regime shifts are found when changing nutrient input, temperature and light intensity forcing functions. Finally, a re-interpretation in terms of sensitivity to initial and operating values is discussed for mesocosm experiments.

6.2 Methods

6.2.1 Model formulation

The model is based on previous existing and validated models developed for Mediterranean coastal lagoons, i.e. Venice lagoon (Italy) and Etang de Thau (France). This approach was chosen because it would allow the flexibility of analyzing different scenarios for these types of ecosystems which are subjected to strong anthropogenic pressures. In addition, previously validated models can offer more robust results than a de novo approach when there is no experimental data adequate for their validation.

Zostera marina model

The Z. marina sub-model is based on the model described in Bocci et al. (1997) and Coffaro and Bocci (1997). State variables in this sub-model are: Zs (shoot biomass, gdwm^{-2}), Zr (rhizome-root biomass, gdwm^{-2}) and Nz (internal nitrogen quota, mgNgdw^{-1}).

Figure 6.1: *Zostera marina*

Zostera growth is described as fol-

lows:

$$\frac{dZs}{dt} = (growth_z - trans - respiration_s)Zs \quad (6.1)$$

$$\frac{dZr}{dt} = trans(Zs - respiration_r)Zr \quad (6.2)$$

$$\frac{dNz}{dt} = (uptake_z - growth_z)Nz \quad (6.3)$$

The influence of the limiting factors on Zostera growth is described with a multiplicative formulation:

$$growth_z = \mu^z_{max} f_1(I) f_2(T) f_3(Nz) f_4(Zs) f_5(NO_3^-) \quad (6.4)$$

The functional forms as well as the parameters of the model are described in Table 6.1. The f_5 term has been introduced in the Bocci et al. (1997) model to take into account that water-column nitrate enrichment promotes decline of Z. marina independently of algal light attenuation. According to Burkholder et al. (1992) this is probably due to internal imbalances in nutrient supply ratios.

In this formulation, the growth of rhizome depends on the translocation of photosynthetic products from leaves to below-ground parts of the plant. This translocation is proportional to the rate of growth:

$$trans = K_{trans} \times growth_z \quad (6.5)$$

The parameter K_{trans} was estimated by Olesen and Sand-Jensen (1993) as 25% of the growth, i.e. K_{trans} = 0.25. Shoot biomass losses are expressed as a function of shoot respiration rate at 20 °C, SR_{20}, corrected by the actual temperature:

$$respiration_s = SR_{20} \times f_s(T) \quad (6.6)$$

where

$$f_s(T) = 0.098 + exp(.4.690 + 0.2317T) \quad (6.7)$$

Following a similar approach, rhizome-root biomass loss processes are considered as a function of a respiration coefficient, RR_{20}, with a temperature correction:

$$respiration_r = RR20 \times f_s(T) \tag{6.8}$$

Internal nitrogen quota in Zostera has been modelled as a function of nitrogen uptake. Shoots can uptake nitrates and ammonium, whereas the rhizome-root can only uptake ammonium.

$$uptake_z = (uptake_s + uptake_r)\, f_u(Nz) \tag{6.9}$$

$$uptake_s = uptake_s^{NH_4^+} + uptake_s^{NO_3^-} \tag{6.10}$$

$$uptake_s^{NH_4^+} = V_{max_s}^{NH+4} \frac{[NH_4^+]}{[NH_4^+] + K_s^{NH_4^+}} \tag{6.11}$$

$$uptake_s^{NO_3^-} = V_{max_s}^{NO_3^-} \frac{[NO_3^-]}{[NO_3^-] + K_s^{NO_3^-}} \tag{6.12}$$

$$uptake_r = V_{max_r}^{NH_4^+} \frac{[NH_4^+]_s}{[NH_4^+]_s + K_r^{NH_4^+}} \tag{6.13}$$

$$f_u(Nz) = \frac{Nz_{max} - Nz}{Nz_{max} - Nz_{min}} \tag{6.14}$$

The values of parameters are summarized in Table 6.1.

Ulva rigida model

The U. rigida sub-model is based on the model described in Solidoro et al. (1997a,b). State variables in this sub-model are: U (Ulva biomass, $gdwl^{-1}$) and Nu (internal nitrogen quota, $mgNgdw^{-1}$). The model can be written as

Figure 6.2: *Ulva rigida*

Table 6.1. Parameters and computed quantities used in the Zostera marina model from Bocci et al. (1997) and Coffaro and Bocci (1997).

Parameters computed quantities	*Description*	*Value*
μ^z_{max}	*Maximum specific growth*	$0.0025h^{-1}$
$f_1(I)$	$f_1(I) = \frac{I}{I+K_z}$	
K^z_I	*Semisaturation constant for light*	$500kcalm^{-2}d^{-1}$
	$I = I_0 exp[.(\varepsilon_w + \varepsilon_u U)z]$	
ε_w	*Water extinction coefficient*	$0.4m^{-1}$
ε_u	*Ulva shading coefficient*	$40lgdw^{-1}m^{-1}$
$f_2(T)$	$f_2(T) = exp\left[-\left(\frac{T-T^z_{opt}}{T^z_{width}}\right)^2\right]$	
T^z_{opt}	*Optimal temperature*	$20°C$
T^z_{width}	*Temperature range, sigmoid width*	$3.6°C$
$f_3(Nz)$	$f3(Nz) = \frac{Nz-Nz_{min}}{Nz_{crit}-Nz_{min}}$	
Nz_{min}	*Minimum internal nitrogen quota*	$5.0mgNgdw^{-1}$
Nz_{max}	*Maximum internal nitrogen quota*	$30.0mgNgdw^{-1}$
Nz_{crit}	*Critical internal nitrogen quota*	$15.0mgNgdw^{-1}$
$f_4(Zs)$	$f_4(Zs) = 1 - exp\left[-\left(\frac{Zs-Zs_{max}}{Zs_{width}}\right)^2\right]$	
Zs_{max}	*Maximum shoot biomass*	$500gdwm^{-2}$
Zs_{width}	*Growth dependence on space availabilit*	$5gdwm^{-2}$
	$f_5(NO_3^-) = exp\left[-\left(\frac{NO_3^- - NO^-_{3_{opt}}}{NO^-_{3_{width}}}\right)^2\right]$	
$NO^-_{3_{opt}}$	*Optimal nitrate concentration*	$5.0mmolm^{-3}$
$NO^-_{3_{width}}$	*Nitrate concentration range*	$80.0mmolm^{-3}$
SR_{20}	*Shoot respiration rate at* $20°C$	$1.0042 \times 10^{-3}h^{-1}$
RR_{20}	*Rhizome-root respiration rate at* $20°C$	$6.25 \times 10^{-4}h^{-1}$
$V^{NH_4^+}_{max_s}$	*Shoot maximum uptake for* NH_4^+	$0.3mgNgdw^{-1}h^{-1}$
$K_z^{NH_4^+}$	*Shoot half saturation constant for* NH_4^+	$9.29mmolNm^{-3}$
$V^{NO_3^-}_{max_s}$	*Shoot maximum uptake for* NO_3^-	$0.06mgNgdw^{-1}h^{-1}$
$K_z^{NO_3^-}$	*Shoot half saturation constant for* NO_3^-	$16.43mmolNm^{-3}$
$V^{NH_4^+}_{max_r}$	*Rhizome-root maximum uptake for* NH_4	$0.02mgNgdw^{-1}h^{-1}$
$K^{NH_4^+}_{max_r}$	*Rhizome-root half saturation constant for* NH_4^+	$5.0mmolNm^{-3}$

$$\frac{dU}{dt} = (growth_u - death_u)U \tag{6.15}$$

The influence of the limiting factors on Ulva growth was described with a multiplicative formulation:

$$growth_u = \mu^u_{max} \times g_1(I) \times g_2(T) \times g_3(Nu) \tag{6.16}$$

The functional forms of the algae model are described in Table 6.2. As we do not consider oxygen dynamics explicitly, the mortality in this model does not follow Solidoro et al. (1997a,b) model. In this case, the mortality term has been expressed as a simple constant and a density dependent function:

$$death_u = k^u_d + k^u_t exp\left[-\left(\frac{U - U_{max}}{U_{width}}\right)^2\right] \tag{6.17}$$

Like Z. marina, Ulva is able to store nitrogen, therefore Solidoro et al. (1997a,b), introduced the tissue concentration of this element (Nu) as a separated state variable. Its dynamics can be expressed as

$$\frac{dNu}{dt} = (uptake_u - growth_u)Nu \tag{6.18}$$

The specific uptake rate of nitrogen depends on the chemical form available and on the level Nu of nitrogen tissue concentration. Hence, uptake can be written as

$$uptake_u = (uptake_u^{NH_4^+} + uptake_u^{NO_3^-})\, f_u(Nu) \tag{6.19}$$

Table 6.2. Parameters and computed quantities used in the Ulva model from Solidoro et al. (1997a) and Solidoro et al. (1997b).

Parameters, computed quantities	*Description*	*Value*
μ^u_{max}	*Maximum specific growth*,	$0.0167h^{-1}$
$g_1(I)$	$g_1(I) = \frac{I}{I+K^u_I}$	
K^u_I	*Semisaturation constant for light*	$239kcalm^{-2}d^{-1}$
$g_2(T)$	$g_2(T) = \frac{1}{1+exp(-\zeta(T.T_U))}$	
ζ	*Temperature coefficient*	$0.2°C^{-1}$
T_U	*Temperature reference*	$12.5°C$
$g_3(Nu)$	$g_3(Nu) = \frac{Nu-Nu_{min}}{Nu-Nu_{crit}}$	
Nu_{min}	$Min.value\,for N quota$	$10.0mgN/gdw$
Nu_{crit}	*Critical N quota level*	$7.0mgN/gdw$
Nu_{max}	*Max. value for N quota, uptake limitation*	$42.0mgN/gdw$
k^u_d	*Mortality rate*	$6.2.10^{-3}h^{-1}$
k^u_t	*Mortality rate due to biomass*	$1.0h^{-1}$
U_{max}	*Growth dependence on space availability*	$0.01gdwl^{-1}$
$V^{NH_4^+}_{max_u}$	*Max. specific uptake rate for ammonium*	$8.5mgNgdw^{-1}h^{-1}$
$V^{NO_3^-}_{max_u}$	*Max. specific uptake rate for nitrate*	$0.45mgNgdw^{-1}h^{-1}$
$K^{NH_4^+}_u$	*Half-saturation for ammonium*	$7.14mmol/m^3$
$K^{NO_3^-}_u$	*Half-saturation for nitrate*	$3.57mmol/m^3$

whereas

$$uptake^{NH_4^+}_u = V^{NH_4^+}_{max_u} \frac{[NH_4^+]}{[NH_4^+] + K^{NH_4^+}_u} \tag{6.20}$$

$$uptake^{NO_3^-}_u = V^{NO_3^-}_{max_u} \frac{[NO_3^-]}{[NO_3^-] + K^{NO_3^-}_u} \tag{6.21}$$

$$f_u(Nu) = \frac{Nu_{max} - Nu}{Numax - Nu_{min}} \tag{6.22}$$

Phytoplankton model

A simple phytoplankton module was introduced in the model. The module, developed for Etang de Thau (France), has been adapted from Plus et al. (2003). Phytoplankton will compete for nutrients in the water column and will have a shadowing effect less pronounced than that of Ulva on benthic vegetation.

Figure 6.3. Phytoplankton of winter-spring proliferation in the Catalan-Balearic sea. Photo: Marta Estrada

$$\frac{dP}{dt} = (growth_P - death_P)P \qquad (6.23)$$

The influence of the limiting factors on phytoplanton growth was described with a multiplicative formulation (Plus et al., 2003):

$$growth_P = \mu^P_{max} \times h_1(I) \times h_2(T) \times h_3(N) \qquad (6.24)$$

whereas mortality is also described as a function of temperature:

$$death_P = m_0 e^{\varepsilon T} \qquad (6.25)$$

As we do not explicitly consider zooplankton grazing explicitly, the mortality function in this model has been changed accordingly. Phytoplankton nutrient uptake can be expressed as a function of the nutrient limitation expression and phytoplankton biomass as in Plus et al. (2003). The functional forms of the phytoplankton growth model as well as the main parameters are described in Table 6.3.

Dissolved inorganic nitrogen (DIN) model

To model the competition between Zostera and Ulva it is necessary to include nutrient consumption. The nutrients included are nitrogen in the

Table 6.3. Parameters and computed quantities used in the phytoplankton model from Plus et al. (2003).

Parameters, computed quantities	*Description*	*Value*
μ^P_{max}	*Maximum specific growth*,	$0.021h^{-1}$
$h_1(I)$	$h_1(I) = (1 - e^{-I/I_k})$	
I_k	*Saturation constant for light*	$620.1kcalm^{-2}d^{-1}$
$h_2(T)$	$h2(T) = e^{\varepsilon \cdot T}$	
ε	*Temperature Coefficient*	$0.07°C^{-1}$
$h_3(N)$	$\frac{[NH_4^+]}{[NH_4^+]+K_N} + \frac{NO_3^-}{NO_3^-+K_N} e^{-\psi[NH_4^+]}$	
K_N	*Half-saturation constant for N limitation*	$2.0mmolm^{-3}$
ψ	*Wroblewski inhibition factor*	$1.5m^3mmol^{-1}$
m_0	*Mortality rate at*$0C$	$1.15 \times 10^{-2}h^{-1}$

oxidized and reduced forms. Furthermore, in shallow water bodies, sediments play a fundamental role in the nutrient dynamics and in this case Zostera is able to uptake ammonium from sediments (Coffaro and Bocci, 1997). For these reasons, the dynamics of DIN in sediments has been introduced as well. The model, adapted from Chapelle (1995), can be written as

(a) Dissolved Inorganic Nitrogen (DIN) in the water column

$$\frac{d[NO_3^-]}{dt} = Nitrif_w - uptake^{NO_3^-} + \frac{Qd^{diffusion}_{NO_3^-}}{watervol} + Q^{input}_{NO_3^-} - Q^{output} NO_3^- \tag{6.26}$$

$$\frac{d[NH_4^+]}{dt} = -Nitrif_w - uptake^{NH_4^+} + \frac{Q^{diffusion}_{NH_4^+}}{watervol} + Q^{input}_{NH_4^+} - Q^{output}_{NH_4^+} \tag{6.27}$$

Nitrification rates in the water column are functions of water temperature and oxygen concentration, and they can be expressed as

$$Nnitrif_w = k_{nit} exp(k_t T)[NH_4^+] \tag{6.28}$$

$[NO_3^-]$ uptake ($mmolNm^{-3}h^{-1}$) can be divided into Ulva, Zostera and phytoplankton uptake:

$$uptake^{NO_3^-} = \alpha_1(uptake_u^{NO_3^-} + uptake_z^{NO_3^-}) + uptake_p^{NO_3^-} \tag{6.29}$$

whereas α_1 is a conversion factor to pass from mgN to mmol N. $[NH_4^+]$ uptake ($mmolNm^{-3}h^{-1}$) can also be divided into Ulva, Zostera and phytoplankton uptake:

$$uptake^{NH_4^+} = \alpha_1(uptake_u^{NH_4^+} + uptake_z^{NH_4^+}) + uptake_p^{NH_4^+} \tag{6.30}$$

At the interface between the water column and the interstitial water, diffusion is responsible for [NO-3] and [NH+4] fluxes ($mmolNm^{-3}h^{-1}$).

These fluxes can be represented as

$$Q_{NO_3^-}^{diffusion} = D_{NO-3}\frac{A\beta}{z_s}([NO_3^-]_s - [NO_3^-]) \quad (6.31)$$

$$Q_{NH_4^+}^{diffusion} = D_{NH_4^+}\frac{A\beta}{z_s}([NH+4]_s - [NH_4^+]) \quad (6.32)$$

whereas D_X are the sediment diffusion coefficients (m^2h^{-1}), A the exchange area ($1m^2$), z_s the distance between the centres of the water and sediment layers, and β is the sediment layer porosity (Chapelle, 1995).

This DIN submodel behaves as a CSTR (Continuous Stirred Tank Reactor), where the forcing is given by the fluxes of nutrients. For example, for nitrate it can be written:

$$Q_{NO_3^-}^{input} = \frac{F[NO_3^-]_{initial}}{V} \quad (6.33)$$

$$Q_{NO_3^-}^{output} = \frac{F[NO_3^-]}{V} \quad (6.34)$$

where F refers to the water flow (m^3/h), V the total volume ($1m^3$) and $[NO_3^-]$initial is the initial concentration of nitrate that enters into the system. (b) DIN in the sediments

$$\frac{d[NO_3^-]_s}{dt} = Nitrif_s - Ndenit - \frac{Q_{NO_3^-}^{diffusion}}{interstvol} \quad (6.35)$$

$$\frac{d[NH_4^+]_s}{dt} = (1-\alpha_{denit})Ndenit - Nitrif_s - uptake_r - \frac{Q_{NH_4^+}^{diffusion}}{interstvol} \quad (6.36)$$

Nitrification in the sediments, $Nitrif_s$, can be described as a first order process in ammonium concentration at the sediment:

$$Nnitrif_s = k_{nit} \times f_1(T) \times f_2(O) \times [NH_4^+]_s \quad (6.37)$$

whereas nitrate reduction can be expressed as a first order process in nitrate concentration at the sediment:

$$Ndenit = k_{denit} \times f_1(T) \times f_3(O) \times [NO_3^-]_s \tag{6.38}$$

Nitrogen mineralization has not been taken into account in this model. Oxygen concentration is considered constant. The values of parameters taken form Chapelle (1995) are summarized in Table 6.4.

6.2.2 Forcing functions and parameters

In all the runs, the model has been forced by imposing temperature and solar radiation sinusoidal forcing, which have the following form:

$$T = A_T \ sin\left(2\pi\left(\frac{t-114.74}{365}\right)\right) + T_m \tag{6.39}$$

$$I = A_I \left[sin\left(2\pi\left(\frac{t-90}{365}\right)\right) + 1\right] + I_m \tag{6.40}$$

Parameters, amplitude and mean value, were adjusted using meteorological data from several Mediterranean stations, but, in any case, their influence is going to be analyzed.

Nutrient inputs and flows have been maintained constant during each simulation run. This is not typical under natural conditions where nutrient loadings delivered to coastal systems undergo seasonal variations due to rainfall regimes. In addition in the Mediterranean climate region, nutrient loadings to coastal marine systems can attain short-term peaks following heavy rainfall events (Plus et al., 2006). Furthermore, oxygen concentrations were set constant at $8.0 gm^{-3}$ during all simulations, whilst in transitional water ecosystems they undergo daily and seasonal variations from supersaturation to anoxia (Viaroli and Christian, 2003).

Table 6.4: Nutrient and sediment parameters, from Chapelle (1995).

Parameters, computed quantities	*Description*	*Value*
k_{nit}	*Nitrification rate at* $0°C$	$0.0083h^{-1}$
$f_1(T)$	$f_1(T) = exp[k_T T]$	
k_T	*Temperature increasing rate*	$0.07°C^{-1}$
$f_2(O)$	$f_2(O) = \frac{[O_2]_s}{K_{NitO}+[O_2]_s}$	
k_{NitO}	*Half-saturation coefficient for* O_2 *limitation of nitrification*	$4.0g/m^3$
$RUPC$	*Ulva stoichiometric ratio*	$2.5mgP/gdw$
QPS	*Photosynthetic ratio*	1.5
$RPHY$	*Phytoplankton respiration rate at* $0°C$	$2.083 \times 10^{-3}h^{-1}$
ψ	*Stoichiometric ratio*	$1450gO_2/gdw$
RPS	O_2 *produced*$/N$	$0.212gO_2/mmol$
D_{NO}	*Diffusion coefficient for nitrate in the sediment*	$0.00072m^2/h$
D_{NH}	*Diffusion coefficient for ammonium in the sediment*	$0.00072m^2/h$
A	*Surface of computational cell*	$1m^2$
z_S	*Distance between the centre of water cell and sediment layer*	$0.51m$
$watervol$	*Volume of the water cell*	$1m^3$
$interstvol$	*Interstitial water volume for a cell*	$0.008m^3$
k_{denit}	*Denitrification rate at* $0°C$	$0.0125h^{-1}$
$f_3(O)$	$f_3(O) = 1 - \frac{[O_2]_s}{K_{denitO}+[O_2]_s}$	
$[O_2]$	*Oxygen concentration*	$8g/m^3$
K_{denitO}	*Half-saturation coefficient for* O_2 *limitation of denitrification*	$2.0g/m^3$
α_{denit}	*Percentage of N denitrified into* N_2	0.6
$f_4(O)$	$f4(O) = \frac{[O2]_s}{K_{minO}+[O_2]_s}$	
K_{minO}	*Half-saturation coefficient for* O_2 *limitation of mineralization*	$0.5g/m^3$

6.2.3 Assessment of mesocosm data

Mechanistic experiments dealing with phanerogams-macroalgae- phytoplankton competition were carried out using mesocosms under controlled conditions (Nixon et al., 2001, Taylor et al., 1999). In this work we have re-assessed the mesocosms experiments reported by Taylor et al. (1999). In these experiments (five settings, each with two replicates: Control, C, Low, L, Medium, M, High, H and Very High, VH) enrichment with ammonium and phosphate at several levels was performed and results monitored from April to September.

The following assumptions were made to simulate these experiments:

- Light intensity was assumed to be not a limiting factor for any of the three taxa.
- Temperature was simulated using a sinusoidal function as in Eq.(6.39) with $T_m = 10.5$ and $A_T = 10.1^{\circ}C$, respectively.
- Dissolved inorganic phosphorous (DIP) was not considered.
- Dissolved inorganic nitrogen (DIN) was equally partitioned between nitrates and ammonium in the background concentration.
- Initial conditions of Zostera above-ground biomass were taken constant at $50 gdwm^{-2}$ whereas the influence of initial conditions of Ulva and phytoplankton was assessed.
- A constant flow,$F = 5.3 \times 10^{-3} m^3 h^{-1}$ was assumed during all the experiment, as well as a constant concentration input of nitrate, $[NO^{-3}]_{input} = 2.4 mmol m^{-3}$ and ammonium, $[NH+4]_{input} = 2.4$, 20.6, 38.7, 75.1, 148.0 $mmol m^{-3}$, for the different experimental conditions (C, L, M, H and VH).

6.3 Results

6.3.1 Competition between Zostera and Ulva

The first set of simulations was run excluding phytoplankton, to compare with field observations for which no phytoplankton data were mentioned. At low DIN_{input} concentrations $(5 mmol m^{-3})$ Zostera survives and Ulva disappears (Figure 6.5).

Figure 6.4. Rocks and submerged algae in "Abrolhos" (Brasil). Photo: André Luis Sousa Sena.

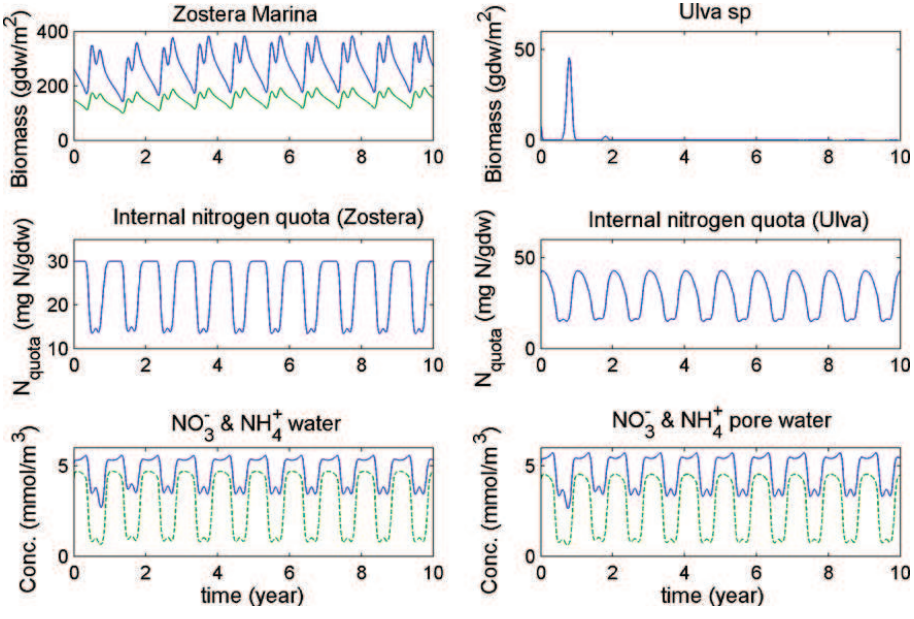

Figure 6.5. Zostera biomasses Zs (shoot biomass, gdwm-2) and Zr (rhizome-root biomass, gdwm-2, in green); Ulva biomasses (gdwm-2); internal nitrogen quotas; DIN concentrations (NO_3^- : blue, NH_4^+ : green) in the water column and in the sediments (pore water). $F = 0.1 m^3 h^{-1}$, and $[NO^{-3}]_{input} = [NH_4^+]_{input} = 5 mmol m^{-3}$ (low nutrient situation).

In addition, due to the relatively high flow of DIN into the system, nitrogen is not completely depleted and the dynamics in the water column and in the sediments are tightly coupled. However, there is a certain transient period of few years before the limit cycle is reached, during which both vegetation types coexist.

Figure 6.6. A green tide in Brittany, beach of Saint-Michel en Grève/Saint Efflam (IFREMER), Northern Brittany (France)

The contrary effect, i.e. dominance by Ulva, may be observed at high input DIN concentrations ($50 mmol m^{-3}$, see Figure 6.7). Keeping high nutrient loads, Zostera will disappear after a few years while Ulva will tend to prevail.

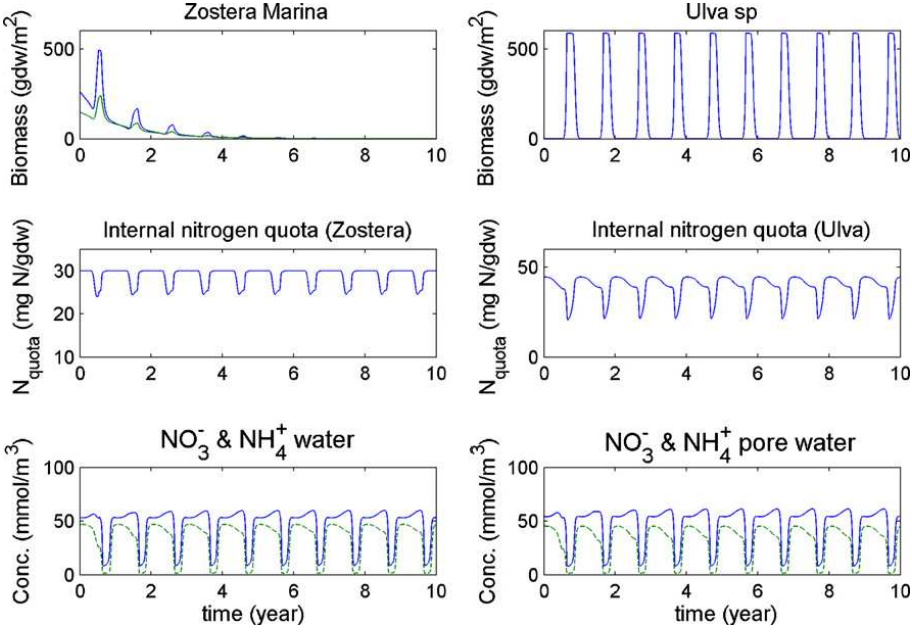

Figure 6.7. Zostera biomasses: Z_s (shoot biomass, $gdwm^{-2}$) and Z_r (rhizome-root biomass, $gdwm^{-2}$, in green); Ulva biomasses ($gdwm^{-2}$); internal nitrogen quotas; DIN concentrations (NO^{-3} : blue, NH^{+4} : green) in the water column and in the sediments (pore water). $F = 0.1 m^3 h^{-1}$, and $[NO_3^-]_{input} = [NH_4^+]_{input} = 50 mmol m^{-3}$ (high nutrient situation).

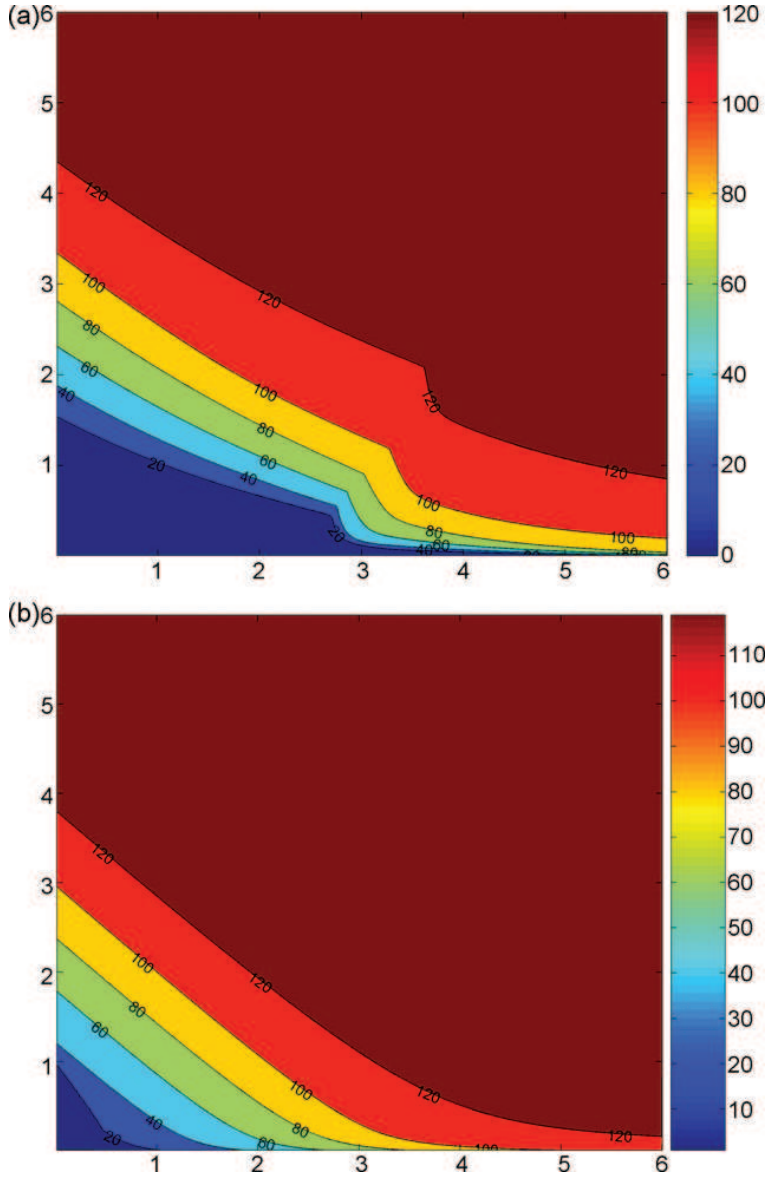

Figure 6.8. Ulva annual mean biomass ($gdwm^{-2}$) as a function of nitrate (x-axis) and ammonium loads (y-axis) in $mmolh^{-1}$. Top: $F = 0.1m^3h^{-1}$; bottom: $F = 0.01m^3h^{-1}$.

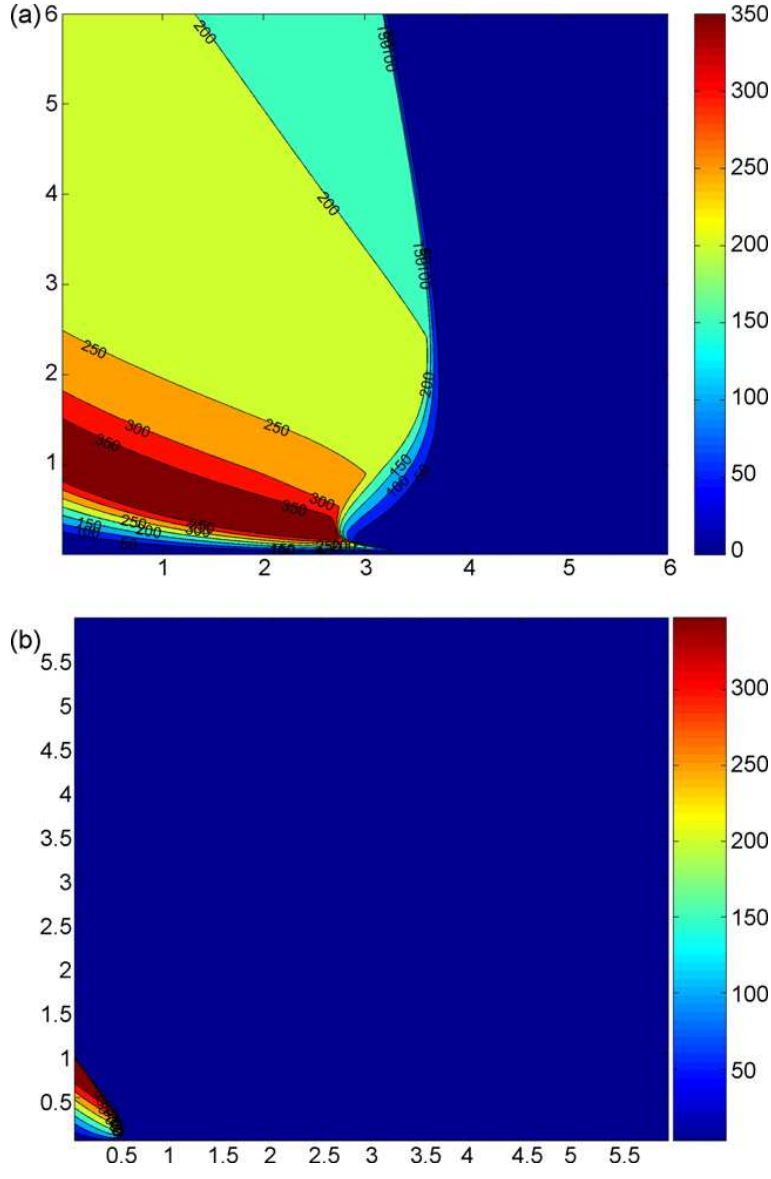

Figure 6.9. Zostera annual mean biomass ($gdwm^{-2}$) as a function of nitrate (x-axis) and ammonium (y-axis) loads in $mmolh^{-1}$. Top: $F = 0.1m^3h^{-1}$; bottom: $F = 0.01m^3h^{-1}$.

In order to analyze the effects of DIN inputs in the Zostera−Ulva competition model, we have run the model for a set of flow conditions with the same forcing. Figs.6.8 and 6.9 present the results in terms of average biomass over the year. Zostera dominates the regions with low DIN concentrations whereas the opposite applies to Ulva. In addition, due to the fact that in the Zostera model the rhizome-root is assumed to only uptake ammonium (Bocci et al., 1997), there is an asymmetry concerning the effects ammonium and nitrate in the figures.

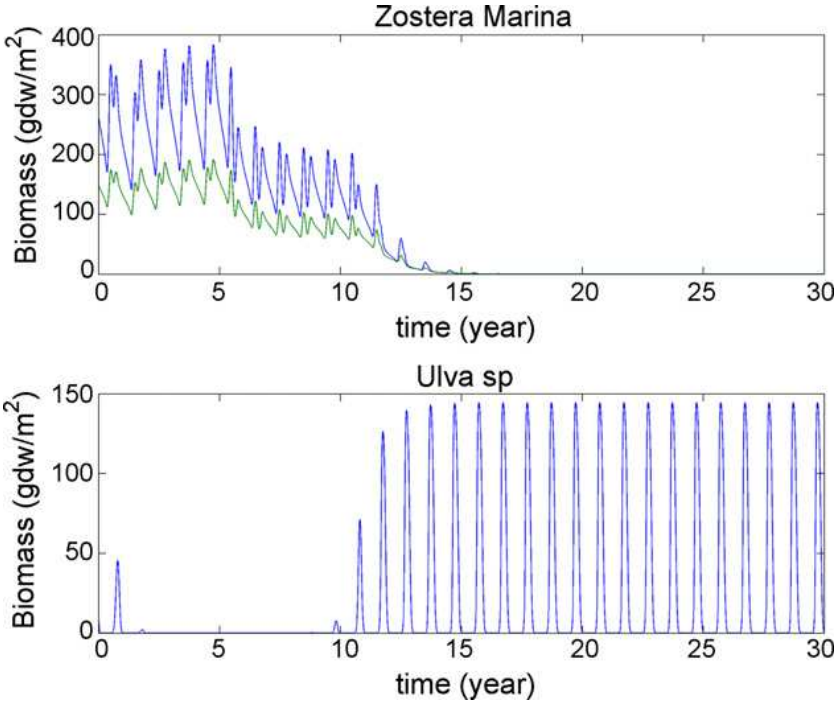

Figure 6.10. Zostera biomasses: Z_s (shoot biomass, $gdwm^{-2}$, blue) and Zr (rhizome-root biomass, $gdwm^{-2}$, green) and Ulva biomasses ($gdwm^{-2}$). Same parameters as in Figure 6.5, but after the fifth year of simulation the temperature forcing function increases by $1.0°C$.

Since we consider explicitly the DIN dynamics, the results represented in Figs.6.8 and 6.9 will change as a function of the flow (F, m^3h^{-1}),

assuming the same initial concentrations of nutrients. Likely, at low flows depletion of DIN may occur in the water column as well as in the sediments during the periods of maximum growth. This affects the dynamics in the system and, consequently, the competition between the two taxa. In order to highlight these differences, we have plotted the results obtained with 0.1 and $0.01 m^3 h^{-1}$ flows.

To verify the sensitivity of the competition in relation to changes in temperature, several simulations were set up, with the same conditions as in Figure 6.5, but with average temperature increased from 0.2 to $2°C$. Results obtained for a temperature increase of $1°C$ after the fifth year are presented in Figure 6.10. In this case, the outcome is the opposite as in Figure 6.5 with Ulva dominating the competition. Dynamics and timing of the regime shift are not a simple function of the temperature increase, as shifts have been observed in all the temperature ranges studied depending on the initial and forcing conditions.

The model was also run changing mean temperatures (Tm) and annual temperatures (A_T) ranges, Eq.(6.39). Results are presented in Figure 6.11, showing that an increase of both parameters tends to favor Ulva growth, even in environments with low nutrient concentrations.

Finally, the results of the model were analyzed as a function of the incident light. A series of simulation were run by modifying the average light intensity (Im) and its annual range (AI), see Eq. (6.40). From the results presented in Figure 6.12 it can be inferred that Zostera is adapted to narrower light ranges while Ulva seems able to cope with high variable light regimes (Dahlgreen and Kautsky, 2004). However, there is a certain realm of lighting conditions within which Zostera dominates even at high DIN concentrations. All simulated results showed that the system was in a transient and the final limit cycle was reached after a few years.

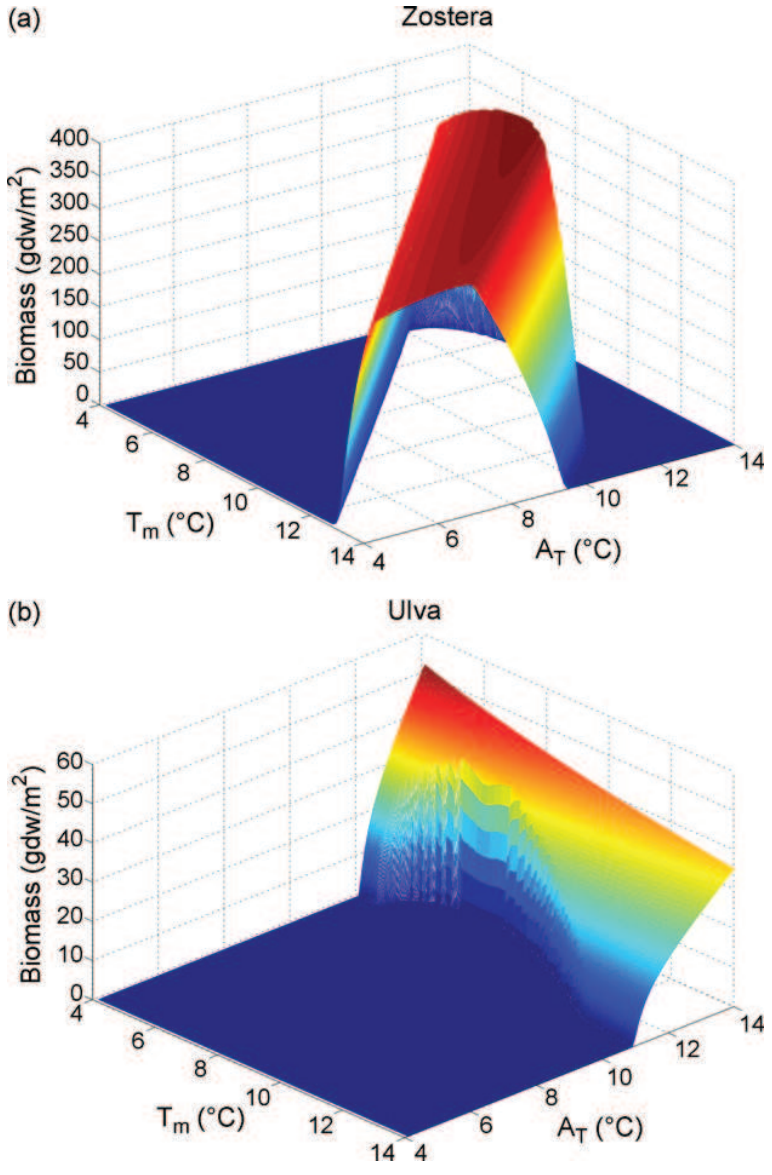

Figure 6.11. Zostera and Ulva annual mean biomass ($gdwm^{-2}$) as a function of mean temperatures, Tm, and its amplitude of annual variation, AT, for the low nutrient regime, $F = 0.1m^3h^{-1}$ and $[NO_3^-]input = [NH_4^+]_{input} = 5mmolm^{-3}$.

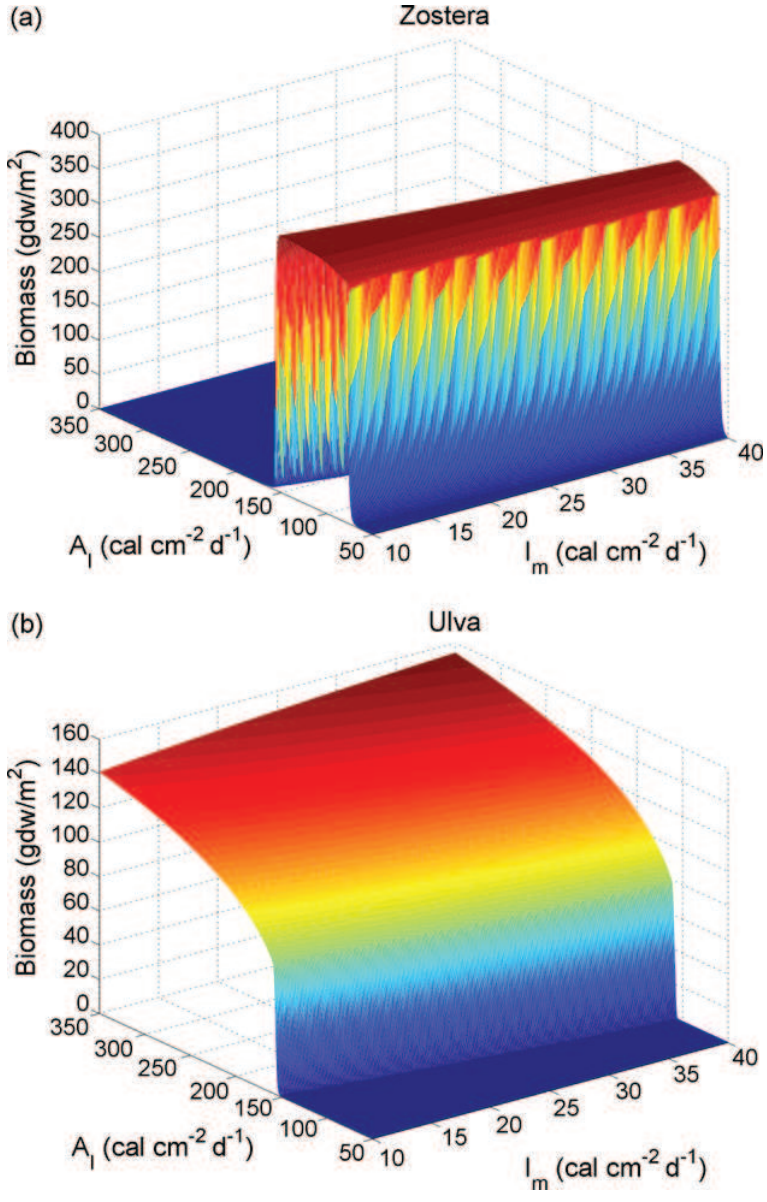

Figure 6.12. Zostera and Ulva annual mean biomass ($gdwm^{-2}$) as a function of mean light intensity, I_m, and its amplitude of annual variation, A_I , for the high nutrient regime, $F = 0.1m^3h^{-1}$ and $[NO_3^-]_{input} = [NH_4^+]_{input} = 50mmolm^{-3}$.

6.3.2 The influence of phytoplankton on competition between Zostera and Ulva

The partitioning of primary production among the different taxa was analyzed under different set of conditions as a function of DIN inputs with high ($F = 0.1 m^3 h^{-1}$) and low flows ($F = 0.01 m^3 h^{-1}$), see Figure 6.13. Overall, phytoplankton was able to compete with Ulva for nutrients in the water column, thus favoring Zostera due to its lower shadowing effect. At high DIN loadings phytoplankton outcompeted both Ulva and Zostera, thus becoming the dominant group. This is due to its higher maximum growth rate ($0.021 h^{-1}$) compared to Ulva ($0.017 h^{-1}$) and Zostera ($0.0025 h^{-1}$) when no nutrient, temperature or light limitation exists.

6.3.3 Assessment of mesocosm experiments

The model has been used to simulate the mesocosm experiments which tested competition between Z. marina, Ulva lactuca and phytoplankton under several nutrient enrichment conditions (Nixon et al., 2001, Taylor et al., 1999). The authors concluded that no significant effect of loading could be detected for Z. marina, epiphytic material, drift macroalgae or for all plant components combined. This contradictory result could be due to several reasons; therefore in this work we have tried to assess two: sensitivity to initial conditions and transient behavior.

Concerning the sensitivity to initial conditions, results obtained from two identical runs imitating the mesocosm experiments, but with different initial biomass of Ulva and phytoplankton are reported in Figs. 6.14 and 6.15, as an example. In the first case, Zostera biomasses increased steadily with nutrient enrichment, from C to M and decreased from M and VH. In parallel, Ulva and phytoplankton increased with nutrient enrichment from C to VH (Figure 6.14). However, in the second case (Figure 6.15), even though Ulva and phytoplankton behaved in a similar way but with delayed dynamics and with different values, Zostera showed a different behavior with higher biomasses at higher concentrations.

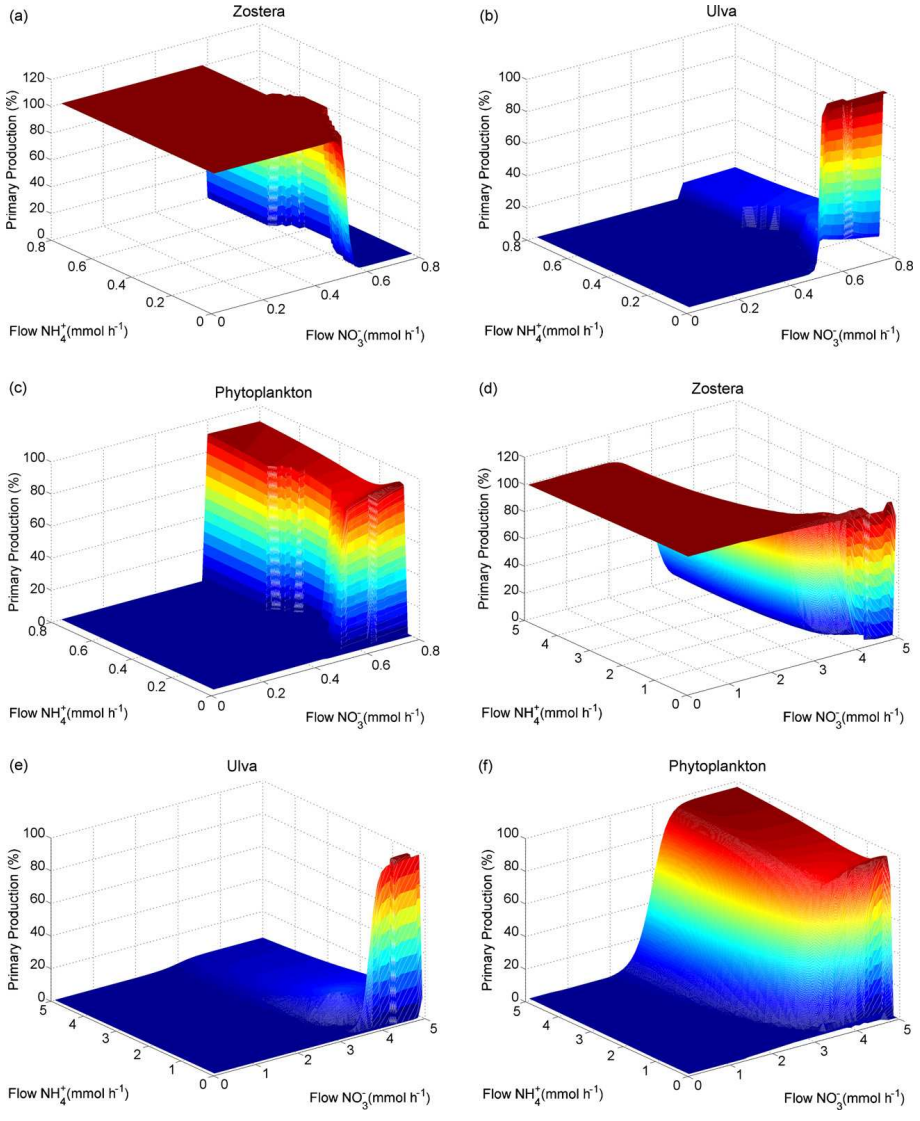

Figure 6.13. Percentage of primary production for each compartment: Zostera, Ulva and phytoplankton as a function of nutrient flows. Top: $F = 0.01m^3h^{-1}$; bottom: $F = 0.1m^3h_{-1}$

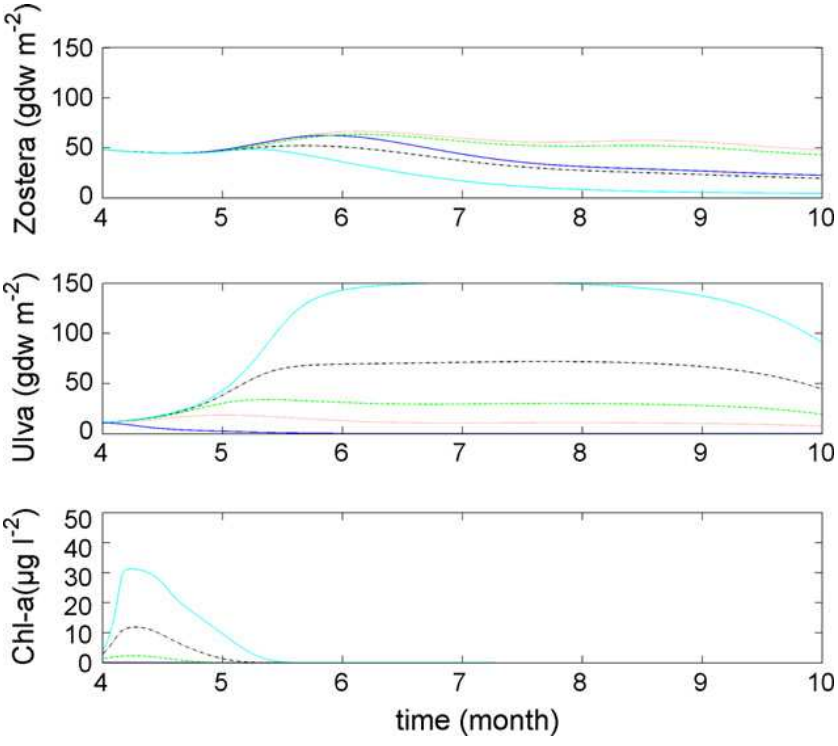

Figure 6.14. Simulated biomasses of Zostera, Ulva and phytoplankton under the conditions of the mesocosm experiments from Taylor et al. (1999). Control (C): continuous blue line; Low (L): dotted red line (L); Medium (M): dashed green line; High (H): dash-dot black line; Very high (VH): continuous cyan line.

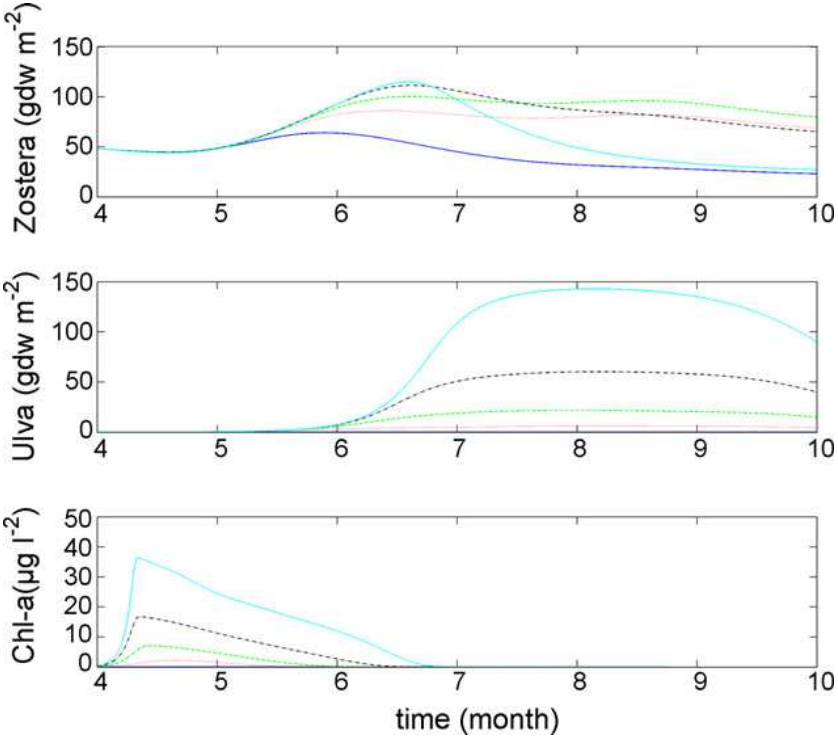

Figure 6.15. Simulated biomasses of Zostera, Ulva and phytoplankton under the conditions of the mesocosm experiments from Taylor et al. (1999). Control (C): continuous blue line; Low (L): dotted red line (L); Medium (M): dashed green line; High (H): dash-dot black line; Very high (VH): continuous cyan line. Conditions as Figure 6.14 but the initial conditions of Ulva and phytoplankton have been reduced by a factor of 10.

6.4 Discussion

The simulated results from the competition between Zostera and Ulva are in agreement with field observations. For example, DIN concentrations around $\sim$ 5 mmol m^3 are typical from Etang de Thau (France), which is covered by Zostera meadows; whereas high DIN concentrations $\sim$ 50 mmol m^3 have occurred during some years in Sacca di Goro (Italy), which is dominated by Ulva. Similar observations have also been reported by Nelson (2003) with Ulva starting to appear at DIN concentrations higher than 18.0mmolm.3. However, the regime shift would be more abrupt since, with such high Ulva biomasses, Zostera would disappear not only due to nutrient competition, but also due to alteration of sediment biogeochemistry (Holmer et al., 2003) and anoxic crises triggered off by the biomass decomposition (Zaldívar et al., 2003).

Biomasses and Ulva−Zostera competition are more correlated with DIN loads than with mean DIN concentrations, since with high growth rates nutrients become depleted. This is one of the reasons why field observations are difficult to use for defining a regime shift value.

Simulation outcomes evidenced that system responses to DIN loadings are complex depending on multiple parameters. For example, environmental conditions, such as temperature and light intensity, seem to play an important role in controlling the competition between benthic and pelagic species. Therefore, attempts to develop a simple nutrient scale for detecting regime shift in benthic vegetation seems not possible. This is probably one of the reasons why experimental observations and mesocosm data do not provide a clear threshold/range of values for regime shifts.

The results of simulations considering the influence of temperature and light intensity can be informative on climatic conditions and depths at which Zostera is able to grow when competing with Ulva by providing plausible values at which regime shifts will occur. The simulations can also help the debate on how changes in incident lights spectrum and intensity would affect the benthic vegetation.

The simulation of mesocosm experiments highlighted that the model of benthic vegetation is very sensitivity to initial (biomass concentrations) and operating (temperature, light intensity, DIN flows) conditions. Such result is in agreement with high variability detected in data, where biomasses differed by a factor of two between the experimental replicates (Taylor et al., 1999). In addition, transient regimes last longer (years) than the duration of the experiments (months); therefore, results could be not adequate to demonstrate the effects of nutrient enrichment on plant competition. Differences could be amplified by manipulations, e.g. when setting mesocosms with sediment transfer and phanerogams transplanting.

6.5 Conclusions

In this work a competition model has been developed with the aim of analyzing the succession of primary producer communities in coastal shallow ecosystems and identifying possible nutrient thresholds which cause shifts between alternative stable states.

The integrated model is able to simulate succession of dominance states, with different resilience characteristics according with the conceptual scheme that sees floating macroalgae as the optimal competitors for light, and submerged phanerogams as most efficient in recovering and storing nutrients from the sediments and from the water column. The shift from phanerogams to macrolgae, and finally to phytoplankton dominated communities, conformed to the general theory of succession in coastal lagoons (Viaroli et al., 2008). Field observations support the view that in nutrient poor ecosystems, rizophytes dominate until they are not limited by light penetration (depth effect) or by turbidity and shading by floating vegetation and phytoplankton (Dahlgreen and Kautsky, 2004). Increasing loading rates support the development of macroalgae, whilst high loaded water masses become dominated by phytoplankton.

Regime shifts are found when changing the input of nutrients, but

also, model simulations were sensitive to environmental forcing: temperature and light.

Overall, model runs evidenced a clear tendency towards a shift from seagrass to macroalgae under increasing temperatures. However, it is expected that the occurrence and severity of the shifts will be site specific depending on local conditions and past history. These results point out that one of the possible outcomes of an average air temperature increase will be the increase in macroalgae and decrease in benthic vegetation. However, the results of the analysis of a competition model between two species are not sufficient to sustain this point.

The model shows a high sensitivity to initial conditions as well as to forcing parameters, but this effect is also observed in mesocom experiments (Taylor et al., 1999). Furthermore, model simulations show that, when initial conditions do not correspond to steady state conditions, seagrasses communities require time periods to attain steady state, which usually are longer than the duration of the mesocosm experiments. In addition, ecosystems, as other nonlinear dynamical systems, are sensitive to initial conditions and even a small difference may drive the system to a completely different position in state space after a certain time (Pahl-Wostl, 1995). Our results suggest that this is probably the main reason behind the high variability found by Taylor et al. (1999) in their experiments, which did not allow finding a clear correlation between nutrient increase and regime shifts.

In its present form, the model does not take into consideration several important aspects such as hydrodynamics, buffering capacity (de Wit et al., 2001, Viaroli et al., 2008), salinity, organic nutrient, oxygen, zooplankton and bacteria as well as interactions between Ulva and aquaculture activities. In order to develop a more realistic assessment of regime shifts in terms of range of concentrations and temperature, we plan to consider a real case study in which the studied taxa coexist. Future efforts will aim to implement the competition model using a 3D hydrodynamic approach such as COHERENS (Luyten et al., 1999) for Thau lagoon (France).

Bibliography

Bocci, M., Coffaro, G., Bendoricchio, G., 1997. Modelling biomass and nutrient dynamics in eelgrass (zostera marina l.): applications to the lagoon of venice (italy) and oresund (denmark). Ecol. Model. 102, 6780.

Borum, J., 1996. Shallow waters and land/sea boundaries. Coast. Estuar. Stud. 52, 179203.

Burkholder, A., Mason, K., GlasgowJr., H., 1992. Water-column nitrate enrichment promotes decline of eelgrass zostera marina: evidence from seasonal mesocosm experiments. Mar. Ecol. Prog. Ser. 81, 163178.

Burkholder, J., Tomasko, D., Touchette, B., 2007. Seagrasees and eutrophication. J. Exp. Mar. Biol. Ecol. 350, 4672.

Chapelle, A., 1995. A preliminary model of nutrient cycling in sediments of a mediterranean lagoon. Ecol. Model. 80, 131147.

Coffaro, G., Bocci, M., 1997. Resources competition between ulva rigida and zostera marina: a quantitative approach applied to the lagoon of venice. Ecol. Model. 102, 8195.

Dahlgreen, S., Kautsky, L., 2004. Can different vegetative states in shallow coastal bays of the baltic sea be linked to internal nutrient levels and external nutrient loads? Hydrobiologia 514, 249258.

de Wit, R., Stal, L., Lomstein, B., Herbert, R., van Gemerden, H., Viaroli, P., Ceccherelli, V., Rodríguez-Valera, F., Bartoli, M., Giordani, G., Azzoni, R., Shaub, B., Welsh, D., Donnely, A., Cifuente, A., Anton, J., Finster, K.,

Nielsen, L., Underlien Pedersen, A., Neubauer, A., Colangelo, M., Heijs, S., 2001. Robust: The role of buffering capacities in stabilising coastal lagoon ecosystems. Cont. Shelf Res. 21, 20212041.

Flindt, M., Pardal, M., Lillebø, A., Martins, I., Marques, J., 1999. Nutrient cycling and plant dynamics in estuaries: a brief review. Acta Oecol. 20, 237248.

Hauxwell, J., V. I., 2004. Estuarine Nutrient Cycling: The Influence of Primary Producers. Kluwer Academic Publishers, Dordrecht, The Netherlands, Ch. Nielsen, S.L., Banta, G.T.,Pedersen, M.F., Effects of nutrient loading on shallow seagrassdominated coastal systems: patterns and processes, p. 5992.

Hemminga, M., 1998. The root/rhyzome system of seagrasses: an asset and a burden. J. Sea Res. 39, 183196.

Holmer, M., Duarte, C., Marbà, N., 2003. Sulphur cycling and seagrass (posidonia oceanica) status in carbonate sediments. Biogeochemistry 66, 223239.

Kjerfve, B., 1994. Coastal Lagoon Processes. Elsevier Science Publishers, Amsterdam.

Levin, L., Boesch, D., Covich, A., Dahm, C., Erséus, C., Ewel, K., Kneib, R., Moldenke, A., Palmer, M., Snelgrove, P., Strayer, D., Weslawski, J., 2001. The function of marine critical transition zones and the importance of sediment biodiversity. Ecosystems 4, 430451.

Luyten, P., Jones, J., Proctor, R., Tabor, A., Tett, P., Wild-Allen, K., 1999. Coherens a coupled hydrodynamical-ecological model for regional and shelf seas: User documentation. Tech. rep., MUMM Report, Management Unit of the Mathematical Models of the North Sea.

Marinov, D., Galbiati, L., Giordani, G., Viaroli, P., Norro, A., Bencivelli, S., Zaldívar, J., 2007. An integrated modelling approach for the management of clam farming in coastal lagoons. Aquaculture 269, 306320.

McLusky, D., Elliott, M., 2007. Transitional waters: a new approach, semantics or just muddying the waters? Estuar. Coast. Shelf Sci. 71, 359363.

Nelson, T.A., N. A. T. M., 2003. Seasonal and spatial patterns of green tides(ulvoid algal blooms) and related water quality parameters in the coastal waters ofwashington state usa. Bot. Marina 46, 263275.

Nienhuis, P., 1992. Ecology of coastal lagoons in the netherlands (veerse meer and grevelingen). Vie Milieu 42, 5972.

Nixon, S., Buckley, B., Granger, S., Bintz, J., 2001. Responses of very shal-

low marine ecosystems to nutrient enrichment. Hum. Ecol. Risk Assess 7, 14571481.

Olesen, B., Sand-Jensen, K., 1993. Seasonal acclimatation of eelgrass zostera marina growth to light. Mar. Ecol. Prog. Ser. 94, 9199.

Orth, R., Carruthers, T., Dennison, W., Duarte, C., Fourqurean, J., Heck, K., Hughes, A., Kendrick, G., Kenworthy, W., Olyarnik, S., Short, F., Waycott, M., Williams, S., 2006. A global crisis for seagrass ecosystems. BioScience 56, 987996.

Pahl-Wostl, C., 1995. The DynamicNature of Ecosystems: Chaos and Order Entwined. Wiley.

Plus, M., Chapelle, A., Lazure, P., Auby, I., Levavasseur, G., Verlaque, M., Belsher, T., Deslous-Paoli, J., Zaldívar, J., Murray, C., 2003. Modelling of oxygen and nitrogen cycling as a function of macrophyte community in the thau lagoon. Cont. Shelf Res. 23, 18771898.

Plus, M., La Jeunesse, I., Bouraoui, F., Zaldívar, J., Chapelle, A., Lazure, P., 2006. Modelling water discharges and nutrient inputs into a mediterranean lagoon impact on the primary production. Ecol. Model. 193, 6989.

Ralph, P., Tomasko, D., Moore, K., Seddon, S., Macinnis-Ng, C., 2006. Human impacts on seagrasses: eutrophication sedimentation and contamination. Springer, The Netherlands, Ch. Larkum, A.W.D., Orth, R.J., Duarte, C.M. (Eds.), Seagrasses: Biology, Ecology and Conservation, p. 567593.

Sacchi, C., 1995. Le lagune costiere come ambienti di transizione. In: Atti VI Congresso Nazionale S. It. E. Vol. 16. p. 149154.

Sand-Jensen, K., Borum, J., 1991. Interactions among phytoplankton, periphyton, and macrophytes in temperate freshwater and estuaries. Aquat. Bot. 41, 137175.

Scheffer, M., Carpenter, S. R., 2003. Catastrophic regime shifts in ecosystems: linking theory to observation. Trends Ecol. Evol. 18, 648–656.

Scheffer, M., Carpenter, S. R., Foley, J. A., Folke, C., Walker, B., 2001. Catastrophic shifts in ecosystems. Nature 413, 591–596.

Schramm, W., 1999. Factors influencing seaweed responses to eutrophication: some results from eu-project eumac. J. Appl. Phycol. 11, 6978.

Short, F., Koch, E., Creed, J., Magalhaes Fernandez, E., Gaeckle, J., 2006. Seagrassnet monitoring across the americas: case studies of seagrass decline.

Mar. Ecol. 27, 277289.

Solidoro, C., Brando, V., Dejak, C., Franco, D., Pastres, R., Pecenik, G., 1997a. Long term simulations of population dynamics of Ulva rigida in the lagoon of Venice. Ecol. Model. 102, 259272.

Solidoro, C., Pecenik, G., Pastres, R., Franco, D., Dejak, C., 1997b. Modelling macroalgae (ulva rigida) in the venice lagoon: Model structure identification and first parameters estimation. Ecol. Model. 94, 191206.

Taylor, D., Nixon, S., Granger, S., Bu Kley, B., 1999. Responses of coastal lagoon plant communities to levels of nutrient enrichment: a mesocosm study. Estuaries 22, 10411056.

Valiela, I., McLelland, J., Hauxwell, J., Behr, P., Hersh, D., Foreman, K., 1997. Macroalgal blooms in shallow estuaries: controls and ecophysiological and ecosystem consequences. Limnol. Oceanogr. 42, 11051118.

Viaroli, P., Bartoli, M., Bondavalli, C., Christian, R., Giordani, G., Naldi, M., 1996. Macrophyte communities and their impact on benthic fluxes of oxygen, sulphide and nutrients in shallow eutrophic environments. Hydrobiologia 329, 105119.

Viaroli, P., Bartoli, M., Giordani, G., Naldi, M., Orfanidis, S., Zaldívar, J., 2008. Community shifts, alternative stable states, biogeochemical controls and feedbacks in eutrophic coastal lagoons: a brief overview. Aquat. Conserv. Freshwater Mar. Ecosyst. 18, S105S117.

Viaroli, P., Christian, R., 2003. Description of trophic status of an eutrophic coastal lagoon through potential oxygen production and consumption: defining hyperautotrophy and dystrophy. Ecol. Indic. 3, 237250.

Vollenweider, R., 1976. Advances in defining critical loading levels for phosphorous in lake eutrophication. Mem. Ist. Ital. Idrobiol. 33, 5383.

Wall, D., Palmer, M., Snelgrove, V., 2001. Biodiversity in critical transition zones between terrestrial, freshwater and marine soils and sediments: processes, linkages, and management implications. Ecosystems 4, 418420.

Webster, I., Harris, G., 2004. Anthropogenic impacts on the ecosystems of coastal lagoons: modelling fundamental biogeochemical process and management implications. Mar. Freshwater Res. 55, 6768.

Zaldívar, J., Cardoso, A., Viaroli, P., Newton, A., deWit, R., Ibañez, C., Reizopoulou, S., Somma, F., Razinkovas, A., Basset, A., Holmer, M., Murray,

N., 2008. Eutrophication in transitional waters: an overview. Transit.Waters Monogr. 2, 172.

Zaldívar, J. M., Cattaneo, E., Plus, M., Murray, C. N., Giordani, G., Viaroli, P., 2003. Long-term simulation of main biogeochemical events in a coastal lagoon: Sacca di Goro (Northern Adriatic coast, Italy). Cont. Shelf Res. 23, 1847–1876.

Patterns in Savannas

Photo: Claudius van de Vijver

7 Savanna-Fire Model

7.1 Introduction

Savanna ecosystems are characterized by the robust coexistence of trees and grass. The mechanisms allowing for the persistence of both types of plants, despite their obvious competition, and governing the population dynamics and spatial arrangement of savanna trees are poorly understood (Bond, 2008, Scholes and Archer, 1997). Of the many potential driving mechanisms investigated, local-scale interactions among trees have received increasing attention in recent years (Barot et al., 1999, Calabrese et al., 2010, Meyer et al., 2008, 2007a,b, Scanlon et al., 2007, Wiegand et al., 2006).

Such tree-tree interactions can roughly be divided into two classes: facilitative and competitive. Facilitation among trees promotes tree clustering and may be mediated by a variety of mechanisms. Among these are dispersal limitation, improvement of local resource conditions, and protection from fire (Belsky et al., 1989, Calabrese et al., 2010, Hochberg et al., 1994, Holdo, 2005, Scanlon et al., 2007). Alternatively, competition among trees for water, nutrients, and light may alleviate the tree-grass competition, favoring their coexistence, and tends to promote separation among trees (Barot et al., 1999, Calabrese et al., 2010, Meyer et al., 2008).

There is evidence for both classes of interactions in the savanna literature; sometimes coming from the same region. For example, several studies have found evidence consistent with competition in the Kalahari (Jeltsch et al., 1999, Meyer et al., 2008, Moustakas et al., 2006, 2008, Skarpe, 1991), while others have found evidence suggesting facilitation

(Caylor et al., 2003, Scanlon et al., 2007). Indeed, one of the key difficulties in understanding the forces structuring savanna tree populations is that both classes of local-scale interactions often occur together and it is not obvious whether the net effect of local interactions will be positive or negative (Bond, 2008).

Further studies, both empirical and theoretical, are needed to better understand the interplay between the opposing forces. Specifically, studies that focus on a limited number of processes and their interactions should help illuminate the conditions under which positive or negative local interactions structure savanna tree populations. Mesic savannas that receive $\sim 400 - 800$ mm of mean annual precipitation (MAP) are particularly interesting because there is evidence from such systems that, in addition to local-scale interactions, fire plays also an important role. (Bucini and Hanan, 2007, Sankaran et al., 2005). Both of these factors can act strongly on juvenile trees and can contribute to a demographic bottleneck through which juvenile trees must pass to recruit into the adult population.

In contrast to forest tree species, savanna trees are often more fire resistant, (Hoffmann et al., 2003), thus savanna fires basically burn the grass layer and the young trees included in it, leaving adult trees alive, affecting only tree recruitment and not adult survival (Gignoux et al., 1997)[1]. Recent studies highlighting the importance of tree competition and fire on savannas are Calabrese et al. (2010), D'Odorico et al. (2006), Hanan et al. (2008), Higgins et al. (2000), Meyer et al. (2008), Moustakas et al. (2006, 2008), from which we might expect a kind of tug of war between these forces, the outcome of which affects both the tree-grass balance of the savanna and the spatial arrangement of adult trees.

[1] See Box 1.

Box 1. Fire : disturbance or disaster?

From human point of view, a wildfire is a disaster that can wreak havoc and shake the sense of security and economic well-being. In nature, however, there are no disasters – only disturbances. Fire sets in motion a cycle of death, decay, and re-birth that is vital to all ecosystems.

Figure 7.1. Fire in the savanna grasslands of Kruger National Park, South Africa, September 1992. Photo: J. S. Levine, NASA

Fire can also prepare seedbeds for germination by burning leaf litter. Some seeds require mineral soil for germination, and fire can release nutrients in the soil and make them available for sprouting plants. Likewise, fire can remove overstory plant material permitting sunlight to bathe the lower plant strata. In fact, naturally occurring fires are essential for the survival of many plant species. Trees such as the jack pine actually depend on heat from fire to break open their seeds for germination.

Regarding savanna, fire has an important role on its dynamics, maintenance and evolution. Tree resistance to fire depends largely on the presence of morphological traits that protects critical tissues and on the food reserves for successful recovery. But the regularity of savanna fire, the low flame height, and the short time of exposure to flame give adult trees other possibilities of resistance. Species in fire-prone ecosystems exhibit a diversity of adaptations to burning, such as large carbohydrate reserves and thick bark. The differences in fire-related traits may largely explain the greater capacity of savanna species to persist in the savanna environment.

The role of fire in mesic savannas is two-fold. On the one hand, it provides an indirect way for grass to compete against trees: the higher recovery rates of grasses compared to juvenile trees make grass the dominant form of vegetation shortly after a fire has destroyed both. On the other hand, several studies have suggested that adult trees can protect vulnerable juveniles from fire, thus increasing their chances of survival (Hochberg et al., 1994, Holdo, 2005). Exactly how such protection works has not been intensively studied. However, given the frequent occurrence of fires in many savannas, it seems likely that the protection effect may be one of the most common forms of positive facilitation among savanna trees, and the dominance of grass after fire could be as important as tree-tree competition in restricting the amount of tree-cover in the savanna.

Recently, Calabrese et al. (2010) studied the interaction between competition and fire in a highly simplified savanna model. They showed that these two forces interact non-linearly with sometimes surprising consequences for tree population density and spatial pattern. However, because Calabrese et al. (2010) treated fire in a non-spatially explicit manner, only the negative impact on trees, and not the protection effect, was included and thus could not fully tease apart how these contrasting local interactions function in combination.

Here, we focus on a spatially explicit lattice model of savanna tree and grass population dynamics under the influence of competition and fire. The model is an extension of the semi-spatial model studied by Calabrese et al. (2010). Importantly, both competition and fire are explicit spatial processes in the new model. This allows us to study directly how adult trees influence the survival probabilities of nearby juveniles. Competition was treated the same way as in Calabrese et al. (2010) and fire was implemented in a similar manner as in the Drossel-Schwabl Forest Fire Models (Bak and Chen, 1990, Drossel and Schwabl, 1992). In our model, however, grasses and juvenile trees are the flammable objects, in contrast to adult trees being flammable in the original Drossel-Schwabl model. We highlight the ranges of conditions under which local interactions result in net positive and net negative influences on juvenile tree

survival, and we demonstrate how these local interactions affect the spatial structure of adult tree populations.

In this Chapter, after this introduction, we briefly describe the modeling ideas behind explicit fire models (Sect. 7.2), and then (Sec. 7.3), after reviewing the previous model by Calabrese et al. (2010), we introduce our new Savanna-Fire model. In Sects. 7.4 and 7.5 we describe the effect of fire on the tree-grass balance and in the character of the effective tree-tree interactions, respectively. We conclude with a description of tree patterns and tree cluster statistics (Sect. 7.6). A Summary closes the chapter.

7.2 Spatially explicit fire models

In 1990 Bak and Chen introduced a toy model to demonstrate the emergence of scaling and fractal energy dissipation. Two years later Drossel and Schwabl made an extension of this model by introducing a lightning parameter f. This is the forest fire model we adapted in order to implement the fire spread in savanna. This model is one of the best studied models of non-conservative self-organized criticality (Bak and Chen, 1990, Clar et al., 1999, 1996, Drossel and Schwabl, 1992, Grassberger and Kantz, 1991, Schenk et al., 2000) and has four simple rules. The first three are the same as in the Per Bak and Chen model and the fourth is due to the lightning parameter introduced by Drossel and Schwabl.

The forest fire model is a probabilistic cellular automaton defined on a d-dimensional hypercubic lattice of L^d sites, initialized with a combination of burning trees and green trees, and updated at each time-step with the following rules: (i) A burning tree becomes an empty site. (ii) A green tree becomes a burning tree if at least one of its nearest neighbors is burning. Some immunity can be introduced in this rule, so that a green tree becomes a burning tree with probability $1 - I$ (Clar et al., 1996). (iii) At an empty site a tree grows with probability p. (iv) Trees in the lattice spontaneously (i.e., without the need of a burning neighbor) become

burning trees with probability f. This model is very rich in behavior, and depending on the parameters f and p it displays spiral-like shapes, critical states and phase transitions.

7.3 Savanna-Fire Model (SFM)

Our model is run in a square lattice with periodic boundary conditions. We use a lateral size of $L = 200$ sites, so that there are $N = L \times L = 4\ 10^4$ lattice sites in the simulation domain, each site represents a square of 5 meters side size. In the previous savanna model (SM) of Calabrese et al. (2010) each site in the lattice could be in one of these two states: grass occupied or tree occupied.

In the Savanna-Fire model (SFM) introduced here, a combination between the previous SM and the Drossel-Schwabl Forest Fire model presented in the previous section is made, but the flammable materials being grass and juvenile trees which are the predominant states in savannas (Gignoux et al., 1997, Hoffmann et al., 2003), instead of the trees of the Drossel-Schwabl Forest Fire model. In this way the fire is included in a explicit way being a possible state in the dynamics. Susceptibility to fire leads to distinguish between adult trees and juvenile trees, being only the later flammable. In this way in addition to the two states of SM, grass and adult trees, three more states are considered in SFM, so that each site on the lattice can be in one of the following five states:

- Grass (G)
- Juvenile Tree (JT)
- Adult Tree (AT)
- Burning (B)
- Ashes (A)

We distinguish two sets of neighbors for each lattice site (see Figure 7.2): the *near* neighborhood consists of the sites sharing an edge or a corner with the central one (Moore neighborhood). We assume this is the spatial scale at which there is direct competition effects between trees, as well as direct influence for fire propagation. The *far* neighborhood consists of the sites sharing edges or corners with the *near* ones, and will be assumed to be the farther sites to which seeds from a central tree can arrive.

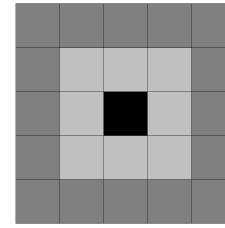

Figure 7.2. Spreading seeds from a central adult tree could reach both the *near* (light gray) and *far* (dark grey) neighborhoods of that central site. Spreading of fire and tree-tree competition occurs only within the *near* neighborhood. Note that the Moore neighborhood (sites sharing edges or corners) is used.

We note that fire propagation is a process much faster (the spread rate may be around 2 m/s, see Cheney and Gould (1995)), than the typical scales for growth, reproduction, death, and the rest of ecological timescales for both trees and grass. Thus we implement the burning process on top of the previous savanna model Calabrese et al. (2010), but acting on a faster scale. More specifically, at each model time step, time advances in an amount of $\Delta t = 0.1$ years, and the whole lattice is scanned in parallel to check for one of the following updates:

1. Growth: A random number is drawn for each site occupied by a juvenile tree so that with probability $a\Delta t$ it becomes an adult tree. Thus a^{-1} is the mean time for a juvenile tree to become adult.

2. Reproduction and establishment: Each adult tree in the lattice sends seeds, with probability $\beta\Delta t/24$, to each of the 24 sites pertaining to its *near* and *far* neighborhood (see Fig. 7.2). If the seed lands on a site in a state which is not G nor A, then nothing happens (establishment fails). If instead a site occupied by grass or ashes is reached a juvenile tree is established.

3. Competition: there is a probability P_c that a juvenile tree survives

from competing adult trees neighbors. This probability of survival due to competition P_c depends only on the competition exerted by neighboring adult trees: $P_c = e^{-\delta z_1}$, where δ is the competition parameter and z_1 is the number of adult trees in the *near* neighborhood.

4. Death: A random number is drawn for each site occupied by an adult tree, so that with probability $\alpha\Delta t$ this tree dies. Thus α^{-1} is the lifetime of adult trees. This mortality could be spontaneous or originated by external agents (e.g. harvesting).

5. Recovery: At each time step, each ash site may recover into grass with probability $p\Delta t$, so that p^{-1} is the mean recovery time of grass from ashes. Note that this forces a delay between successive fire fronts, thus difficulting all the lattice to be burnt out and trees completely disappearing giving place to grassland formation.

6. Spontaneous burning: There is a "lightning parameter", f, so that fire appears spontaneously on the lattice with this rate, affecting grass and juvenile trees. More explicitly, lattice sites occupied by G and JT are checked so that with probability $f\Delta t/N$ they become burning sites.

7. Fire propagation and extinction: After updating with all the above processes, a new pass through the lattice is done, so that if some fire has been introduced in the previous step, fire propagation is simulated until complete extinction. It is assumed that this process is fast and occurs at small time steps, much smaller than the $\Delta t = 0.1$ years introduced above. It is implemented in the following way:

   a) Each G and JT site is checked and if at least one site in its *near* neighborhood is in the B state, the site also burns with probability P_b. This models fire propagation on grass and juvenile trees. We will use a constant ignition probability $P_b = 1 - I$,

with I an *immunity* parameter reducing from unity the probability of burning by contact, thus giving some stochastic component to the fire propagation process. Note that, since adult trees do not burn, fire has less chances to reach JT (and G) sites which are surrounded by some adult trees. In this way the inclusion of fire in a explicit way implements the protection effect from adult trees.

b) End of burning: All sites that were burning before entering the previous step (a) are set to ashes.

Processes a) and b) are repeated until there are no remaining burning sites. Then time advances in Δt and the algorithm repeats again from step (1) on the updated lattice.

Table 7.1: Parameters

Parameters		Units
α	mortality rate	0.1 *or* 0.2 $year^{-1}$
b	sent offspring constant rate	1 $year^{-1}$
δ	competition coefficient	vary
f	lightning parameter	0.2-1 $year^{-1}$
a	growth rate	0.2 $year^{-1}$
p	recovery rate	4 $year^{-1}$
I	Immunity	0.3

The parameters used (see table 7.1) are based in the ones from Calabrese et al. (2010), but with a few modifications. The parameter α, death of adult trees, and f, lightning parameter, were changed according to Hanan et al. (2008, p 852) and Gignoux et al. (1997, p 557). In mesic savannas fire frequency is about once per year or even once each three years. The growth rate, a, was changed according to Hochberg et al. (1994, p 219), so that a tree takes on average 5 years to begin to reproduce (i.e. this is the mean time a juvenile tree becomes adult after seedling).

We note that the main facilitative interaction, the dispersal of seeds from adults to promote new trees, occurs at the spatial scale of the first

and second neighborhood, whereas the main competitive one, adults difficulting the development and juveniles, occurs at shorter distances, the first neighborhood. This is exactly the opposite situation as the one believed to occur in nutrient-poor arid savannas and other dry ecosystems, namely short distance facilitation by local improvement of humidity, and long range competition among trees mediated by long superficial roots. In this last case, tree patterns are expected to be nearly periodic in space (Rietkerk et al., 2004, Rietkerk and van de Koppel, 2008). Our situation is more appropriate for mesic savannas, and would tend to promote tree clustering. But the occurrence of fire may alter the nature of the interactions in a variety of ways, which we investigate in the following.

7.4 The tree-grass balance and phase transition

As expected, stronger tree-tree competition displaces the tree-grass coexistence towards the grass side (Figure 7.3, left). The model was run for 3000 years until an asymptotic state was reached in which we performed the measurements described in Figure 7.3. Simulations were performed to determine under what conditions we have a transition from savannas to grassland.

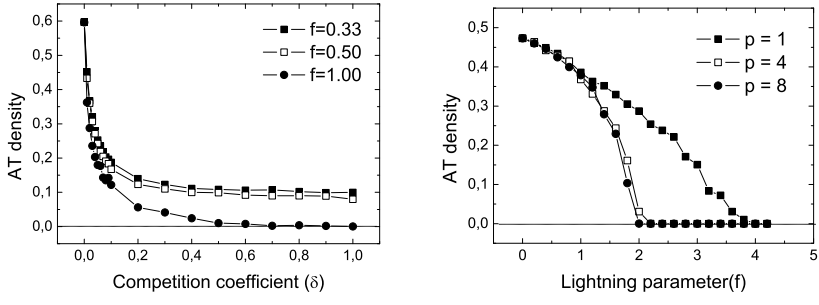

Figure 7.3. Density of adult trees (i.e., the number of adult trees divided by the total number of lattice sites) versus competition (δ, left graph) and versus lightning (f, right graph). Average over 500 snapshots in the long-time asymptotic state. Parameters in Table 7.1 but $\alpha = 0.1$ and in the right graph δ= 0.01.

In the previous study by Calabrese et al. (2010), however, coexistence was observed even for high competition. This is also the outcome in our SFM for small fire rate f (see Figure 7.3). For larger f, however, competition could drive tree extinction, which did not happen in the Calabrese et al. (2010) model. The lightning frequency f turns out to be the parameter most easily driving this savanna-grassland transition: The right part of Figure 7.3 shows a phase transition towards grassland by tree extinction by increasing f.

The indirect effect of fire on the tree-grass balance occurs because increasing fire destroys grass and juvenile trees, but the ashes will be replaced soon by grass, which grows faster. For frequent fire this would result in lack of tree renewal and finally in tree extinction. This mechanism and the subsequent extinction was somehow built-up in the definition of the fire parameter of the previous model by Calabrese et al. (2010). Here the mechanism appears as a consequence of the explicit presence of fire. In Figure 7.3 we can see that the transition from the coexistence state to grassland driven by increasing f is favored by larger grass recovery rates.

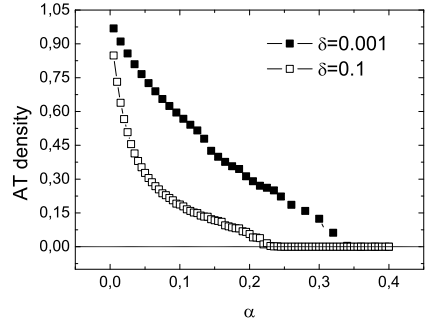

Figure 7.4. Density of adult trees (i.e., the number of adult trees divided by the total number of lattice sites) versus adult tree mortality (α). Parameters: $b = 1$, $a = 0.2$, $I = 0.3$, $p = 4$, $f = 0.33$.

A smooth transition forest-savanna is also present in the model (Figure 7.4). Tree cover increases when adult tree life span increases (i.e. de-

creasing α value). However, when using reasonable values for tree mortality in savannas, the region of parameters in which forest state is reached is strongly reduced and basically only the savanna-grassland transition can be found.

7.5 Positive and negative effects of surrounding adult trees on juvenile's: Protection and competition

In addition to affecting the tree-grass competition, fire has also an indirect effect on tree-tree interactions. In fact, it introduces the positive effect of juvenile-tree protection by surrounding adult trees. In order to analyze this effect in detail we run simulations in which only the fire propagation process (6) above occurs. The lattice is initialized fully with grass except for one unique site occupied by a juvenile tree, and a number of adult trees, from 1 to 8, occupying random positions in the Moore neighborhood of the chosen JT. Once with this initial condition, one sparkling is allowed so that a lattice site chosen randomly among the G sites becomes burning and fire begins to propagate. Step (6) in the SFM algorithm is repeated until fire disappears.

Juvenile trees sufficiently protected by adult trees will not burn. An example is seen in Figure 7.5, where the pass of a fire front does not affect a juvenile protected by five adult trees.

The effect has been quantified by repeating this burning protocol 1000 times for each number of AT neighbors, from 1 to 8. The sparkling site and the position of the surrounding neighbors is changed in these realizations. The resulting survival probability $p_f(z_1)$ is shown in Figure 7.6. The protective effect of an increasing number of ATs is clearly seen when the immunity parameter is not too small. For very small I protection is only effective when the juvenile is completely surrounded by adults, i.e. $z_1 = 8$.

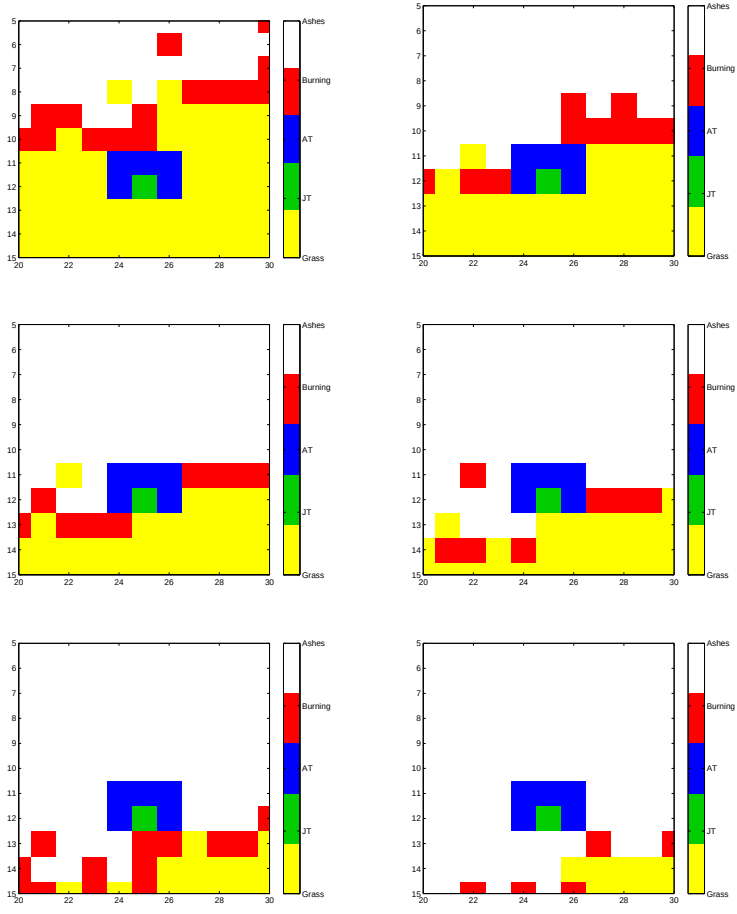

Figure 7.5. Protection effect: Selected snapshots from an example simulation with 5 adult trees (blue) surrounding a juvenile (green). Immunity parameter $I = 0.3$. Time runs from left to right and then from the upper to the lower row. A fire front (red) advances downwards, converting grass (yellow) into ashes (white), but the juvenile survives. Only a 10×10 area of the whole 200×200 lattice is shown.

In order to better quantify the impact of this protective effect on the survival of juveniles and recruitment into adults, we estimate now how

the number of adult trees z_1 in the near neighborhood of a site affects a 'recruiting probability' $P_r(z_1)$, defined as the probability that a grass or ash site becomes successfully colonized by a tree seed during a given time-step, in such a way that the resulting JT would survive successive fires and become adult. This probability is a product of several factors.

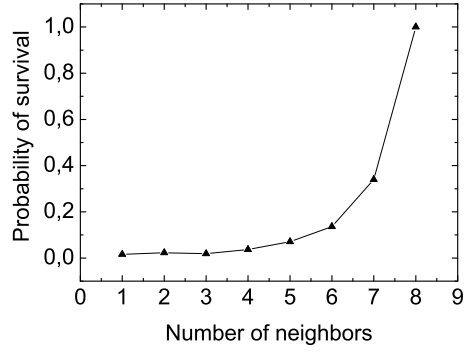

Figure 7.6. The protection effect: The probability $p_f(z_1)$ of a juvenile surviving one fire as a function of the number of surrounding adult trees in its first neighborhood. This probability has been obtained from 1000 realizations of the process in which fire is initiated at one grass site, as described in the text, using immunity $I = 0.3$.

First, the grass or ash site should receive in that time step seeds from the adult trees in the near or in the far neighborhood (the number of adult trees there is $z_1 \in (0,8)$ and $z_2 \in (0,16)$, respectively). This is given by $p_s(z_1,z_2) = 1-(1-\beta\Delta t/24)^{z_1+z_2}$. Then, the seed, turned on a juvenile tree, should survive competition at successive time steps which is given by the factor $P_e = \exp(-\delta z_1)$. Since a^{-1} is the growth time from juvenile to adult tree, $a\Delta t^{-1}$ time steps occur during the growth, and $\exp(-\frac{\delta z_1}{a\Delta t})$ is the total survival factor to adulthood under competition.

Finally, the growing JT should resist the first and successive fires occurring during its growing time a^{-1}. The survival to a single fire is the function $p_f(z_1)$ numerically calculated and shown in Figure 7.6 for the

case in which the considered site is surrounded just by z_1 trees in the near neighborhood (i.e., $z_2 = 0$).

An estimation of the survival probability to successive fires, which neglects any correlations arising from successive fire fronts and from the lattice configuration beyond the immediate neighborhoods would be $p_f(z_1)^{f/a}$, since f/a is the expected number of fires suffered by the JT during its growing time a^{-1}. The probability $p_s(z_1, z_2)$ depends on the number of AT both in the near and in the far neighborhood. For consistence with the calculation of $p_f(z_1)$ we will take $z_2 = 0$. This (as in the case of $p_f(z_1)$) will underestimate the probability of establishment, survival and recruitment, as the trees in the far neighborhood do not compete with the central one. In this way we will obtain an estimation of the recruitment probability $P_r(z_1)$ which would be smaller than the exact one. Thus, if this function shows positive effects of surrounding adult trees (as it will do), the result has an enhanced value, since it is obtained in a *worst case* situation.

Summarizing all the factors above, with $z_2 = 0$, our estimation of the recruitment probability of a grass site surrounded by z_1 adult trees is

$$P_r(z_1) \approx \left[1 - \left(1 - \frac{\beta \Delta t}{24}\right)^{z_1}\right] e^{-\frac{\delta z_1}{a \Delta t}} p_f(z_1)^{\frac{f}{a}} \tag{7.1}$$

This is plotted in Figure 7.7, and reveals both the positive and the negative effects of the presence of neighboring trees (but remember that the positive effects are underestimated). For medium values of the competition parameter and above four neighboring adult trees the positive protective effect of fire (in combination with local dispersal) overcomes the negative effect of direct competition, but for high values of competition the negative effect predominates. For frequent fire, however, the protection effect is no longer effective.

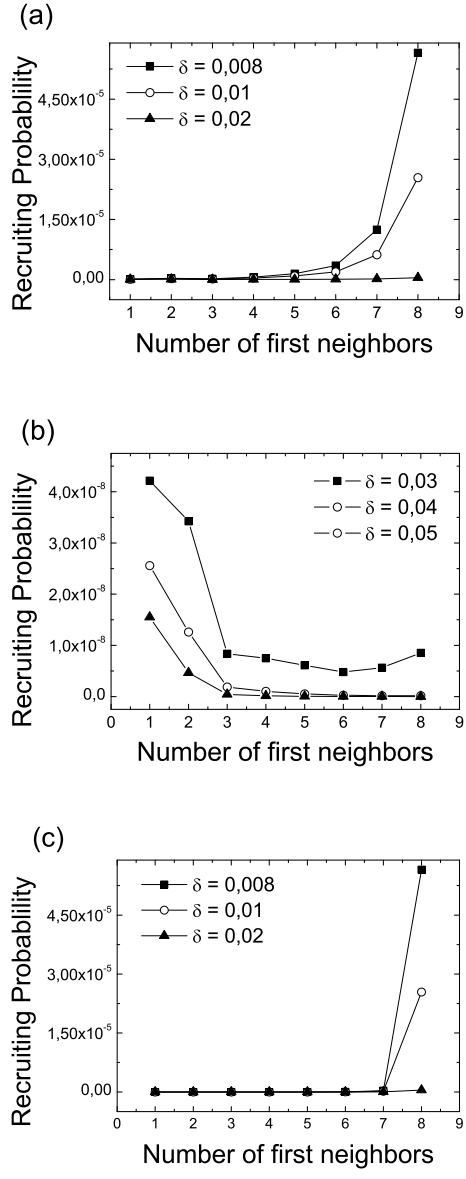

Figure 7.7. Estimation of the recruiting probability $P_r(z_1)$, as a function of the number of adult trees z_1 in the near neighborhood, from Eq. (7.1), showing the positive and negative effects of these neighbors. (a) and (b) $I = 0.3$, $f = 0.33/year$ (triennial fire). (c) $I = 0.3$, $f = 1/year$ (annual fire).

7.6 Clustering patterns

7.6.1 Spatial pattern under different fire scenarios

We characterize spatial patterns of adult trees by the pair correlation function, $g(r)$:

$$g(r) = \frac{\rho_{AA}(r)}{(\rho_A)^2} \tag{7.2}$$

ρ_{AA} is the proportion of pairs of adult trees at a distance r with respect to the total number of pairs of sites at that distance, and the denominator is the expected value of this ratio under a random distribution with the density of the adult trees ρ_A. At large distances $g(r)$ is expected to approach 1, as correlations indicating a departure from random distribution would decay. For short distances, $g(r)$ characterizes how the particles are packed together (see Dieckmann et al., 2001, chap. 14), values higher than 1 indicating a proportion of pairs at that distance greater than in the random case, and a smaller proportion indicated by values of g smaller than 1. We will not use the Euclidean distance for r but instead we will measure r in number of cell layers so that $g(1)$ and $g(2)$ will denote the pair correlation function for the first and for the second Moore neighborhood, respectively.

Comparison of Figure 7.8 with the results of Calabrese et al. (2010) shows that all the patterns found in the SM model are present also here. In that case the patterns can be understood from the fact that there is direct competition only between nearest neighbors, whereas the facilitation effect of local seed dispersal reaches first and second neighbors. In consequence, all these patterns have an enhanced probability of ATs having other ATs as second neighbors (far Moore neighborhood), as seen by the high value of $g(2)$. As in Calabrese et al. (2010), two types of configurations are distinguished by having a value of $g(1)$ smaller or larger than 1, i.e. smaller or larger proportion of ATs in the near neighborhood than the one expected from a random distribution. The balance between positive and negative tree-tree interaction effects determines these values. The

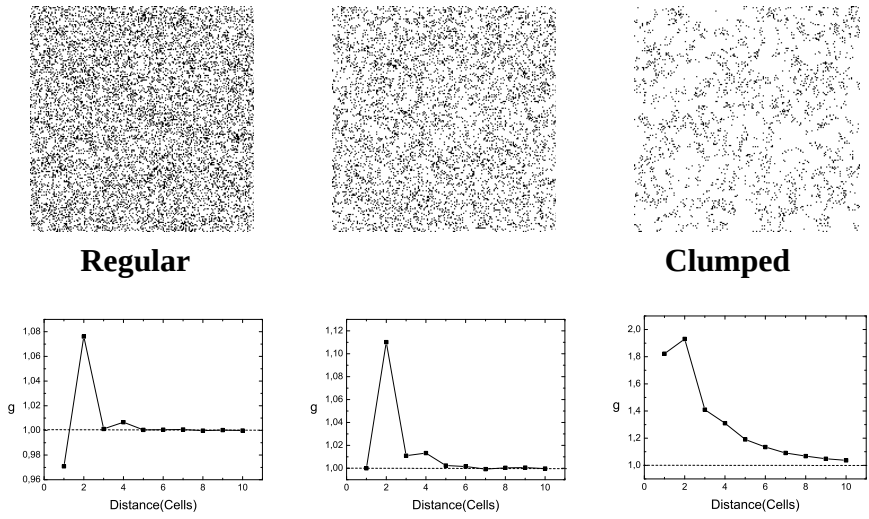

Figure 7.8. Patterns in the SFM. Parameters as in Table 1 and $p = 4.0$, $\delta = 0.02$. Regular case: $f = 0.10$. Clumped case: 0.60. The central panel shows an intermediate state ($f = 0.24$) in which $g(1) = 1$, which indicates the same number of AT near pairs as in a random case.

case $g(1) < 1$ is a *regular* case in which trees appear more regularly spaced than in the random case. The case $g(1) > 0$ is a *clumped state*, in which, although the density of near-neighbor pairs is still smaller than the one of far-neighbor pairs, it is larger than in the random case. The transition between the two states, that in the SM model was ruled by the parameter σ (representing the probability of surviving fire), is here determined by the explicit fire parameter f.

In the clumped patterns just described, plotted in Figure 7.9, the clusters are *open* in the sense that there are more neighbors in the far neighborhood than in the near neighborhood. This a clear effect of the competition existing in the near neighborhood, and was the only clumped state present in the previous SM model. The novelty here is that, in addition, there is a second type of clustered state not present in the SM model. A clumped state made of *closed* clusters is shown in Figure 7.10. The clusters are closed in the sense that there are more AT neighbors in

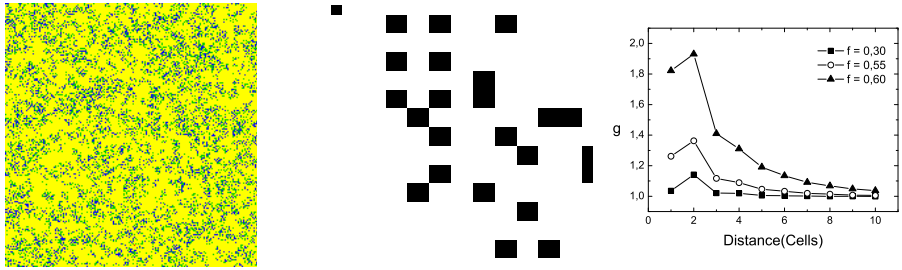

Figure 7.9. Savanna configuration in the clumped state at parameters $\alpha = 0.2$, $b = 1$, $a = 0.2$ and $I = 0.3$, $\delta = 0.02$, $p = 4$, $f = 0.55$ and an example of open cluster of ATs, the typical configuration here. The right panel shows the pair correlation function for this and similar parameters, similar to the one in the SM model in the clumped state. The yellow represents grass state, green the juvenile tree state and blue the adult tree state.

the near neighborhood than in the far neighborhood. Thus, the positive effect of fire protection (and local dispersion) has completely overcome the competition effect occurring in the near neighborhood. The transition from one type of pattern to the other occurs when changing the competition or the lightning parameters, δ and f, as shown in Figure 7.11 and 7.12.

7.6.2 Cluster size distributions

A cluster is a group of neighbor sites occupied by the same type of vegetation (e.g. adult trees). The distribution of cluster sizes is a powerful indicator of the different mechanisms occurring in ecosystem (Pascual and Guichard, 2005, Pascual et al., 2002). The distributions of sizes of adult-tree clusters in regions of southern Africa have been investigated by Scanlon et al. (2007), finding that in most cases a power-law fit can describe the data (although the fit was not of uniform quality). Scanlon et al. (2007) showed that resource constraints, together with positive local interactions of the type identified in the previous section, could generate cluster size distributions similar to the observed ones.

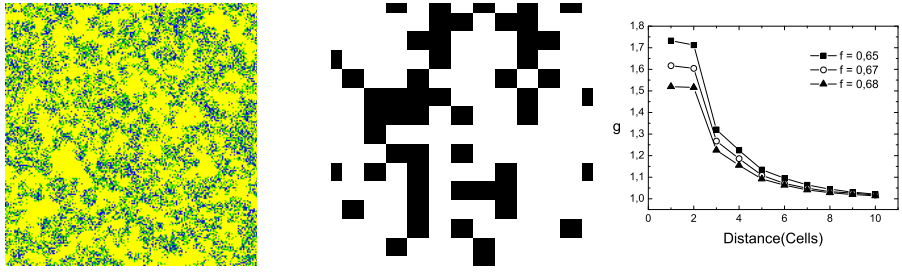

Figure 7.10. Savanna configuration in the clumped state at parameters $\alpha = 0.2$, $b = 1$, $a = 0.2$ and $I = 0.3$, $\delta = 0.008$, $p = 4$, $f = 0.65$ and an example of closed cluster of ATs, the typical configuration here. The right panel shows the pair correlation function for this and similar parameter, which is different to the one in the SM model in the clumped state because the maximum of $g(r)$ occurs at $r = 1$, i.e. in the near neighborhood. Colors are the same as in Figure 7.9.

Figure 7.13 shows the cumulative adult-tree cluster size distributions from our model. The Moore neighborhood has been used to define clusters. It is seen that, although the distributions have fat tails (and even plateaux at large sizes, see the small-f curves in Fig. 7.13), a single power law does not provide a good description except in particular parameter ranges. One of such cases in which cluster size distribution follow a relatively good power law is seen in Fig. 7.13 at $f \approx 0.9$. Inspection of the tree distributions above and below such value indicates that a percolation transition occurs precisely at that point: there is a giant adult-tree cluster spanning the whole area for smaller lightning, and just disconnected tree patches for higher values. Power-law cluster distributions are observed close to the percolation transition. Then, power-law behavior in our model seems to be associated to the *percolation* mechanism discussed in Pascual and Guichard (2005), although in a parameter range not as broad as suggested there. The reason is not difficult to understand: tree cover in Fig. 7.13 is just of 0.4 for $f \approx 0.9$, and can not be increased much more (see Fig. 7.3, right panel), which makes difficult to attain percolation through the whole lattice because of the absence of very large clusters. By artificially changing parameters, in particular reducing tree mortality (see Fig. alfadensity), larger tree densities could be achieved

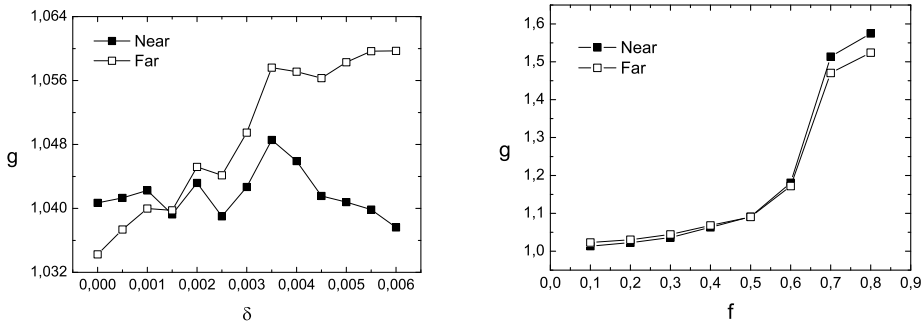

Figure 7.11. Values of the pair correlation function for near neighbor pairs $g(1)$ and for far neighbors $g(2)$. Left graph: Parameters: $\alpha = 0.2$, $b = 1$, $a = 0.2$ and $I = 0.3$, $p = 4.0$, $f = 0.33$. Closed clusters occur for $\delta < 0.0014$ and open ones for $\delta > 0.0014$. The second graph corresponds the same as in the left one but for fixed $\delta = 0.003$ and varying lightning parameter f.

which makes easier to cross a percolation transition when moving the remaining parameters. In such situations, we observe more robust power-law behavior (not shown), but the system is then closer to a forest than to a realistic savanna. We do not find systematic correlation between the small-scale character of the tree patterns (regular, clumped, open, closed, ...) and the type of cluster-size distributions, despite one could expect that positive short-range correlations would favor power-laws (Scanlon et al., 2007). This can be explained because in our model stronger positive correlations are generally associated to lower tree-densities (compare Figs. 7.11 with 7.9) which are far from the percolation point since large clusters are necessarily absent.

7.7 Summary

We have introduced a model for the savanna structure which includes, in addition to the standard ecological interactions and competition, the explicit effect of spatial fire. Fire introduces some effective tree-grass

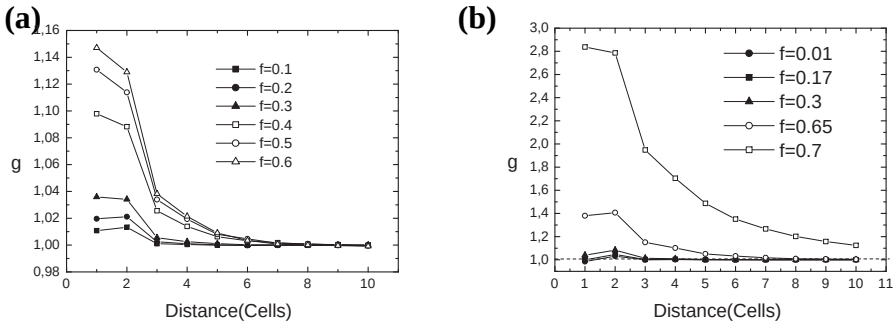

Figure 7.12. Pair correlation functions showing the transition open-closed clusters. Parameters: $\alpha = 0.2$, $b = 1$, $a = 0.2$ and $I = 0.3$, $p = 4.0$. (a)$\delta = 0.001$. (b) $\delta = 0.01$

and tree-tree interactions which are important in shaping demography and spatial pattern. First, the presence of fire improves competitiveness of grass because of its faster recovery after a fire. Second, adult trees may provide protection against fire to juveniles surrounded by them. This gives a positive tree-tree interaction which can overcome the explicit tree-tree competition for resources. As a result of these direct and indirect interactions a variety of tree distributions are observed, which we have characterized by the pair correlation function. As the short-range positive interactions gain importance as compared to the negative ones, a succession of regular to clumped states is observed. Clumped states can have "open" clusters, as the ones present in the previous Calabrese et al. (2010) model, but also "closed" for the cases with stronger positive interactions. Adult-tree cluster-size distributions are of power-law type in some cases because of the proximity of a percolation transition, but for much of the realistic parameter range tree cover is small and far from percolating. The tails of the distributions, although fat, seem to decay faster than power laws, as in fact is seen to occur in several of the sites reported by Scanlon et al. (2007).

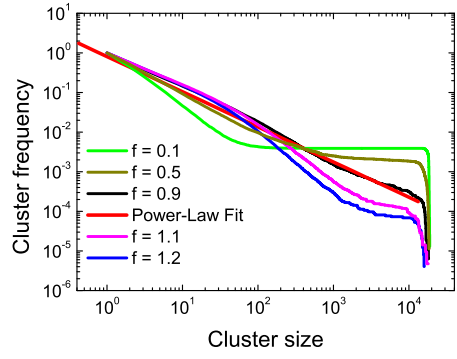

Figure 7.13. Adult-tree cluster-size distributions, represented by means of the complementary cumulative distributions. Parameters in Table 7.1 but $\alpha = 0.1$ andδ= 0.01. Power-law behavior is found around $f \approx 0.9$, when adult-tree biomass fraction reaches values around 0.4. At lower values of f (higher tree biomass), a plateau develops at large cluster size.

Bibliography

Bak, P., Chen, K., 1990. A forest-fire model and some thoughts on turbulence. Physics Letters A 147 (5,6), 297–300.

Barot, S., Gignoux, J., Menaut, J. C., 1999. Demography of a savanna palm tree: Predictions from comprehensive spatial pattern analyses. Ecology 80 (6), 1987–2005.

Belsky, A. J., Amundson, R. G., Duxbury, J. M., Riha, S. J., Ali, A. R., Mwonga, S. M., 1989. The effects of trees on their physical, chemical and biological environments in a semi-arid savanna in kenya. Journal of Applied Ecology 26 (3), pp. 1005–1024.

Bond, W. J., 2008. What limits trees in c_4 grasslands and savannas? Annual Review of Ecology, Evolution, and Systematics 39, 641–659.

Bucini, G., Hanan, N. P., 2007. A continental-scale analysis of tree cover in african savannas. Global Ecology and Biogeography 16, 593–605.

Calabrese, J. M., Vazquez, F., Lopez, C., Miguel, M. S., Grimm, V., 2010. The independent and interactive effects of tree-tree establishment competition and fire on savanna structure and dynamics. The American Naturalist 175 (3), 44–65.

Caylor, K. K., Shugart, H. H., Dowty, P. R., Smith, T. M., 2003. Tree spacing along the Kalahari transect in Southern Africa. Journal of Arid Environments 54, 281–296.

Cheney, N., Gould, J., 1995. Fire growth in grassland fuels. International Journal of Wildland Fire 5, 237–247.

Clar, S., Drossel, B., Schenk, K., Schwabl, F., 1999. Self-organized criticality in forest-fire models. Physica A 266, 153–159.

Clar, S., Drossel, B., Schwabl, F., 1996. Forest fires and other examples of self-organized criticality. Journal of Physics:Condensed Matter 8, 6803–6824.

Dieckmann, U., Law, R., Metz, J. A. J., 2001. The geometry of ecological interactions: Simplifying spatial complexity. Cambridge University Press.

D'Odorico, P., Laio, F., Ridolfi, L., March 2006. A probabilistic analysis of fire-induced tree-grass coexistence in savannas. The American Naturalist 167 (3), E79–E87.

Drossel, B., Schwabl, F., 1992. Self-organized critical forest-fire model. Physical Review Letters 69 (11), 1629–1632.

Gignoux, J., J., C., J.-C., M., 1997. Alternative fire resistance strategies in savanna trees. Orcologia 110, 576–583.

Grassberger, P., Kantz, H., 1991. On a forest fire model with supposed self-organized criticality. Journal of Statistical Physics 63 (3/4), 685–700.

Hanan, N. P., Sea, W. B., Dangelmayr, G., Govender, N., June 2008. Do fires in savannas consume woody biomass? a comment on approaches to modeling savanna dynamics. The American Naturalist 171 (6), 851–856.

Higgins, S. I., Bond, W. J., Trollope, W. S. W., 2000. Fire, resprouting and variability: A recipe for grass-tree coexistence in savanna. Journal of Ecology 88, 213–229.

Hochberg, M. E., Menaut, J. C., Gignoux, J., 1994. The influences of tree biology and fire in the spatial structure of the West African savannah. Journal of Ecology 82, 217–226.

Hoffmann, W. A., Orthen, B., Nascimento, P. K. V. D., Dec. 2003. Comparative fire ecology of tropical savanna and forest trees. Functional Ecology 17 (6), 720–726.

Holdo, R. M., 2005. Stem mortality following fire in kalahari sand vegetation: Effects of frost, prior damage, and tree neighbourhoods. Plant Ecology 180, 77–86.

Jeltsch, F., Moloney, K., Milton, S. J., 1999. Detecting process from snapshot pattern: Lessons from tree spacing in the southern Kalahari. Oikos 85, 451–466.

Meyer, K. M., Ward, D., Wiegand, K., Moustakas, A., 2008. Multi-proxy evidence for competition between savanna woody species. Perspectives in Plant Ecology, Evolution and Systematics 10 (1), 63 – 72.

Meyer, K. M., Wiegand, K., Ward, D., Moustakas, A., 2007a. The rhythm of savanna patch dynamics. Journal of Ecology 95, 1306–1315.

Meyer, K. M., Wiegand, K., Ward, D., Moustakas, A., 2007b. Satchmo: A spatial simulation model of growth, competition, and mortality in cycling savanna patches. Ecological Modelling 209 (2-4), 377 – 391.

Moustakas, A., Guenther, M., Wiegand, K., Mueller, K. H., Ward, D., Meyer, K. M., Jeltsch, F., 2006. Long-term mortality patterns of the deep-rooted *Acacia erioloba*: The middle class shall die! Journal of Vegetation Science 17, 473–480.

Moustakas, A., Wiegand, K., Getzin, S., Ward, D., Meyer, K. M., Guenther, M., Mueller, K. H., 2008. Spacing patterns of an Acacia tree in the Kalahari over a 61-year period: How clumped becomes regular and vice versa. Acta Oecologica 33, 355–364.

Pascual, M., Guichard, F., 2005. Criticality and disturbance in spatial ecological systems. Trends Ecol. Evol. 20 (2), 88–95.

Pascual, M., Roy, M., Guichard, F., Flierl, G., 2002. Cluster size distributions: signatures of selforganization in spatial ecologies. Philosophical Transactions of the Royal Society of London. Series B: Biological Sciences 357 (1421), 657–666.

Rietkerk, M., Dekker, S. C., de Ruiter, P. C., van de Koppel, J., 2004. Self-Organized Patchiness and Catastrophic Shifts in Ecosystems. Science 305 (5692), 1926–1929.

Rietkerk, M., van de Koppel, J., 2008. Regular pattern formation in real ecosystems. Trends in Ecology & Evolution 23 (3), 169 – 175.

Sankaran, M., Hanan, N. P., Scholes, R. J., Ratnam, J., Augustine, D. J., Cade, B. S., Gignoux, J., Higgins, S. I., Roux, X. L., Ludwig, F., et al., 2005. Determinants of woody cover in african savannas. Nature 438, 846–849.

Scanlon, T. M., Caylor, K. K., Levin, S. A., Rodriguez-Iturbe, I., Sep 2007. Positive feedbacks promote power-law clustering of Kalahari vegetation. Nature 449, 209–212.

Schenk, K., Drossel, B., Clar, S., Schwabl, F., 2000. Finite-size effects in the

self-organized critical forest-fire model. The European Physical Jounal B 15, 177–185.

Scholes, R. J., Archer, S. R., 1997. Tree-grass interactions in savannas. Annual Review of Ecology and Systematics 28, 517–544.

Skarpe, C., 1991. Spatial patterns and dynamics of woody vegetation in an arid savanna. Journal of Vegetation Science, 565–572.

Wiegand, K., Saitz, D., Ward, D., 2006. A patch-dynamics approach to savanna dynamics and woody plant encroachment - insights from an arid savanna. Perspectives in plant ecology evolution and systematics 7 (4), 229–242.

Male Biased Parasitism

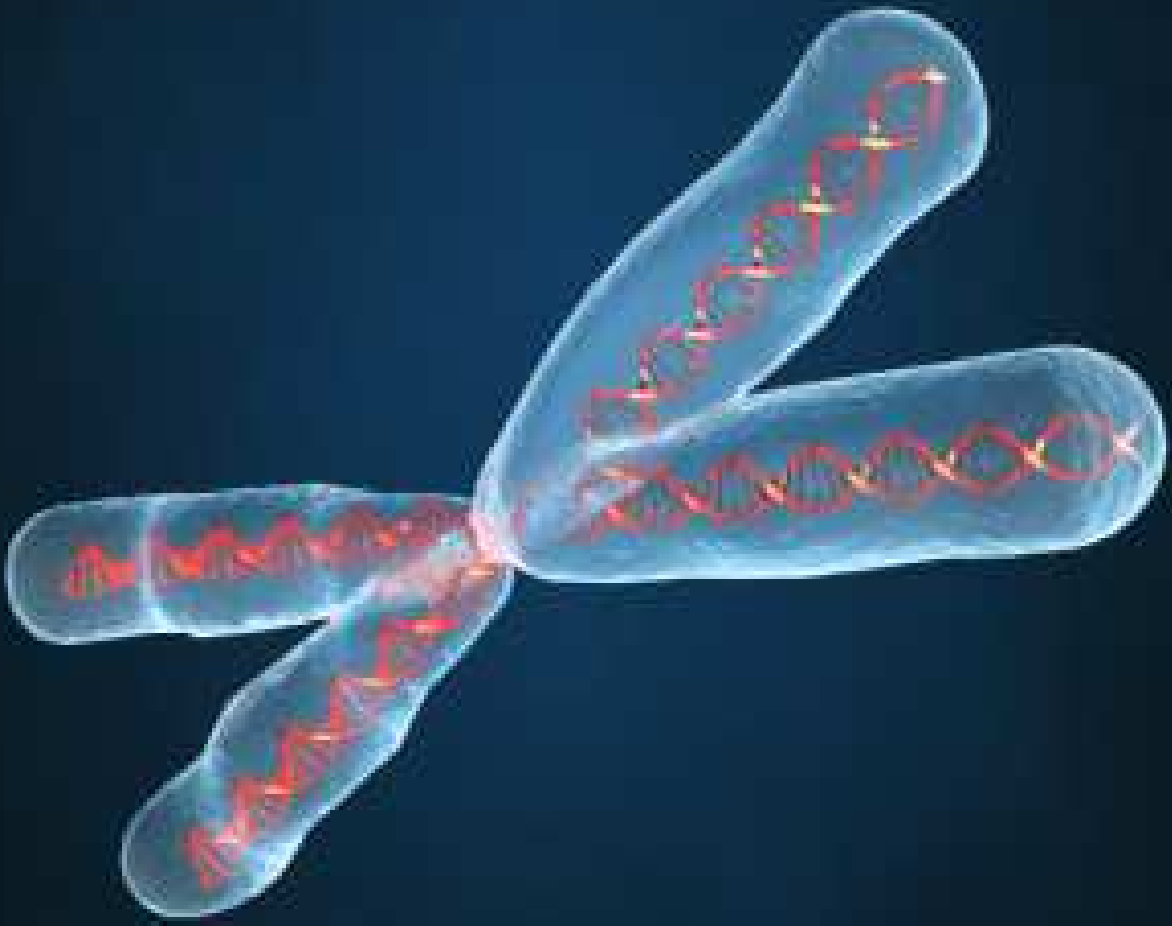

8

Life history and mating systems select for male biased parasitism mediated through natural selection and ecological feedbacks

8.1 Introduction

Sex bias in parasitism is often found across a diverse range of taxa, with males commonly the 'sicker' sex (Zuk, 1990, 2009). Although such male-biased parasitism is the most commonly reported (Ferrari et al., 2004, Perkins et al., 2003, Poulin, 1996, Schalk and Forbes, 1997), higher rates of parasitism and less investment in immunity have also been reported for females (McCurdy et al., 1998, McKean and Nunney, 2005, Zuk et al., 2004). It remains unclear what processes can account for sex-biased parasitism and in particular the higher prevalence of disease in males. One possibility is that males exhibit different behavior that leads to greater exposure (i.e. larger home ranges or more risk of infection for any given exposure because of damage caused by fighting) (Bundy, 1988, Restif and Amos, 2010). Bias may also result from underlying differences in life-history characteristics between males and females (Moore and Wilson, 2002) including the idea that the larger physical size and growth rates of males make them a more accessible and attractive target for parasites (Moore and Wilson, 2002). There is also clear evidence of a physiological basis for differences in susceptibility with for example androgenic hormones in males (testosterone in vertebrates) acting to depress the im-

mune system (Alexander and Stimson, 1988, Folstad and Karter, 1992, Moore and Wilson, 2002).

Beyond physiological mechanisms, it has been proposed that life-history theory could explain immune differences from an adaptive point of view in relation to sex-specific reproductive strategies. In particular, it has been argued that the reduced investment in resistance is due to trade-offs between male mating effort and immune defence. In this scenario as the strength of sexual selection on males increases, the magnitude of the sex differences in immunocompetence will increase. In essence the argument is that a reduced immune systems may be the unavoidable price of being male due to sexual selection (Zuk, 1990, 2009). Following on from this a polygynous mating systems should lead to greater differences in male biased parasitism and under polyandry females should be more susceptible (Zuk, 1990, 2009). The basic assumptions of these ideas have recently been examined theoretically by Stoehr and Kokko (2006) who determine optimal allocation of resources between immunity, survival and reproduction in males and females, under varying levels of sexual selection. This theory has shown that sexual selection may explain male-biased parasitism (Stoehr and Kokko, 2006, Zuk, 2009). In addition, Moore and Wilson (2002) carried out a meta-analysis using two measures of the strength of sexual selection (mating system and sexual size dimorphism) and showed that sexual selection was associated with sex differences in parasitism.

There is a large body of theoretical work that has emphasized the importance of ecological feedbacks to the evolution of host defence to infectious disease (see Boots et al. (2009) for a review). It is clear from this theory that host life-history is critical to level of defence that evolves. In particular, it is often, although not always the case, that increased resistance to parasites is more likely to evolve for long-lived hosts (Miller et al., 2007a). Differences between males and females in terms of their life-histories may therefore be enough to explain the evolution of different levels of investment in defence through natural rather than sexual selection. In particular differences in ecological feedbacks between males and

females due to differences in their life-histories may underpin the evolution in reduced investment by males in defence and therefore result in higher transmission of infection. Furthermore, the ecological feedbacks due to monogamous and polygynous mating systems may have different effects on the evolution of male and female investment in defence. In particular, different mating systems could cause different patterns in the way in which densities of males and females feedback into the evolutionary dynamics.

A recent model (Restif and Amos, 2010) has shown the importance of epidemiological feedbacks in determining male-biased parasitism through natural selection. Restif and Amos (2010) develop a model with explicit genetics (two diploid loci with a link between genotype and phenotype) to investigate how the evolution of sex-specific investment in immune defenses (through recovery from, or tolerance to, infection) are affected by a combination of life-history trade-offs and pre-existing differences between male and female phenotypes (in particular an imposed sex-specific difference in exposure to disease). Our aim is to investigate how the mating system and differences in competitive ability and longevity between sexes influence the level of resistance to infection that evolves. Our study additionally differs from Restif and Amos (2010) in that we examine the effect of mating system on the level of evolved resistance in each sex and we do not impose pre-existing sex-specific differences in disease parameters. We also examine the effects of mating system and host life-history under natural selection that includes epidemiological dynamics, focusing on how ecological feedbacks affect the evolutionary process. We find that differences in lifespan are enough to explain male biased parasitism. Differences in the mating system act only to accentuate an existing bias. Our work further emphasizes the importance of including epidemiological feedbacks when studying the evolution of defence.

8.2 Methods

The underlying host-parasite framework is based on the classical approaches for modelling the population dynamics of directly transmitted microparasites (see Anderson and May (1981)) and which have been successfully extended to understand the evolution of host resistance (Boots et al., 2009, Boots and Haraguchi, 1999). This framework is modified following the techniques of Lindström and Kokko (1998) and Miller et al. (2007b), to represent a two-sex host parasite model that considers the dynamics of males and females separately. This is achieved by representing births as the harmonic mean function proposed by Caswell and Weeks (1986), that depends on the densities of the two sexes and declines to zero in the absence of either sex. This function can also be modified to approximate different mating systems (monogamy, polygyny and polyandry)[1]. The theoretical framework is therefore represented by the following system of nonlinear ordinary differential equations for the densities of susceptible, S, and infected, I, males and females, represented by the subscripts m and f respectively.

$$\begin{aligned}
\frac{dS_m}{dt} &= \frac{1}{2}B(S_m,S_f)(1-q_mH) - d_mS_m - \beta_mS_m(I_f+I_m) \\
\frac{dI_m}{dt} &= \beta_mS_m(I_f+I_m) - (d_m+\alpha)I_m \\
\frac{dS_f}{dt} &= \frac{1}{2}B(S_m,S_f)(1-q_fH) - d_fS_f - \beta_fS_f(I_f+I_m) \\
\frac{dI_f}{dt} &= \beta_fS_f(I_f+I_m) - (d_f+\alpha)I_f
\end{aligned} \tag{8.1}$$

Here $H = S_f + S_m + I_f + I_m$ is the total host density. Births are divided equally between males and females according to the harmonic

[1]Monogamy: males and females have one mate. Polygyny: a male has more than one female mate. Polyandry: a female has more the one male mate.

birth function, $B(S_m, S_f)$, which describes the dependency of the birth rate on the density of either sex and mating strategy. The birth rate is modified due to density-dependent competition for resources with the parameter q, and the population has a natural death rate, d. Infection can occur through contact between susceptible and infected individuals with transmission coefficient, β, and the disease induces an additional mortality while infected at rate α. (The subscripts on some parameters distinguishes between male and female specific parameters.) The harmonic birth function, $B(S_m, S_f)$, is derived from (Caswell and Weeks, 1986), and takes the following form.

$$B(S_m, S_f) = \frac{c_m S_m c_f S_f}{S_m + \frac{S_f}{h}} \tag{8.2}$$

Here, c_m and c_f represent the contribution that males and females make to the birth rate and h represents harem size and can be manipulated to represent different mating systems. When $h > 1$ it represents a polygynous mating system (births are maximized when females exceed males), when $h < 1$ it represents polyandry (births are maximized when males exceed females) and when $h = 1$ it represents monogamy (births are maximized when males and females are equally abundant) (Caswell and Weeks, 1986).

To examine the evolution of parasite resistance we follow the techniques of adaptive dynamics (Boots et al., 2009, Geritz et al., 1998). We assume a 'mutant' strain of host can occur at low density and attempt to invade the established 'resident' strain which is at its equilibrium density. The mutant male host strain differs from the resident strain in terms of its transmission coefficient $\tilde{\beta}_m$ compared to β_m for the resident (a similar difference can occur for the female transmission coefficient and we will use '˜' to represent the mutant parameters). In line with previous studies into the evolution of host resistance it is assumed and that a benefit in terms of increased resistance to infection is bought at a cost in terms of a reduced birth rate (Boots and Haraguchi, 1999). For this study we impose

the trade-off $c_m = g(\beta_m)$ and $c_f = g(\beta_f)$. The trade-off is defined by

$$c_m = c_{max} - \left((c_{max} - c_{min}) \frac{\left(1 - \frac{\beta m - \beta min}{\beta max - \beta min}\right)}{\left(1 + \gamma \frac{\beta m - \beta min}{\beta max - \beta min}\right)} \right) \tag{8.3}$$

which is a smooth curve between the minimum and maximum values of the birth and transmission rates and in which the parameter γ controls the curvature (and therefore cost structure) of the trade-off, see Figure 8.1. (We will discuss other possible trade-offs later.)

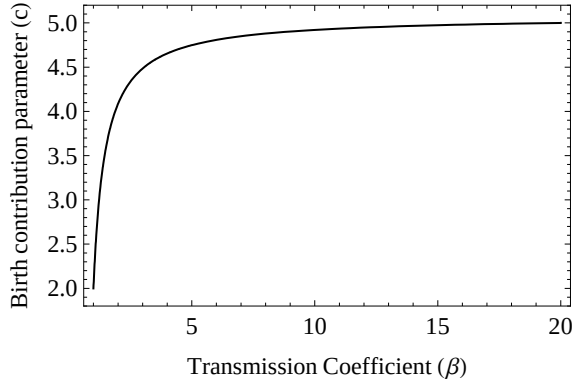

Figure 8.1. A trade-off with accelerating costs as defined by Eq. (8.3). Parameters are $c_{min} = 2$, $c_{max} = 5$, $\beta_{min} = 1$, $\beta_{max} = 20$ and $\gamma = 40$.

The fitness is the long-term exponential growth rate of a phenotype in a given environment. We initially consider the situation where the female parameters are fixed and we allow the male parameter β_m (and c_m via the trade-off) to evolve. A proxy for the fitness, R, can be calculated as the determinant of the jacobian matrix, J, at the steady state $(S_m, S_f, I_m, I_f, \tilde{S}_m, \tilde{I}_m) = (S_m^*, S_f^*, I_m^*, I_f^*, 0, 0)$ (Miller et al., 2005) where

$$J = \begin{pmatrix} \frac{\partial \tilde{S}_m}{\partial \tilde{S}_m} & \frac{\partial \tilde{S}_m}{\partial \tilde{I}_m} \\ \frac{\partial \tilde{I}_m}{\partial \tilde{S}_m} & \frac{\partial \tilde{I}_m}{\partial \tilde{I}_m} \end{pmatrix} \tag{8.4}$$

and therefore, R, can be represented by the following expression

$$R = -b_m - (I_f^* + I_m^*)\tilde{\beta}_m + \frac{c_f a_m g(\tilde{\beta}_m) S_f^* (1 - q_m H^*)}{2(\frac{S_f^*}{h} + S_m^*)} \quad (8.5)$$

$$\text{where } H^* = S_m^* + S_f^* + I_m^* + I_f^*$$

The fitness proxy, R, can be used to determine the position of evolutionary singular points and the evolutionary behavior at the singular point. Evolutionary singular points are determined when the fitness gradient $\frac{\partial R}{\partial \tilde{\beta}_m}\Big|_{\beta_m = \tilde{\beta}_m} = 0$ which equates to solving the following expression

$$-I_f - I_m + \frac{1}{2(\frac{S_f}{h} + S_m)} a_m c_f S_f (1 - q_m H^*) g'(\widetilde{\beta}_m) = 0 \quad (8.6)$$

The evolutionary behavior at the singular point is determined by analyzing the second order partial derivatives of R with respect to the mutant and resident parameters (Geritz et al., 1998). Previous studies have assessed how the trade-off cost structure or underlying population dynamics can influence the evolutionary behavior and also induce evolutionary branching leading to diversity in host strategies (Boots et al., 2009, Boots and Haraguchi, 1999). The focus here is to examine whether different levels of resistance can evolve between males and females. To allow us to concentrate on this issue we ensure that the underlying population dynamics are point equilibrium and that the trade-off has sufficiently accelerating costs that the singular point is an evolutionary stable attractor. We can then assess how the position of the singular point changes as other life history parameters are varied.

To examine the coevolution of male and female resistance properties we determine the female fitness function (which depends on the evolving parameter β_f and c_f via the trade-off). The male singular points are plotted against β_f (for a fixed female strategy using the method outlined above) and the female singular points (against a fixed male strategy) are plotted against β_m . The intersection of these lines produces a coevolutionary attracting singular point (Restif and Koella (2003), note that again

the trade-off is chosen to ensure the population dynamics exhibit a point equilibrium and that the singular point is a coevolutionary stable attractor). Using this method it is possible to determine how the coevolutionary singular point varies with changes in underlying life history parameters.

8.3 Results

The evolutionary behavior is dependent on feedbacks that arise in the ecological dynamics and therefore it is useful to first understand how changes in life history parameters will affect the equilibrium density of the different classes in the model system (Figure 8.2). Increases in the harem size, h, or the overall birth rate leads to an increase the total density of males and females (equally since the sex ratio is 50:50). If the male death rate is reduced (relative to the female death rate) then there is an increase in the overall density of males (through an increase in infected males) and a decrease in female density. As the male death rate is increased then there is an increase in the overall density of females (through an increase in susceptible females) and a decrease in male density. Note also that the prevalence of infection decreases as the male death rate increases (relative to the female death rate). When there is a reduction in the competition parameter for males there is an increase in male density through increases in susceptible and infected males and female density in both susceptible and infected classes is reduced. When there is an increase in the competition parameter for males then overall male density and female infected density decreases while female susceptible density increases. The overall susceptible density remains constant as the competition parameter is varied but the proportion of susceptible males to susceptible females decreases as the competition parameter for males is increased. Also, the prevalence of infection remains relatively constant when the male competition parameter is less than the female parameter but the prevalence decreases when the male competition parameter is greater than the female parameter.

When interpreting the remaining results it is worthwhile recalling

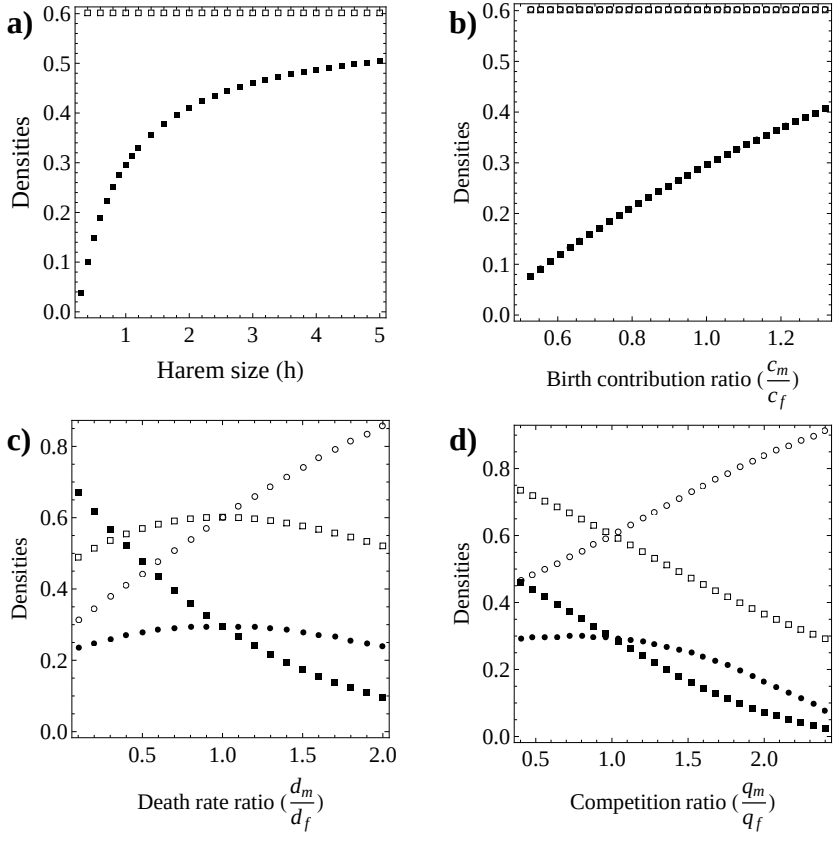

Figure 8.2. Changes in the density of the different classes as other parameters are varied where '○' represents S_f, '•' represents I_f, '□' represents S_m and '■' represents I_m. Parameter values (unless varied in the figure) are $c_m = c_f = 3.79$, $q_m = q_f = 0.25$, $d_m = d_f = 1$, $\alpha_m = \alpha_f = 1$, $\beta_m = \beta_f = 1.6625$, $h = 1$. In a) h a is varied, b) c_m is varied, c) d_m is varied and d) q_m is varied. In a) and b) $S_f = S_m$ and $I_f = I_m$ so the results are just shown for males.

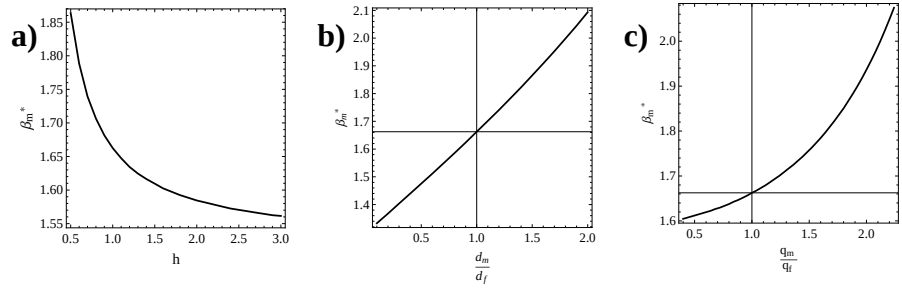

Figure 8.3. Change in the singular value of disease transmission for males, β_m^*, when males can evolve (and females do not evolve). Parameters values (unless varied in the figure) are $c_f = 3.79$, $q_m = q_f = 0.25$, $d_m = d_f = 1$, $\alpha_m = \alpha_f = 1$, $\beta_f = 1.6625$, $h = 1$. The parameters for the trade-off (Eq. (8.3)) are $\beta_{min} = 1$, $\beta_{max} = 20$, $c_{min} = 2$, $c_{max} = 5$ and $\gamma = 40$. In a) harem size, h is varied, b) death rate, d_m is varied and c) male competition q_m is varied.

that a decrease/increase in disease transmission equates to an increase/decrease in disease resistance and that male biased parasitism occurs when $\beta_m > \beta_f$.

8.3.1 Evolving male characteristics.

The results when the male characteristics are allowed to evolve against fixed female parameters are shown in Figure 8.3. As harem size increases the level of resistance to disease in males increases (the singular value of β_m decreases). The evolved level of disease resistance in males decreases as the male death rate increases and the male competition parameter increases. The decrease in disease resistance in males is a response to decreased levels of prevalence of infection (see Figure 8.2) which reduces the need to avoid infection (as individuals are less likely to become infected). Male-biased parasitism is therefore evident under polyandrous mating systems and when males have a higher death rate or suffer more severe competition than females.

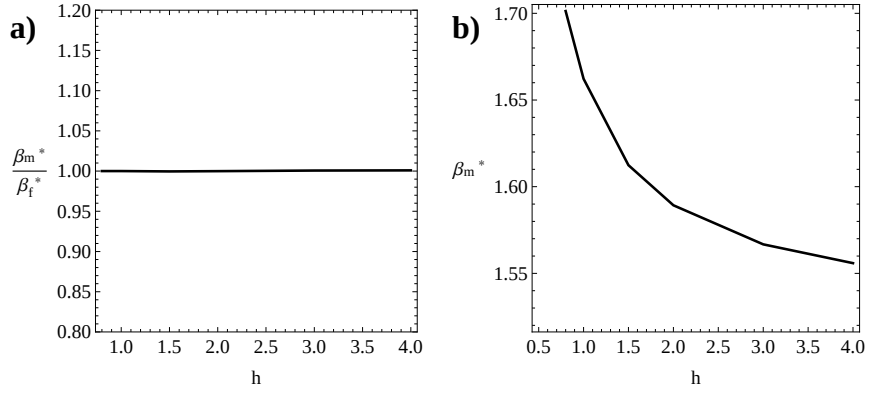

Figure 8.4. Change in the coevolutionary singular value of disease transmission, β_m^* and β_f^* plotted against changes in harem size, h. Parameter values are $q_m = q_f = 0.25$, $d_m = d_f = 1$, $\alpha_m = \alpha_f = 1$. The parameters for the trade-off (Eq. (8.3)) are as in Fig.8.3. a) shows the relative values of β_m and β_f at the coevolutionary singular point and b) shows the actual value of β_m^* at the coevolutionary singular point (note the value of β_f^* is identical here).

8.3.2 Coevolving male and female characteristics

When both male and female characteristics are allowed to evolve variation to the harem size does not produce a bias between male and female infection rates (Figure 8.4a). Both males and females will evolve increased levels of resistance as harem size increases (Figure 8.4b) in response to the associated increases in prevalence.

When the male death rate exceeds that of females then male biased parasitism can result from coevolution (Figure 8.5a). Here the increased death rate for males means they have, on average, a shorter lifespan and this increases the possibility of dying from natural causes before becoming infected. This is reflected in the fact that the proportion of female to male susceptible increases as the male death rate increases. Since there are more susceptible females than males it implies that females are more likely to be infected and therefore males can afford to evolve decreased resistance. When male biased parasitism occurs the bias increases as harem

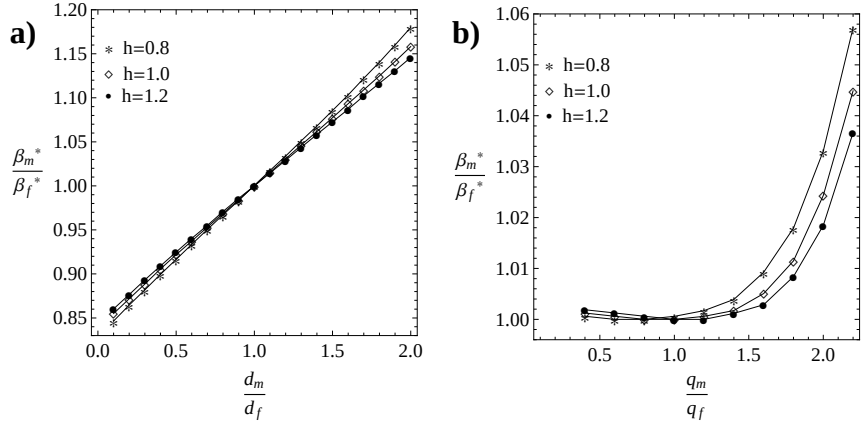

Figure 8.5. Change in the coevolutionary singular value of disease transmission β_m^* and β_f^* plotted against changes in a) male death rate, d_m and b) male competition, q_m. Parameter values (when not varied in the figure) are $d_m = d_f = 1$, $q_m = q_f = 0.25$, $\alpha_m = \alpha_f = 1$, $\beta_m = \beta_f = 1.6625$. The parameters for the trade-off (Eq.(8.3)) are as in Fig.8.3.

size decreases. Here, as harem size decreases the prevalence of infection decreases and the evolved level of disease resistance decreases (and therefore transmission of infection increases) for both males and females (Figure 8.4). This accentuates the relative bias in the transmission of infection between males and females in a multiplicative manner.

A similar response occurs when male competition exceeds that of females (Figure 8.5b) and can again be attributed to changes in the proportion of female to male susceptible as the male competition parameter increases. When the male competition parameter is reduced below that of the female parameter the evolved level of resistance remains relatively constant. This occurs as the prevalence of infection also remains relatively constant and therefore there is no selection for a change in resistance to infection.

8.3.3 Generality of results for other trade-offs

We have undertaken the above analysis when the level of parasitism, β, is traded-off against the competition parameter, $q(q = g(\beta))$, and where we have imposed a trade-off such that a decrease in parasitism rate for females results in an increase in the parasitism rate for males $(\beta_m = g(\beta_f))$. We find the results are analogous to those presented above. The changes in the mating system do not produce a bias in parasitism between males and females. Male biased parasitism occurs when the males have a short lifespan (or where appropriate suffer increased competition) in comparison to females. Again the type of mating system can only accentuate this bias rather than cause it.

8.4 Discussion

Differences in the rate of parasitism between sexes, in particular male biased parasitism, is often observed in nature (see Moore and Wilson (2002), Skorping and Jensen (2004), Zuk (1990, 2009)). We examined whether parasite bias between the sexes could arise as a result of the mating system or through differences in the underlying life history characteristics between males and females through natural selection due to the epidemiological feedbacks that they cause. As such we are examining the evolutionary ecological implications of life-history and mating system in isolation from the role that they may play in sexual selection. Male-biased parasitism was selected for when males have a shorter lifespan than females or when males were subject to greater competition for resources than females (provided the overall level of competition was not too low). Changes to the mating system did not produce a bias in parasitism but could accentuate an existing bias. In particular as harem size decreases an existing male bias in parasitism is increased as a result of a decrease in overall prevalence. We therefore predict more male biased parasitism when males have shorter life spans than females in monogamous or polyandrous species.

Selection for biased rates of parasitism requires there to be underlying differences in the life history characteristics of males and females. Male-biased mortality rates have been reported in vertebrate and invertebrate systems (Promislow, 1992, Rolff, 2002) and it has been shown to have a positive correlation with male-biased parasitism (Moore and Wilson, 2002). It has therefore been suggested that male-biased parasitism may drive the increased mortality rates in males (Moore and Wilson, 2002). Our study indicates the converse, that male-biased parasitism may evolve as a consequence of male-biased mortality. (Moore and Wilson (2002) noted this as a possible interpretation of their empirical findings.) We show that increased mortality in males leads to differences in the population dynamics, with a greater proportion of susceptible females than males. This reduces the likelihood of infection for males and so they can afford to evolve decreased resistance. Fundamentally our argument is that non-disease causes of higher mortality in males *per se* may select for the observed decrease in immune investment. This increase in mortality can come from processes such as increased risks from larger range size or fighting over females. By examining how natural selection operates through the ecological feedbacks we show in general terms that if males are shorter lived they will invest less in resistance.

The mating system, determined by the choice of the harem size, does not directly select for differences in parasitism between males and females in our models. However, we do find that differences in life-history characteristics that select for parasitism bias can be accentuated by the mating system. This is because as the harem size reduces, total prevalence levels also reduce leading to selection for reduced levels of host resistance. The mating system, which in this study acts via the harmonic birth function, affects population density and the overall level of disease resistance that evolves. If there is less selection for resistance then given an existing bias, it becomes accentuated. Taken as a whole, our results on the importance of mating systems are very different to those expected from sexual selection theory and shown in comparative studies (Moore and Wilson, 2002, Stoehr and Kokko, 2006, Zuk, 1990, 2009). Generally polygynous species are expected to have stronger selection and therefore

more male biased parasitism. Our results show that for a 50-50 sex ratio the ecological feedbacks that operate due to natural selection affect males and females equally. Therefore, the mating system *per se* does not lead to a sexual bias through ecological feedbacks. Furthermore, the effect of mating system on accentuating existing biases runs counter to the prediction from sexual selection studies. Monogamous or polyandrous mating systems are more likely to accentuate the bias and therefore show male biased parasitism. Therefore the selection pressures due to ecological feedbacks may run counter to those that result from sexual selection. The outcome will depend on the relative strength of the different selection pressures in particular natural systems.

The model results can be used to examine when female biased parasitism can evolve. By swapping the male and female labels on population classes and parameters it would indicate the female biased parasitism could evolve if females had higher mortality rates or were subject to greater competition for resources that males. This further emphasizes the idea that it is differences in the underlying mortality/competition rates between the sexes that can drive a bias in their rates of parasitism. The evolved bias would be accentuated in monogamous or polygynous mating systems (since when the labels are swapped a value of $h < 1$ indicates polygyny). This is again counter to the ideas from sexual selection studies in which polyandrous mating systems are predicted to produce female biased parasitism (Zuk (1990, 2009)).

The mating system can have important consequences for the population dynamics that are exhibited and can lead to complicated (cycles, chaos) dynamical behavior (Lindström and Kokko, 1998, Miller et al., 2007b). Recently, the population dynamical effects of male-biased parasitism for different case mortalities and both monogamous and polygamous mating systems (Miller et al., 2007b) have been examined. The population dynamics exhibited (point stability, cycles, chaos) did not show clear trends with increasing male-biased parasitism and the outcome depended on a complex interaction between the hosts mating system, demography and parasite virulence (Miller et al., 2007b). Here we focus

on the situation where the underlying population dynamics are at a stable point equilibrium to allow analysis of the fitness expression. We also choose the trade-off to ensure the singular point is an evolutionary stable attractor. Studies which examine the evolutionary behavior for non-equilibrium underlying dynamics are rare but report that the evolutionary behavior would not change for trade-offs where an attractor is predicted under equilibrium conditions (Hoyle et al., 2010, White et al., 2006). We would therefore expect our finding to extend to non-equilibrium underlying dynamics.

Our results confirm previous general work on the evolution of resistance to parasites (Boots et al., 2009, Miller et al., 2007a) in that we find that the evolved level of host resistance increases as the average lifespan of the host increases. This result is linked to increased levels of prevalence which occur as lifespan increases. In our study the prevalence levels also increase as the harem size increases or as the level of competition for resources is reduced (until the competition for resources is low) (Figure 8.2). As prevalence of infection increases it is beneficial to evolve higher levels of resistance in an attempt to avoid infection. Throughout we have assumed that there is no long-lived immunity after recovery from infection. In principle this may have important consequences with circumstances under which longer-lived individuals do not invest more in immunity. As such male biased parasitism may be less likely in disease with long lasting immunity, but a full theoretical analysis has not as yet been carried out.

This theoretical study examines the evolution of male-biased parasitism in the context of the complex epidemiological feedbacks in disease systems. A recent paper has also shown the importance of epidemiological feedbacks to the evolution of male biased parasitism (Restif and Amos, 2010). In a comprehensive study, they examine how differential exposure between males and females affects various aspects of investment in immunity under a range of trade-offs including one between recovery and lifespan (Restif and Amos, 2010). The model includes diploid genetics mapped onto a quantitative trait and fundamentally includes the

epidemiological feedbacks caused by different investments under monogamous mating systems. Restif and Amos (2010) show that reduced investment in males can evolve when there is more exposure to parasites (achieved by imposing differences in some of the disease characteristics between males and females). Their results further emphasize the importance of epidemiological feedbacks. Our model system does not include explicit genetics but allows female/male phenotype characteristics to be inherited directly from the maternal/paternal parent respectively. This is clearly a simplification of inheritance but where direct comparisons can be made with the study of Restif and Amos (2010) our results are qualitatively similar. Our study does not impose underlying differences in disease characteristics but focuses on the role of host life history and mating system. We have shown that male-biased parasitism can evolve as a consequence of sexual differences in life history characteristics that produce a greater proportion of susceptible females than males. Our results extend to different choices of trade-offs. Future studies should extend the analysis to examine the importance of the choice of underlying infectious disease framework and the representation of the two-sex birth function that may include assessing the effects of a non-equal sex ratio. Throughout we are focusing on the role of natural selection in the context of epidemiological feedbacks. Future work could combine this approach with models of sexual selection in order to gain a full understanding of the mechanisms that underpin male biased parasitism. The combined genetic and quantitative trait model of Restif and Amos (2010) could be extended to provide a framework in which to examine these different processes.

Bibliography

Alexander, J., Stimson, W., 1988. Sex hormones and the course of parasitic infection. Parasitol. Today 4 (7), 189 – 193.

Anderson, R. M., May, R. M., 1981. The population dynamics of microparasites and their vertebrate hosts. Phil. Trans. R. Soc. B 291 (27), 451–524.

Boots, M., Best, A., Miller, M. R., White, A., 2009. The role of ecological feedbacks in the evolution of host defence: what does theory tell us? Phil. Trans. R. Soc. B 364 (1513), 27–36.

Boots, M., Haraguchi, Y., 1999. The evolution of costly resitance in host-parasite systems. Am. Nat. 153 (4), 359–370.

Bundy, D., 1988. Gender-dependent patterns of infections and disease. Parasitol. Today 4 (7), 186 – 189.

Caswell, H., Weeks, D. E., 1986. Two-sex models: Chaos, extinction, and other dynamic consequences of sex. Am. Nat. 128 (5), 707–735.

Ferrari, N., Cattadori, I. M., Nespereira, J., Rizzoli, A., Hudson, P. J., 2004. The role of host sex in parasite dynamics: field experiments on the yellow-necked mouse *Apodemus flavicollis*. Ecol. Lett. 7 (2), 88–94.

Folstad, I., Karter, A. J., 1992. Parasites, bright males, and the immunocompetence handicap. Am. Nat. 139 (3), 603.

Geritz, S., Kisdi, E., Meszéna, G., Metz, J., 1998. Evolutionarily singular strategies and the adaptive growth and branching of the evolutionary tree. Evol. Ecol. 12, 35–57.

Hoyle, A., Bowers, R., White, A., 2010. Evolutionary behaviour, trade-offs and cyclic and chaotic population dynamics. Bull. Math. Biol. In Press.

Lindström, J., Kokko, H., 1998. Sexual reproduction and population dynamics: the role of polygyny and demographyc sex differences. Proc R. Soc Lod.B 265, 483–488.

McCurdy, D. G., Shutler, D., Mullie, A., Forbes, M. R., 1998. Sex-biased parasitism of avian hosts: Relations to blood parasite taxon and mating system. Oikos 82 (2), 303–312.

McKean, K. A., Nunney, L., 2005. Bateman's principle and immunity: phenotypically plastic reproductive strategies predict changes in immunological sex differences. Evolution 59 (7), 1510–1517.

Miller, M. R., White, A., Boots, M., 2005. The evolution of host resistence: Tolerance and control as distinct strategies. J. Theor. Biol. 236, 198–2075.

Miller, M. R., White, A., Boots, M., 2007a. Host life span and the evolution of resistance characteristics. Evolution 61 (1), 2–14.

Miller, M. R., White, A., Wilson, K., Boots, M., 2007b. The population dynamical implications of male-biased parasitism in different mating systems. PLoS ONE 2 (7), 1–8.

Moore, S. L., Wilson, K., 2002. Parasites as a viability cost of sexual selection in natural populations of mammals. Science 297, 2015–2018.

Perkins, S. E., Cattadori, I. M., Tagliapietra, V., Rizzoli, A. P., Hudson, P. J., 2003. Empirical evidence for key hosts in persistence of a tick-borne disease. Int. J. Parasitol. 33 (9), 909 – 917.

Poulin, R., 1996. Sexual inequalities in helminth infections: A cost of being a male? Am. Nat. 147 (2), 287–295.

Promislow, D. E. L., 1992. Costs of sexual selection in natural populations of mammals. Proc. Biol. Sci. 247 (1320), 203–210.

Restif, O., Amos, W., 2010. The evolution of sex-specific immune defences. Proc. R. Soc. B. 277 (1691), 2247–2255.

Restif, O., Koella, J. C., 2003. Shared control of epidemiological traits in a coevolutionary model of host-parasite interactions. Am. Nat. 161 (6), 827–836.

Rolff, J., 2002. Batemans principle and immunity. Proc Biol Sci. 269 (1493), 867–872.

Schalk, G., Forbes, M. R., 1997. Male biases in parasitism of mammals: Effects of study type, host age, and parasite taxon. Oikos 78 (1), 67–74.

Skorping, A., Jensen, K. H., 2004. Disease dynamics: all caused by males? Trends Ecol. Evol. 19 (5), 219 – 220.

Stoehr, A. M., Kokko, H., 2006. Sexual dimorphism in immunocompetence: what does life-history theory predict? Behav. Ecol. 17, 751–756.

White, A., Greenman, J. V., Benton, T. G., Boots, M., 2006. Evolutionary behaviour in ecological systems with trade-offs and non-equilibrium population dynamics. Evol. Ecol. Res. 8, 387–398.

Zuk, M., 1990. Reproductive strategies and disease susceptibility: an evolutionary viewpoint. Parasitol. Today 6 (7), 231 – 233.

Zuk, M., 2009. The sicker sex. PLoS Pathog 5 (1), e1000267.

Zuk, M., Simmons, L. W., Rotenberry, J. T., Stoehr, A. M., 2004. Sex differences in immunity in two species of field crickets. Can. J. Zoo 82 (4), 627–634.

9

Conclusion and perspectives

In this thesis different models of non-linear ecological systems with regime shifts were explored. Different sort of mathematical analysis were used, either equation-based models or individual-based models. Half of the results were obtained in marine ecology using analysis in differential equations. One part explored patterns in savanna using a cellular automata tool and the last part focused on adaptive dynamics to study evolutionary behavior in mating systems. In this chapter the main results will be summarized divided by chapters, following the same order presented in the body of the thesis.

Chapter 5: Joint effects of nutrients and contaminants on the dynamics of a food chain in marine ecosystems. In this work a model for a marine food chain (nutrient, phytoplankton, zooplankton and fish) was analyzed by means of the tools of dynamical systems theory (qualitative and numerical analysis of differential equations, and bifurcation theory), aiming at considering the join effects of nutrient supply and pollution by a contaminant on the system dynamics. Contaminant having toxic effects in each species of the trophic chain was introduced in the model by altering their mortalities. The influence of contaminants on species mortalities was assumed to have a sigmoidal dose-response relationship. This generates delay in the transitions to complex dynamical states occurring at higher nutrient load values. Apart from that, more counterintuitive consequences arise from indirect effects related to the non-linearities pertained to the food chain dynamics. In particular, the top predator seems to be the species more affected by pollutants, even when contaminant is toxic only to lower trophic levels. Besides, contaminants increase the stability

of the food chain with respect to oscillations which would occur under increased nutrient input.

Chapter 6: Modeling approach to regime shifts of primary production in shallow coastal ecosystems. In this work a competition model between rooted seagrass (Zostera marina), macroalgae (Ulva sp.), and phytoplankton has been developed to analyze the succession of primary producer communities in these systems. This model is an integrated model that uses previous existing and validated models developed for Mediterranean coastal lagoons. In order to deal with the ability of seagrass to survive at low nutrient conditions, the dynamics of inorganic nitrogen (nitrates and ammonium) in the water column and in the sediments have also been included. The model described successions of dominance states, with different resilience characteristics when changing input of nutrients and the seasonal temperature and light intensity forcing. The model simulations show a general agreement with the experimental results reported in literature concerning thresholds of nutrient concentrations at which a regime shift occurred. Namely the model shows the algae bloom phenomenon caused by eutrophication process (high nutrient levels), also a regime of Ulva dominance, the dominance of Zostera in low nutrients concentrations dissolved in the water column and the regimes in which both vegetation types coexist. Apart from competition between rooted seagrass and macroalgae, the model showed the implications of the presence of phytoplankton in the system and showed that phytoplankton is able to compete with Ulva for nutrients in the water column, thus favoring Zostera due to the lower shadowing effect.

Chapter 7: Savanna-Fire Model. Savannas are characterized by a discontinuous tree layer superimposed on a continuous grass layer. Savannas occur across a wide range of climatic, edaphic, and ecological conditions covering approximately one fifth of the earth's land area. In some countries these grass- dominated ecosystems are a principal biotic resource playing important roles in both the configuration of natural landscapes and in local economies. Identifying the mechanisms that facilitate tree-grass coexistence in savannas has remained a persistent chal-

lenge in ecology and is known as the ”savanna problem”. In this work, a model was proposed to combine the previous savanna model (Calabrese et al., 2010) with the Drossel-Schwabl forest fire, therefore representing fire in a spatially explicit manner. The model was used to explore how the pattern of fire-spread, coupled with an explicit, fire-vulnerable tree life stage, affects tree density and spatial pattern. Tree density depends strongly on both fire frequency and tree-tree competition and under extreme conditions can drive tree extinction (grassland). However fire frequency appears to be the crucial factor on tree extinction. By increasing fire frequency a phase transition happens between the savanna (coexistence) state and grassland. Since fire is an explicit state in the model, fire fronts can spread following different paths that can lead to different regular or clumped patterns, the last ones of compact- or open-clusters type. In the study of cluster distributions , we find fat tails which approach power-law behavior in some cases.

Chapter 8: Life history and mating systems select for male biased parasitism mediated through natural selection and ecological feedbacks. In a range of ecological systems, there is evidence that the level of infection from parasites is higher in males than in females. Previous theoretical studies have shown that this has implication for the population dynamics of the host. In this study, modern game-theoretical approaches (adaptive dynamics) was used to examine the circumstances under which male-biased parasitism would evolve. A system of ordinary differential equations that represents a host-parasite system and also distinguishes between males and females was examined. In addition studies were performed examining the evolution of resistance to infection when males and females have a trade-off between the level of host resistance and the birth rate. Male-biased parasitism was selected for when males have a shorter lifespan than females or when males were subject to greater competition for resources than females (provided the overall level of competition was not too low). Changes to the mating system did not produce a bias in parasitism but could accentuate an existing bias. In particular as harem size decreases an existing male bias in parasitism is increased as a result of a decrease in overall prevalence. Therefore the model predicts more

male biased parasitism when males have shorter life spans than females in monogamous or polyandrous species.

Open jobs

Different tools in the analysis of complex and non-linear systems were used to study different problems in biology during this thesis. However during these years much more was done in searching interesting phenomena to be analyzed and understood. I will list some works that are still in process and that are worth finishing.

Hysteresis: Shifting baselines affect ecosystem restoration targets

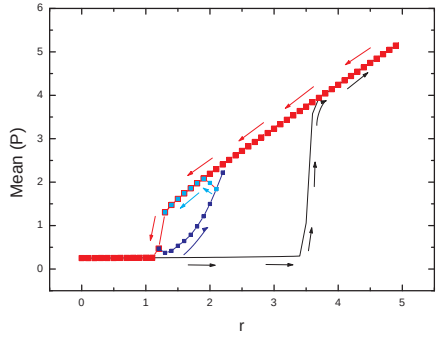

Figure 9.1. Phosphorous values (P) in a lake model (Carpenter et al., 1999): $\frac{dP}{dt} = F - SP + r\frac{P^q}{P^q+K^q} - D\nabla^2 P$ in the presence of quenched (static) disorder. K is a static Gaussian white noise. Small cycles can be found inside the hysteresis cycle hardly changing forward and backward in response to slow shifts in the control parameter (nutrient load).

The idea is to provide a scientific framework to study ecosystems impacted by human pressures that could be reverted to their original condition by suppressing the pressure (e.g.eutrophication/ oligotrophication) (Duarte et al., 2009). The starting point was to analyze models that have alternative attractors subjected to random spatial dispersion, this helps the understanding of ecosystem response to multiple shifting baselines in order to set reliable targets for restoration efforts. Two models were chosen, the Carpenter model (Carpenter et al., 1999) and the Noy-Meir model (Noy-Meir, 1975). Similarly to Van Nes and Scheffer (2005) some studies were performed to observe the effect of static gaussian noise. Preliminary analysis was performed using a dynamical colored noise in the spatial heterogeneity and adding heterogeneity in all parameters and changes in the control parameter of

each time step.

A continuous model of Savannas

This work is a complementary study of the mean field approximation of Calabrese et al.(2010) work. The idea is the obtain the patterns of tree distribution in savanna (see Figure 9.2) through a continuous model adding the non-local interactions in the competition term:

$$\dot{\rho}_1 = be^{-\delta \int H(r-r')\rho_1(r',t)dr'} \frac{\sigma}{\sigma+1-\rho_1(r,t)}(\rho_1(r,t)-\rho_1(r,t)^2) - \alpha\rho(r,t) \tag{9.1}$$

where H is the step-function kernel: $H(r)=\begin{cases} 1, & if\ r \leq R; \\ 0, & if\ r > R. \end{cases}$

Some stability analysis was performed using the same theory in the studies of pattern formation in López and Hernández-García (2004) (Figure 9.3). Uniform and periodic patterns can be obtained, but it is a challenge to model clumped states in terms of continuous fields.

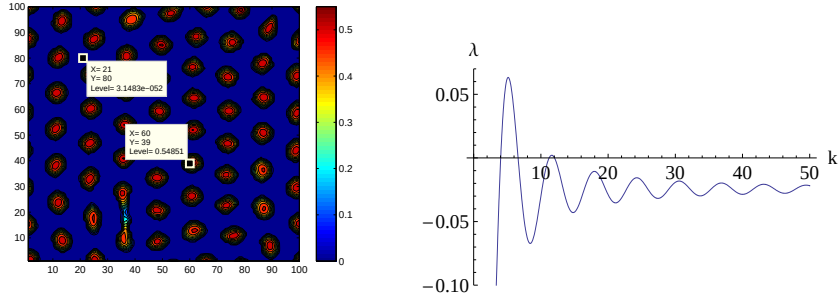

Figure 9.2. Spot pattern in savanna model. Parameters: $\sigma = 0.33$, $\delta = 2.5$, $\alpha = 1$ and $b = 8$. Right: growth rate of a function of wave number.

The effects of prey switching on predator persistence in a one predator-two prey system with a refuge.

In many predator-prey situations, the predator has a preferred prey. However, in many cases this preferred prey has a refuge in which it is safe from predation. If it does not search for alternate prey, the predator

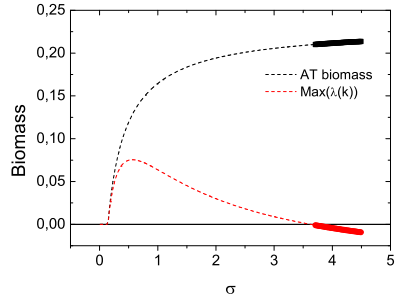

Figure 9.3. Adult tree biomass versus related fire parameter in black and in read the maximum eigenvalue of the coexistence solution. Thick lines represent the stable homogeneous solution, what means that no pattern arises in this region.

may well go extinct. Each time the preferred prey attempts to increase its population beyond the refuge, the predator switches its predation to its preferred prey, driving the population back into small numbers in the refuge (Bergerud, 1983).

Figure 9.4. Lynx preying on snowshoe hare.

In this work a system of four ordinary differential equations is studied to describe one example of such a predator-prey system. A case in point is a predator-prey system on the island of Newfoundland in Atlantic Canada, where the predator population, Canada lynx prefers the snowshoe hare, but switches to the arctic hare when the former population becomes scarce. Studies of equilibria and their stabilities was analyzed. The next step is to determine the criteria for periodic solutions and persistence.

Bibliography

Bergerud, A., 1983. Prey switching in a simple ecosystem. Scientific American 249, 130–141.

Carpenter, S. R., Ludwig, D., Brock, W. A., Aug 1999. Management of eutrophication for lakes subject to potentially irreversible change. Ecological Applications 9 (3), 751–771.

Duarte, C. M., Conley, D., Carstensen, J., Sanchez-Camacho, M., 2009. Return to neverland: Shifting baselines affect eutrophication restoration targets. Estuaries and Coasts 32 (1), 29–36.

López, C., Hernández-García, E., 2004. Fluctuations impact on a pattern-forming model of population dynamics with non-local interactions. Physica D: Nonlinear Phenomena 199 (1-2), 223 – 234.

Noy-Meir, I., Jul. 1975. Stability of grazing systems: An application of predator-prey graphs. Journal of Ecology 63 (2), 459–481.

Van Nes, E. H., Scheffer, M., 2005. Implications of spatial heterogeneity for catastrophic regime shifts in ecosystems. Ecology 86 (7), 1797–1807.

A

Numerical continuation Programs

A.1 XPPAUT

Although there is a good explanation of how XPPAUT can be used to continue your equations in the webpage *http://www.math.pitt.edu/ bard/xpp/ xpp.html*, a breath explanation to start using AUTO from XPP will be given in this appendix. Besides some tips are given in order to help the reader to get rid of some trick problems. In the home page cited before you can download the XPPAUT program and follow the instructions how to install it.

XPP is a freely available tool written in C-language for solving differential equations, difference equations, delay equations, functional equations, boundary value problems, and stochastic equations. Besides, it contains the code for the popular bifurcation program, AUTO, (Doedel et al., 1997). It can be used in the following platforms: Linux, MacOs, Unix and Windows.

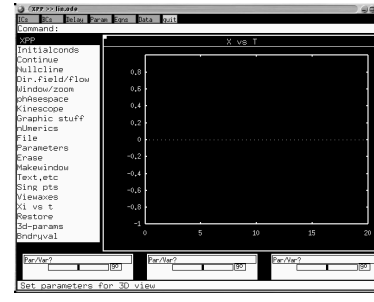

Figure A.1: XPP window.

Before start using XPPAUT it is needed to write the studied system into a **ode** file. This file must contain the system to be studied, the initial conditions, the parameter values and , if wanted, some numerical specifications, such as the time step size, the amount of time to integrate, the

parameter range and tolerance error in the algorithm used. Observe the following example of an ode file.

```
# RMA model
dX1/dt=X1*(R*(1-X1/K)-A2*X2/(B2+X1))
dX2/dt=X2*(E2*A2*X1/(B2+X1)-A3*X3/(B3+X2)-D2)
dX3/dt=X3*(E3*A3*X2/(B3+X2)-D3)

# D3=0.015+0.015*cont^6+h^6

#The initial condition
#par D2=0.01,D3=0.005
X1(0)=0.181022
X2(0)=0.0333333
X3(0)=1.65108

#D2=0.01,D3=0.015
X1(0)=0.0939155
X2(0)=0.128571
X3(0)=1.57478

#The parameters
par D2=0.01,D3=0.015
par R=0.5,K=0.2
par A2=0.4,B2=0.1,E2=1
#par h=0.5,cont=0
par A3=0.05,B3=0.3,E3=1

#The XPP options
@ total=2000, bounds=1000
@ Nmax=2000, Ds=0.005,Dsmin=0.001
@ EPSL=1e-06,Dsmax=0.01,EPSU=1e-06,EPSS=1e-06
@ ParMin=0, ParMax=0.3
@ Xmin=0,Ymin=0
@ Xmax=1,Ymax=1

done
```

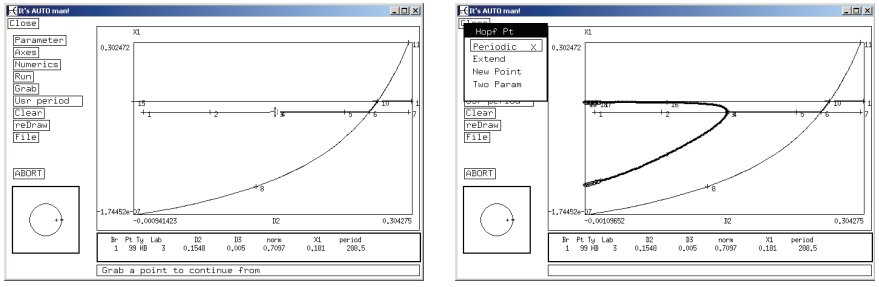

Figure A.2. Auto window: Bifurcation Diagram showing fixed points and periodic solutions.

Bifurcation analysis must be started from either a fixed point or a periodic orbit. Sometimes, there are complicated parameter zones in which AUTO calculation is too slow or does not converge. To solve this kind of numerical complications i)the tolerances (EPSL, EPSS, EPSU) can be reduced, which sets the default value to 10^{-4}, but usually the better value of the tolerances is 10^{-7} or ii)the study can be started from another fixed point value in order to scape from the complicated zone of parameters. In the ode file example two set of initial conditions can be observed, the set of initial conditions considered by XPP will be the last one you write. Regarding parameters, AUTO considers the first parameter written as the one to continue the solutions. But the parameters can be changed as well as the numerical specifications in the XPP menu without changing the ode file.

XPP can be used to calculate fixed points and then the result can be written in the ode file to avoid calculating them again. To continue a fixed point, go to the AUTO window : click on “Run” and then on “Steady state”. Using the system of equations cited in the example the bifurcation diagram like in the first picture of Figure A.2 will be found. To follow periodic solutions, grab a HP point that designates a Hopf bifurcation and click on “Run” and select “Periodic” as shown in the second picture of Figure A.2 and a branch of periodic solutions will appear.

In order to analyze changes in the phase portrait of the system when

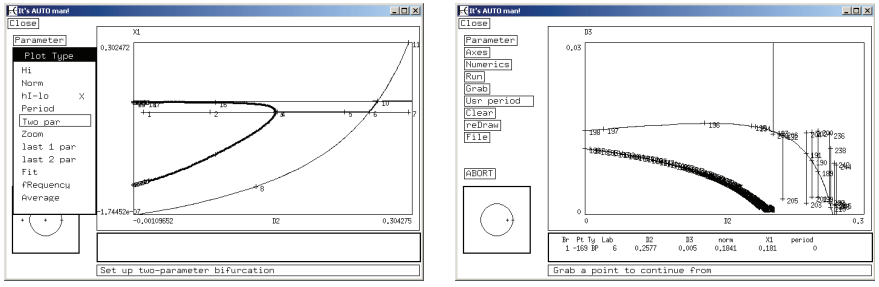

Figure A.3: Two-parameter bifurcation Diagram.

varying two parameters select “Axes” then “Two parameters” and a window will appear to select the main parameter and the second parameter. Never start continuations from two parameter calculus, first continue from one parameter and afterwards grab the special points to study two-parameter curves. As in the same situation with starting points, problems with convergence and speed of calculus can occur, in this way the main and second parameter can be switched to obtain complete two-parameter curves, see Figure A.3.

The AUTO window is not convenient to edit the plot. Consequently the postscript is generated without any possibilities of change except by using a postscript editor afterwards. However, from the AUTO window the bifurcation diagram data can be saved, which can be used later to make nicer figures using XPP or another software. Recently it was posted on the XPP’s webpage a link to a worthwhile Matlab function that orders the messy diagram outputs of XPPAUT and generates graph which can be modified using the graph tools of Matlab. But I have made my own Matlab program to solve some plotting problems when there are “MX” points, that means failure to converge. Figure A.4 shows some plots of AUTO data using Matlab, all the plots are related to the second one in Figure A.3. The first plot shows a “messy” plot where all the lines are connected and the lines with convergence failure can not be eliminated. The second plot was generated by my own code in matlab and as can be seen all the lines are disconnected, allowing to cut the undesirable lines

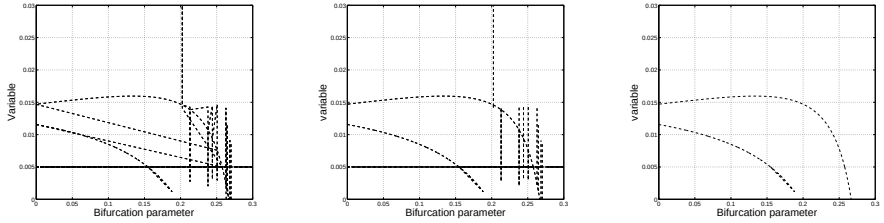

Figure A.4: "Make-up of plots"

as showed in the third plot.

```
%Copyright by Flora Souza Bacelar
%Plot bifurcation diagrams in Matlab that have been saved by XPPAUT
%Tested Under Matlab version 7.4.0.287 (R2007a)

[file_in,path] = uigetfile('*.dat','.dat file saved by AUTO (XPPAUT)');
file_name = [path file_in];
 b=load(file_name);
linhas=size(b(:,1),1);
a=zeros(linhas+2,5);
a(1:linhas,1:5)=b(1:linhas,1:5);
figure;
 m=0;
for i=1:linhas+1

  if a(i,4)==a(i+1,4);
        m=m+1;
        c(m,1)=a(i,1);
        c(m,2)=a(i,2);
        c(m,3)=a(i,3);
        c(m,4)=a(i,5);
        else
```

```
m=m+1;
c(m,1)=a(i,1);
c(m,2)=a(i,2);
c(m,3)=a(i,3);
c(m,4)=a(i,5);
size(c(:,1),1);

 if a(i,4)==1 %STABLE STEADY STATE
      plot(c(:,1),c(:,[2 3]),'linestyle','-','linewidth',3,'color','k');
      hold on;
      elseif a(i,4)==2;%UNSTABLE STEADY STATE
      d=zeros(m+2,4);
      d(1:m,1:4)=c(1:m,1:4);
      n=0;
      for j=1:m+1
      if d(j,4)==d(j+1,4);
      n=n+1;
      f(n,1)=d(j,1);
      f(n,2)=d(j,2);
      f(n,3)=d(j,3);
      else
      n=n+1;
      f(n,1)=d(j,1);
      f(n,2)=d(j,2);
      f(n,3)=d(j,3);
      plot(f(:,1),f(:,[2 3]),'linestyle','--','linewidth',1,'color','k');
      hold on;
      f=zeros(1);
      n=0;
      end

end
elseif a(i,4)==3;%STABLE PERIODIC ORBIT
plot(c(1:5:length(c),1),c(1:5:length(c),[2 3]),'linestyle','o','linewidth',2,
'Markersize',8,'color','r','Markerfacecolor','r');
```

```
        hold on;
        else %a(i,4)==4;%UNSTABLE PERIODIC ORBIT
        plot(c(:,1),c(:,[2 3]),'linestyle','o','linewidth',2,'Markersize',8,'color','b');
        hold on;
        end
        c=zeros(1);
        m=0;
        grid on;
        axis tight
        end

end
```

Of course before starting bifurcation analysis with AUTO it is desirable to know the studied system making some analytical studies, when possible, and numerical analyses in order to obtain the interesting parameter region in which the bifurcations are laid.

A.2 Matcont

Matcont is a freely available graphical Matlab package for the study of dynamical systems. This package can be downloaded from the webpage: http://www.matcont.ugent.be/.

Like XPPAUT, using this tool is possible to integrate numerically the equations and to do the continuation of equilibrium and periodic solutions with respect to a control parameter. Among many possibilities of this tool usage it is also possible continue a equilibrium in two and three control parameters.

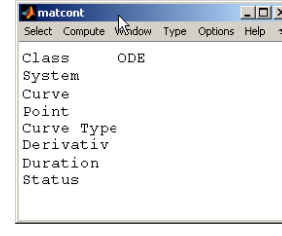

Figure A.5: Matcont window.

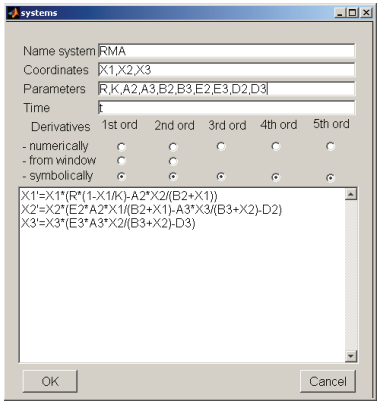

Figure A.6: Matcont system window.

Matcont contains a folder with some systems as an example. In order to write a system to be studied, the better way to do it is choosing one among of the examples and then modify and rename it. In this way follow these steps: open the Matcont window, see Figure A.5, choose “Select” and then “Systems” and click in the option “Edit/Load” instead of the option “New”. As a result a window, Figure A.6, will appear in which it possible to write the system.

Figure A.7. Matcont resume window.

Since the Matlab platform is being used, all the graph tools therein can be used. And also it is possible to see simultaneously the continuation evolution in all variables and in a three dimensional space. For that it necessary to select the “window” option and add how many plots wanted. With Matcont, there are no problems with mixed data or lines in the plots. However, is better stop the process of continuation of each bifurcation point. This allows to access separately each branch of equilibria. So, after selecting the control parameter and the fixed point to continue, click “compute”, then “forward”. The calculation will stop when a bifurcation point is detected and a small window with three options will appear, see Figure A.7. Select “stop” option, and immediately, rename the present curve. To extend the curve select it and restart from the last point of the curve. This will permit to access each branch of the curve in order to edit them separately.

In order to illustrate, see Figure A.8, that shows all the windows that compounds the Matcont tool.

There are others softwares that can be used to study dynamical systems, see the webpage http://www.dynamicalsystems.org/sw/sw/. All of them have advantages and disadvantages, just choose the one that fits a personal style of working. In the present thesis both XPPAUT and Matcont were used. Auto runs faster the continuations while Matcont seems to be more stable in the complicated range of parameters mentioned before.

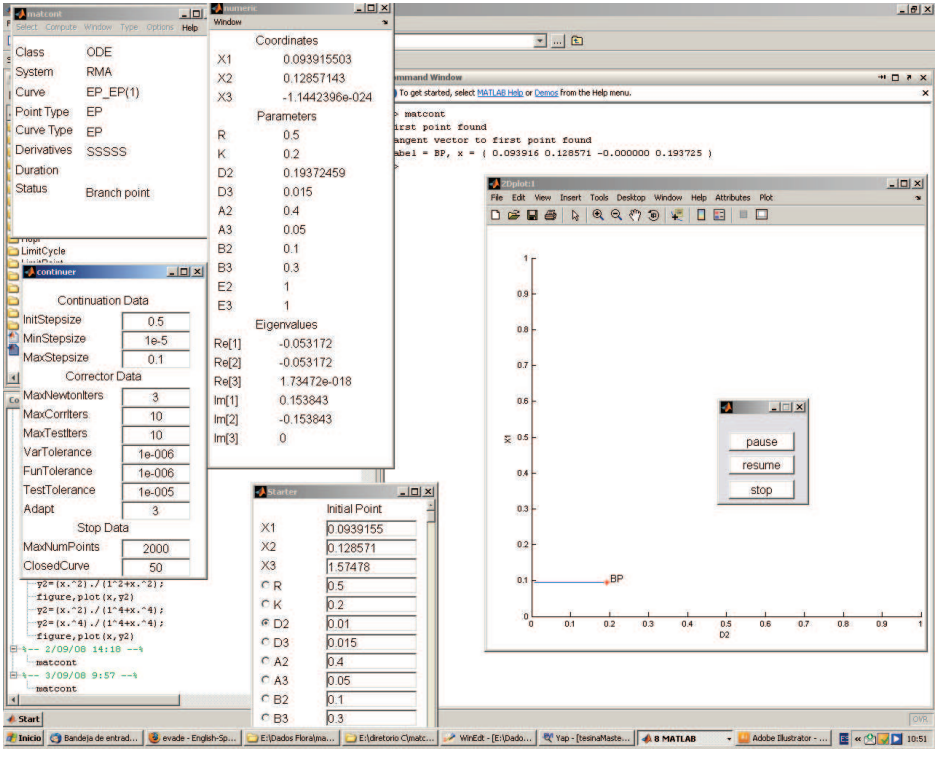

Figure A.8: Matcont windows.

Bibliography

Doedel, E., Champneys, A., Fairgrieve, T., Kuznetsov, Y., Sandstede, B., Wang, X., 1997. Auto 97: continuation and bifurcation software for ordinary differential equations. Technical report, Concordia University, Montreal, Canada.

Index

Curriculum vitæ

Flora Souza Bacelar

Personal Information

Date of birth:	04/01/1978
Place of birth:	Salvador of Bahia
Country:	Brazil
E-mail:	florabacelar@ifisc.uib-csic.es
URL:	http://www.ifisc.uib-csic.es/people/people-detail.php?id=585

Education

- (January 2001) Graduate in Physics.
  Universidade Federal da Bahia (UFBA-Brazil).
- (October 2004) Master degree in Physics.
  Universidade Federal da Bahia (UFBA-Brazil).

Thesis Advisor: Prof. Roberto Fernandes Silva Andrade.
Title: Um modelo de equações diferenciais funcionais com retardo temporal para a dinâmica de infecção pelo VIH

- (Since January 2006) PHD Student in Physics.
  Universitat de les Illes Balears, Palma de Mallorca.
  Thesis Advisor: Prof. Emilio Hernández García.

- (September 2008) Master degree in Physics.
  Universitat de les Illes Balears, Palma de Mallorca.
  Thesis Advisor: Prof. Emilio Hernández García.
  Title: Bifurcation Analysis of a Marine Food Chain

Current Affiliation

- ORGANISM: Universitat de les Illes Balears (UIB)

- CENTER: Instituto de Física Interdisciplinar y Sistemas Complejos, *IFISC*, (CSIC-UIB)

- PROFESSIONAL CATEGORY AND STARTING DATE: PhD student at the UIB and scholarship holder of a Fellowship from the Government of the Balearic Islands since 01/09/2007. PhD supervisor: Prof. Emilio Hernández García .

- POSTAL ADDRESS:

  Instituto de Física Interdisciplinar y Sistemas Complejos (IFISC)
  Edifici Instituts Universitaris de Recerca
  Campus UIB. Carretera de Valldemosa km. 7.5.
  07122-Palma de Mallorca
  Spain

- PHONE: +34 971 259 883

- FAX: +34 971 173 248

Awarded Fellowships

1. “Iniciação científica” . Scholarship sponsor: PIBIC (Programa Institucional de Bolsas de Iniciação Científica), http://www.prp.unicamp.br/pibic/.
   PERIOD: 09/1998-08/1999.
   CENTER: Universidade Federal da Bahia (UFBA-Brazil).
   TITLE:“Caracterização de Fotomultiplicadoras”.
   SUPERVISOR: Iuri Muniz Pepe.

2. “Iniciação científica” . Scholarship sponsor: PIBIC (Programa Institucional de Bolsas de Iniciação Científica), http://www.prp.unicamp.br/pibic/.
   PERIOD: 09/1999-08/2000.
   CENTER: Universidade Federal da Bahia (UFBA-Brazil).
   TITLE: “Desenvolvimento de instrumentação para detecção de luz de baixa intensidade”.
   SUPERVISOR: Iuri Muniz Pepe.

3. “Iniciação científica” . Scholarship sponsor: PIBIC (Programa Institucional de Bolsas de Iniciação Científica), http://www.prp.unicamp.br/pibic/.
   PERIOD: 09/2000-08/2001.
   CENTER: Universidade Federal da Bahia (UFBA-Brazil).
   TITLE:“Propriedades óticas e de transporte de sistemas semicondutores”.
   SUPERVISOR: Antonio Ferrera da Silva.

4. Master of Physics. Scholarship sponsor: CNPQ (Conselho Nacional de Desenvolvimento Científico e Tecnológico), http://www.cnpq.br/.

PERIOD: 09/2001-12/2003.
CENTER: Universidade Federal da Bahia (UFBA-Brazil).
TITLE: “Um modelo de equações diferenciais funcionais com retardo temporal para a dinâmica de infecção pelo VIH ”.
SUPERVISOR: Rorberto Fernandes Silva Andrade.

5. PHD studies. Scholarship sponsor: European community.
THRESHOLDS integrated project(Thresholds of Environmental Sustainability), http://www.thresholds-eu.org/index.html.
PERIOD: 01/02/2006-30/09/2007.
CENTER: Instituto Mediterraneo de Estudios Avanzados (CSIC-IMEDEA)-Cross-Disciplinary Physics Department.
SUPERVISOR: Emilio Hernández García .

Research Lines

- Statistical Physics

  Phase transitions;

  Nonequilibrium instabilities.

- Biological Physics and Nonlinear phenomena in ecology and in Life Science:

  Bifurcation theory of dynamical systems;

  Stochastic Differential Equations;

  Delay differential equations;

  Spatiotemporal pattern formation;

  Population dynamics of ecological systems;

  Predator-prey models;

  Individual-based models (Cellular Automata).

- Evolutionary dynamics

  Evolution of disease(biological trade-offs for evolution)

  Phenotypic evolutionary models(evolutionary branching/speciation)

Participation in Research Projects

1. ”Física Biologica”. Program: 28001010002P-5 FÍSICA - UFBA (2004) Coordinator: Suani Tavares Rubim de Pinho.

2. THRESHOLDS: Thresholds of environmental sustainability Integrated Project (Contract 003933), VI Framework Program, European Union. Priority 6.3 Global Change and Ecosystems” (2005-2008). Coordinator: C. Duarte (RRNN-IMEDEA). Responsible workpackage S2WP1 ’Regime modelling’: E.Hernández-García.

3. Grupo de investigación competitivo de Física Interdisciplinar (Grupo de Excelencia Coherente). Subvención del Govern Balear (2006-2008). Investigador principal : M. San Miguel.

4. FISICOS: Física Interdisciplinar de Sistemas Complejos. Proyecto Fis2007-60327, Ministério de Educación y Ciencia. Investigador principal: M. San Miguel.

5. Integrando níveis de organização em modelos ecológicos preditivos: aportes da epistemologia, modelagem e investigação empírica. Coordenador da pesquisa Dr. Charbel Niño El-Hani. Pronex- Programa de apoio a núcleos de excelência (Pedido $n^{\circ}6714/2009$), Fapesb-Fundação de Amparo à pesquisa do estado da Bahia.

Teaching Experience

1. Classical Mechanics 1. Federal University of Bahia (UFBA), (Brazil). 05/01/2004-05/01/2006.

2. Classical Mechanics 1. Centro Baiano de Ensino Superior (AREA1), (Brazil). 01/03/2005-02/01/2006.

3. Electromagnetism. Centro Baiano de Ensino Superior (AREA1), (Brazil). 01/07/2005-02/01/2006.

Stays at foreign research centers

- From 10/05/2006 to 12/05/2006 under the supervision of Professor José-Manuel Zaldívar, Institute for Environment and Sustainability, Joint Research Center of the European Commission (JRC), Ispra (Italy).

- From 17/11/2006 to 22/11/2006 under the supervision of Professor José-Manuel Zaldívar, Institute for Environment and Sustainability, Joint Research Center of the European Commission (JRC), Ispra (Italy).

- From 25/07/2007 to 27/07/2007 under the supervision of Professor José-Manuel Zaldívar, Institute for Environment and Sustainability, Joint Research Center of the European Commission (JRC), Ispra (Italy).

- From 29/09/2008 to 31/10/2008 under the supervision of Professor Volker Grimm and Dr. Justin Calabrese, Department of Ecological Modelling (OESA), Helmholtz Centre for Environmental Research (UFZ), Leipzig (Germany).

- From 23/04/2009 to 05/07/2009 under the supervision of Dr. Andrew White, Department of Mathematics, Heriott-Watt University, Edinburgh (Scotland)

- From 14/10/2009 to 15/12/2009 under the supervision of Professor Dr. Herb Freedman, Department of Mathematical and Statistical Sciences , University of Alberta , Edmonton (Alberta), Canada

Workshops and Schools

- Summer School -PHYSBIO - Stochastic processes, fluctuations and noise, St. Etienne, France, 13. Aug. - 08. Oct. 2006
- Transylvanian Summer School Series - International Workshop on Complex Systems and Networks, Sovata, Romania, July 15-20, 2007.
- Workshop on Dynamics and Evolution of Biological and Social Networks, Mallorca, Spain 10-20 February, 2008.

Submitted Papers

1. T. R. Pinho, S. ; S. Bacelar, F. ; S. Andrade, R. F.; I. Freedman, H.; *A Model of Vascular Tumor Response to Chemotherapy Combined with Anti-Angiogenic Therapy*, Bulletin of Mathematical Biology (December 2009).
2. Flora Souza Bacelar; Roberto F. S. Andrade; *The dynamics of the HIV infection: a time-delay differential equation approach*, Physical Review E, (April 2010).
3. Bacelar, F. S., Calabrese, J. M., Hernández-García, E.; *Savanna-fire model: Combined effects of tree-tree establishment competition and spatially explicit fire on the spatial pattern of trees in savannas*. Preprint submitted to Journal of Theoretical Biology (2010).

Published Papers

1. Bacelar, F.S.; Dueri, S.;Hernández-García, E. ; Zaldívar,J.M.. " *Joint effects of nutrients and contaminants on the dynamics of a food chain in marine ecosystems*", Mathematical Biosciences 218 (2009) 24-32 .

2. Zaldívar, J.M.;Bacelar, F.S.; Dueri, S.; Marinov, D.; Viaroli, P.; Hernández-García, E.. "*Modeling approach to regime shifts of primary production in shallow coastal ecosystems*", Ecological Modelling 220 (2009) 3100-3110

3. Flora S. Bacelar, Andrew White, Mike Boots; *Life history and mating systems select for male biased parasitism mediated through natural selection and ecological feedbacks*, Journal of Theoretical Biology 269 (2011) 131 - 137.

Seminars Given

1. Investigations on the HIV dynamics with a system of time delayed functional equations.
   Instituto Mediterráneo de Estudios Avanzados (IMEDEA)-Universitat de les Illes Balears.
   May 30th 2006.

2. Regime shifts in shallow coastal ecosystems: Competition between Floating and Submerged plants.
   Istituto de Fisica Interdisciplinar y Sistemas complejos (IFISC).
   February 26th 2008.

3. Savanna-Fire Model: Combined effects of tree-tree establishment competition and spatially explicit fire on the spatial pattern of trees in Savannas.
   Mathematical Biology Seminar Series: Centre for Mathematical Biology. Dept. of Mathematical and Statistical Sciences.

University of Alberta
November 16th 2009.

4. Savanna-Fire Model: Combined effects of tree-tree establishment competition and spatially explicit fire on the spatial pattern of trees in Savannas.
   Istituto de Fisica Interdisciplinar y Sistemas complejos (IFISC).
   March 3rd 2010.

Conference Presentations

[O] = Oral presentation, [P] = Poster presentation

1. "*Caracterização de Fotomultiplicadoras*", XVIII Seminário estudantil, UFBA, Brazil. October (1999). [O]

2. "*Desenvolvimento de instrumentação para detecção de luz de baixa intensidade*", XIX Seminário estudiantil, UFBA, Brazil. October de (2000). [O]

3. "*Propriedades óticas e de transporte de sistemas semicondutores*", XIX Seminário estudantil, UFBA, (Brazil), March (2002). [P]

4. "*Estudo de um modelo de equações diferenciais ordinárias para descrever a dinâmica de infecção pelo HIV*", XXVI encontro Nacional de Física da matéria condensada, Poços de Caldas, (Brazil), May (2004). [P]

5. "*Estudo de um modelo de equações diferenciais ordinárias para descrever a dinâmica de infecção pelo VIH*", II Bienal da Sociedade Brasileira de Matemática, UFBA, (Brazil), 27 octuber (2004). [P]

6. "*Duas escalas de tempo em um modelo de equações diferenciais com retardo temporal para a infecção pelo VIH*", XXII Encontro de Físicos do Norte e Nordeste, Feira de Santana-Ba, (Brazil), 08-12 november (2004). [P]

7. "*Duas Escalas de tempo em um modelo de equações diferenciais com retardo temporal para infecção pelo VIH*", X Congresso Brasileiro de Física Médica poster, Salvador, (Brazil). 26-29 may (2005). [P]

8. "*Analise comparativa de modelos angiogênicos de diferentes terapias do câncer*", XXIII Encontro de Físicos do Norte e Nordeste", Maceió-Al, Brazil. October (2005). [O]

9. Presented by S. T. R. PINHO "*A comparative analysis of nonlinear time delayed angiogenic models of cancer therapies*", PINHO, S. T. R. ; BACELAR, Flora Souza ; ANDRADE, R. F. S..
XIX Latin American Workshop on Nonlinear Phenomena (LAWNP05), Bariloche (Argentina), (2005). [O]

10. Presented by R. F. S. Andrade "*Investigations on the HIV dynamics with a system of time delayed differential equations* ", Andrade, R. F. S.; BACELAR, Flora Souza ; SANTOS, Rita Maria Zorzenon
Work shop on Immunology, International centre of condensed matter physics, Brasilia (Brazil), (2005). [O]

11. Presented by S. T. R. PINHO "*Ação Angiogênica em Modelos de Terapias de Câncer*", PINHO, S. T. R. ; ANDRADE, Roberto Fernandes Silva ; BACELAR, Flora Souza .
XXIX Encontro Nacional de Física da Matéria Condensada (XXIX ENFMC), São Lourenço (Brazil), (2006). [O]

12. "*Integration of Langevin Equations with Multiplicative noise: Using a split-step scheme*", PHYSBIO- Non-equilibrium in Physics and in Biology, St. Etienne, France. October (2006). [O]

13. "*A comparative Analysis of time-delayed models of cancer therapies at the vascular stage. 2nd Conference of the BioSim Network of Excellence*", Calas Viñas, Mallorca (Spain). 18-22 October (2006). [P]

14. Presented by J.-M. Zaldivar-Comenges "*A modelling approach to nutrient-driven regime shifts in shallow coastal systems: competition between seagrass and macroalgae*", J.-M. Zaldívar-Comenges, F.S. Bacelar, S. Dueri, E. Hernández-García, P. Viaroli.
6th International Congress on Industrial and Applied Mathematics (ICIAM07). Zurich, (Switzerland). 16-20 July (2007). [P]

15. Presented by E. Hernández-García "*Regime changes in competing floating-submerged plant ecosystems*", F.S. Bacelar, J.-M. Zaldívar-Comenges, S. Dueri, E. Hernández-García.
European Conference on Complex Systems (ECCS07). Dresden, Germany, 30 September - 6 October (2007). [P]

16. "*Regime changes in competing floating-submerged plant ecosystems*", F. S.Bacelar, J.-M. Zaldívar-Comenges, S. Dueri, E. Hernández-García.
XV Congreso de Física Estadística, FisEs'08 Salamanca, 27 -29 March (2008). [P]

17. "*Join effects of nutrients and contaminants on the dynamics of a food chain in marine ecosystems* ", Flora S. Bacelar, Sibylle Dueri, Emilio Hernández-García and José-Manuel Zaldívar. XV Congreso de Física Estadística, FisEs'08 Salamanca, 27 -29 March (2008). [P]

18. "*Savanna-Fire Model: Combined effects of tree-tree establishment competition and spatially explicit fire on the spatial pattern of trees in savannas* ", Flora S. Bacelar, Justin M. Calabrese, Volker Grimm, Richard Zinc, Emílio Hernández-García. PATRES meeting Paris, 25 -27 March (2009). [O]

19. Presented by R. F. S. Andrade "*A model of partial differential equations for the propagation of HIV in TCD*4^+ *cells*", Andrade, R. F. S.; B. S. Marinho, Euler; Bacelar, Flora Souza
XXXII Encontro Nacional Física da Matéria Condensada (XXXII Brazilian Meeting on Condensed Matter Physics), Águas de Lindóia, State of São Paulo, from May 11 to 15 (2009). [O]

20. "*Savanna-Fire Model: Combined effects of tree-tree establishment competition and spatially explicit fire on the spatial pattern of trees in savannas"*, Flora S. Bacelar, Justin M. Calabrese, Volker Grimm, Emílio Hernández-García. XVI Congreso de Física Estadística, FisEs'09 Huelva,10-12 September (2009). [P]

21. "*The evolution of male-biased parasitism*", Flora S. Bacelar, Andrew White, Mike Boots. XI Latin American Workshop on Nonlinear Phenomena, Lawnp09 Buzios(RJ), Brazil, 05-09 October(2009). [P]

22. "*A model of partial differential equations for the propagation of HIV in TCD*4^+ *cells*", Roberto F. S. Andrade, Euler B. S. Marinho, Flora S. Bacelar. XI Latin American Workshop on Nonlinear Phenomena, Lawnp09 Buzios(RJ), Brazil, 05-09 October(2009). [P]

23. "*The evolution of male-biased parasitism in different mating systems*", Flora S. Bacelar, Andrew White, Mike Boots. Darwin09-International Workshop on 150 Years after Darwin: From Molecular Evolution to Language
Palma de Mallorca, November 23 - 27, 2009. [P]

24. "*Savanna-Fire Model: Combined effects of tree-tree establishment competition and spatially explicit fire on the spatial pattern of trees in savannas"*, Flora S. Bacelar, Justin M. Calabrese, Volker Grimm, Emílio Hernández-García. CMPD3 Conference on Computational and Mathematical Population Dynamics from May 31 to June 4, 2010 - Bordeaux, France. [O]

25. "*Combined effects of tree-tree establishment competition and spatially explicit fire on the spatial pattern of trees in savannas* ", Flora S. Bacelar, Justin M. Calabrese, Emílio Hernández-García. Emergence and Design Robustness: General Principles and Applications to Biological, Social and Industrial Networks, IFISC, Palma de Mallorca, 21-25 September (2010). [P]

26. Presented by Emílio Hernández-García "*Savanna-Fire Model: Combined effects of tree-tree establishment competition and spatially explicit fire on the spatial pattern of trees in savannas* ", Flora S. Bacelar, Justin M. Calabrese, Emílio Hernández-García. Emergence and Design Robustness: General Principles and Applications to Biological, Social and Industrial Networks, IFISC, Palma de Mallorca, 21-25 September (2010). [O]

Computer Skills

- Programming languages: Fortran 77, Python,
- Operating systems: Windows, Unix (basic)
- Mathematics: Matlab, Mathematica.
- Typesetting: LaTeX, Word.

Languages

Portuguese	Mother-tongue
Spanish	Correct(written and spoken)
English	Correct(written and spoken)
French	Basic level

Last updated: December 2, 2010